The Astrophysical Journal Supplement Series, 190:348–417, 2010 October doi:10.1088/0067-0049/190/2/348

THE ARIZONA RADIO OBSERVATORY 1 mm SPECTRAL SURVEY OF IRC +10216 AND VY CANIS MAJORIS (215–285 GHz)

E. D. Tenenbaum[1,2,5], J. L. Dodd[1,2], S. N. Milam[3], N. J. Woolf[1], and L. M. Ziurys[1,2,4]
[1] Department of Astronomy and Steward Observatory, University of Arizona, 933 N. Cherry Ave., Tucson, AZ 85721, USA; tenenbaum@strw.leidenuniv.nl, jldodd@email.arizona.edu, lziurys@email.arizona.edu, nwoolf@as.arizona.edu
[2] Department of Chemistry, University of Arizona, Tucson, AZ 85721, USA
[3] NASA Goddard, Space Flight Center, Astrochemistry Laboratory, Code 691, Greenbelt, MD 20771, USA; Stefanie.N.Milam@nasa.gov
[4] Arizona Radio Observatory, University of Arizona, Tucson, AZ 85721, USA
Received 2010 May 4; accepted 2010 July 28; published 2010 September 29

ABSTRACT

A low noise (1σ rms $\sim$ 3 mK) 1 mm spectral survey (214.5–285.5 GHz) of the oxygen-rich supergiant VY Canis Majoris and the carbon-rich asymptotic giant branch star IRC +10216 has been conducted using the Arizona Radio Observatory's 10 m Submillimeter Telescope. Here the complete data set is presented. This study, carried out with a new ALMA-type receiver, marks the first continuous band scan of an O-rich circumstellar envelope, and the most sensitive survey to date of IRC +10216. In VY CMa, 130 distinct molecular lines were detected, 14 of which cannot be identified; in IRC +10216, 717 lines were observed, with 126 features remaining unidentified. In the 1 mm bands of VY CMa and IRC +10216, emission is present from 18 and 32 different chemical compounds, respectively, with 10 species common to both sources. Many narrow emission lines were observed in both circumstellar shells, arising from vibrationally excited molecules and from refractory-containing species. Line profiles in VY CMa also exhibit a variety of different shapes, caused by the complex, asymmetric outflow of this object. The survey highlights the fact that C-rich *and* O-rich circumstellar envelopes are chemically interesting, and both are sources of new interstellar molecules. The high number of unidentified lines and the unreliable rest frequencies for known species such as NaCN indicate the need for additional laboratory spectroscopy studies.

Key words: astrochemistry – circumstellar matter – stars: AGB and post-AGB – stars: individual (IRC +10216, VY CMa) – supergiants

Online-only material: machine-readable tables

1. INTRODUCTION

Many evolved stars are known to lose mass at prolific rates (Schöier & Olofsson 2001). Besides playing an important role in the feedback of matter into the interstellar medium (Dorschner & Henning 1995; Cherchneff 2006), stellar mass loss creates a dusty, molecular envelope around the central star. A wide range of physical conditions are present in the material composing the circumstellar envelope, or CSE, leading to a rich and varied gas-phase chemistry. Considerable temperature and density gradients exist throughout the CSE, with significant infrared radiation emanating from the star itself and a strong ultraviolet field impinging on the outer shell (Olofsson 2005; Ziurys 2006; Decin et al. 2010). Moreover, circumstellar envelopes have varying C/O ratios, which is the major factor in determining chemical composition (Olofsson et al. 1997).

C-rich envelopes, where C/O is typically $\sim$1.3, have been extensively studied using infrared and radio telescopes, in particular the nearby asymptotic giant branch (AGB) star IRC +10216. The envelope of this star, which is at a distance $\sim$150 pc, is losing mass at a rate of $\sim 3 \times 10^{-5}\ M_{\odot}\ \mathrm{yr}^{-1}$ (Agúndez & Cernicharo 2006). Seven spectral surveys have been conducted of IRC +10216, starting in 1985 (Johansson et al. 1985). The surveys include the recent work by He et al. (2008) in the 1 and 2 mm bands using the Arizona Radio Observatory (ARO) telescopes, the Cernicharo et al. (2000) study in the 2 mm band using the IRAM 30 m dish, the Avery et al. (1992) and Groesbeck et al. (1994) band scans at 0.8 mm with the Caltech Submillimeter Observatory and James Clerk Maxwell telescope, the Onsala survey in the 3–4 mm window (Johansson et al. 1985), the Nobeyama survey at 6–10 mm (Kawaguchi et al. 1995), and the 43–197 μm survey with the *Infrared Space Observatory* (Cernicharo et al. 1996). These surveys, as well as numerous other observations (e.g., Guelin et al. 1990; Turner et al. 1994; Ziurys et al. 2002), have resulted in the identification of 71 distinct molecules in this object, most of which contain carbon. The molecules include unusual carbon chain species such as HC_nN ($n = 2, 3, 4, 5$) and SiC_n ($n = 1, 2, 3$), and the metal cyanides MgNC, NaCN, and AlNC (Cernicharo et al. 2000; Ziurys 2006). The varied chemical makeup of C-rich circumstellar envelopes has inspired many theoretical models which explore the photochemistry, neutral–neutral reactions, and inner envelope shock chemistry taking place in these objects (e.g., Millar & Herbst 1994; Willacy & Cherchneff 1997; Millar et al. 2000; Agúndez & Cernicharo 2006; Cherchneff 2006).

Until recently, molecular studies of oxygen-rich (C/O $\sim$ 0.8) CSEs have been widely neglected compared to their carbon-rich counterparts. Radio and millimeter-wave observations of O-rich envelopes have shown that CO, SO, SiO, SiS, CS, H_2O, HCN, H_2S, SO_2, and NH_3 are present in some O-rich shells (Omont et al. 1993; Bujarrabal et al. 1994; Menten & Alcolea 1995; Menten et al. 2008). However, unlike IRC +10216, these objects have not been sources of new molecular species. This apparent lack of exotic molecules has led to the conclusion that O-rich envelopes are less chemically diverse than their C-rich counterparts, and, in general, are not particularly interesting from the aspect of astrochemistry (Tielens & Charnley 1997; Olofsson 2005).

[5] Current address: Sackler Laboratory for Astrophysics, Leiden Observatory, Leiden University, P.O. Box 9513, 2300 RA Leiden, The Netherlands.

Over the past four years, new, more sensitive molecular-line observations have been carried out toward O-rich circumstellar shells, in particular that of the red supergiant VY Canis Majoris (VY CMa) by Ziurys and collaborators (e.g., Ziurys et al. 2007, 2009; Milam et al. 2007). This star, located at a distance of 1.14 kpc (Choi et al. 2008), is a 25 $M_{\odot}$ object with an effective temperature of 3000 K and an impressively large mass-loss rate of $\sim 3 \times 10^{-4}\ M_{\odot}\ \mathrm{yr}^{-1}$ (Humphreys et al. 2005; Monnier et al. 2000; Smith et al. 2001). VY CMa is a well-known source of SiO, H_2O, and OH masers (Shinnaga et al. 2004; Menten et al. 2006; Bowers et al. 1983), and IR images have shown highly asymmetric dust outflows (Smith et al. 2001). Millimeter-wave observations done using the ARO Submillimeter Telescope (SMT) and 12 m telescope revealed the presence of NaCl, PN, and NS in VY CMa, marking the first detections of these molecules in an O-rich CSE (Ziurys et al. 2007; Milam et al. 2007). Also, diverse line shapes were measured, with several velocity components traced in emission from different chemical species (Ziurys et al. 2007, 2009).

To further explore the unique molecular environment in VY CMa, we have conducted a continuous, low-noise (1σ rms $\sim$ 3 mK at 1 MHz resolution) spectral survey of the 1 mm band (214.5–285.5 GHz) of this object using the ARO SMT. For the purpose of directly comparing C-rich and O-rich circumstellar chemistry, we also observed the same spectral band toward IRC +10216 at an equivalent noise level. Our survey is significantly more sensitive and complete than previous work. For example, in the survey of He et al. (2008), typical noise levels at 1 mm in IRC +10216 were 20 mK, and their band covered 219.5–245.5 GHz and 251.5–267.5 GHz, compared to our typical 1σ noise level of 3 mK and our unbroken coverage from 214.5 to 285.5 GHz. The work reported here marks the first continuous survey of an O-rich CSE, and also the first direct comparative band scan of an O-rich and a C-rich envelope.

The complete survey will be presented in three separate papers. A short "highlights" paper has already been published (Tenenbaum et al. 2010, Paper I). Another forthcoming paper will include detailed chemical modeling of both sources and a complete set of molecular abundances and isotope ratios derived from non-LTE radiative transfer analysis of the observations (J. L. Dodd et al. 2011, in preparation). In this work, we present the details of the observations, the entire survey spectra, assignment of all the detected emission lines, measurement of all line parameters, and a discussion of results that have not been described elsewhere.

2. OBSERVATIONS

The measurements were conducted during the period 2007 February to 2009 December using the ARO's 10 m SMT on Mt. Graham. The observations were done using the SMT's dual polarization, 1 mm receiver employing sideband-separating SIS mixers designed for ALMA Band 6. Rejection was consistently $\geqslant$15 dB, inherent in the mixer architecture, and typical system temperatures ranged from 200 to 450 K, depending on weather and source elevation. Filter banks with 2048 channels at 1 MHz resolution were the backends used for all measurements, operated in parallel mode for the two receiver polarizations ($2 \times$ 1024 channels), and acousto-optical spectrometers (AOS) with 0.9 MHz resolution served as secondary confirming backends. The temperature scale at the SMT is measured as T_A^*, derived by the chopper-wheel method. The radiation temperature is defined as $T_R = T_A^*/\eta_b$, where η_b is the main-beam efficiency. Throughout the data collection process, the main beam efficiency was measured by doing spectral scans of planets immediately after pointing, resulting in an average value of $\eta_b = 0.74$. To convert antenna temperature to flux density, a conversion factor of 46.5 Jy K^{-1} is used for the SMT. Across the frequency span of 214.5–285.5 GHz, the beam size range was $\theta_b = 35''$–$26''$.

Observations were carried out in beam-switching mode with a $\pm 2'$ subreflector throw. For each frequency setting, spectra were accumulated with a 1.024 GHz bandwidth as per parallel mode of the filter banks. The data were typically taken in 2 IF mode, in the LSB of both receiver channels. The default intermediate frequency (IF) used in the survey was 6 GHz, but often a different IF value was chosen in order to avoid contamination from strong lines in the image sideband. (The IF of the 1 mm receiver can be tuned to any value within a range of 5–7 GHz). Local oscillator shifts of $\pm$20 MHz were also done to insure against image contamination. Pointing and focus were monitored approximately every 2 hr on planets. The positions used for VY CMa and IRC +10216 were $\alpha = 07^{\mathrm{h}}20^{\mathrm{m}}54\overset{\mathrm{s}}{.}7\ \delta = -25^{\circ}40'12''$ and $\alpha = 9^{\mathrm{h}}45^{\mathrm{m}}14\overset{\mathrm{s}}{.}8\ \delta = 13^{\circ}30'40''$ (B1950.0), respectively. Data were reduced using the CLASS software package and linear baselines were removed from the spectra.

At the SMT, VY CMa and IRC +10216 are above the tree line from 4–11 LST and 5–15 LST, respectively. Our observing protocol for most sessions consisted of first observing VY CMa for its full 7 hr at a given frequency, and then observing IRC +10216 at the same frequency for the last four hours before it set. In this manner, the integration time was maximized because the receiver only needed to be tuned once per observing session. Despite the difference in observing time, similar noise levels were achieved for these two objects because of the difference in declinations. Overall, about 1700 hr of actual integration time on the sky was devoted to the survey, not taking into account overhead, pointing, receiver tuning, and bad weather. For each frequency setting, typical integration time per source was 7–10 hr.

3. LINE IDENTIFICATION AND ANALYSIS

Spectra from the survey of IRC +10216 and VY CMa are shown sequentially in increasing frequency in Figures 1 and 2, respectively. The intensity scale is T_A^* (K). All spectra have been Hanning smoothed to a resolution of 2 MHz, or 2.1–2.8 km s^{-1} in the 1 mm band, completely acceptable given that the linewidths are 30 km s^{-1} or greater in both sources. Each panel in the figures displays $\sim$1 GHz of the spectrum. For IRC +10216, there is a 30 MHz overlap between successive panels such that lines falling near the edge of a given panel appear at least once in untruncated form. For example, the first panel of Figure 1 (IRC +10216) displays the spectral range 214500–215530 MHz, and the next window displays 215500–216530 MHz. The figures of VY CMa data also have a similar frequency overlap, but the range is 80 MHz to accommodate the wider lines of this source. In most cases, the same 1 GHz frequency range is repeated in two successive panels: one with an intensity scale to accommodate strong lines and the other to show weak lines. For frequency settings where only weak lines are present, just one panel was used to display the spectrum. In the instances where an extremely intense line is present, an inset is used to show the strong feature such that the intensity scale can be set for weaker emission (for example, see the IRC +10216 spectrum at 231 GHz showing the $J = 2 \rightarrow 1$ line of CO). In Figures 1 and 2, each spectral feature is labeled by molecule(s) and in cases when $v \neq 0$ (i.e., not the

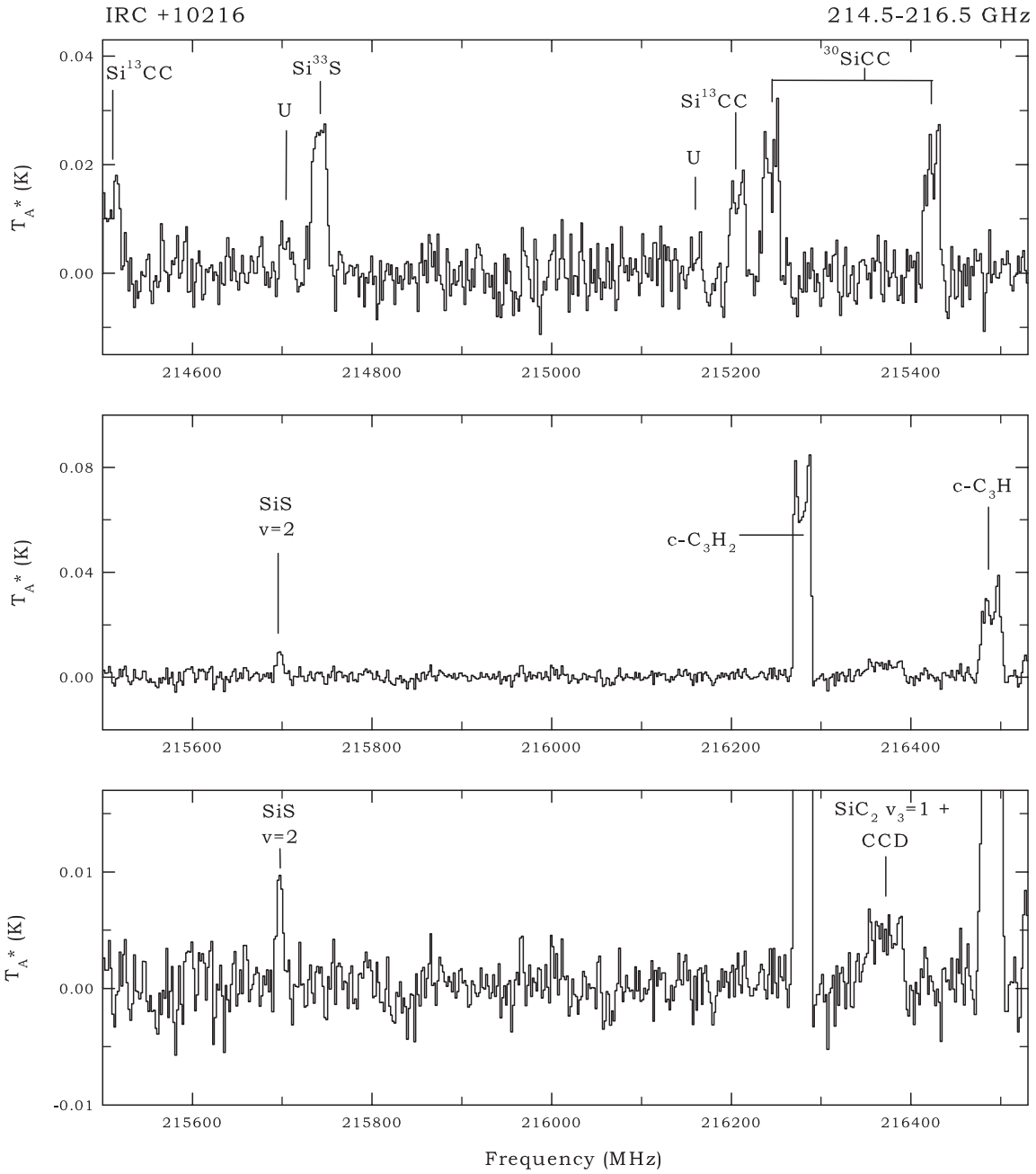

Figure 1. 214.5–285.5 GHz spectrum of IRC +10216 displayed in consecutive 1.03 GHz frequency segments with 2 MHz spectral resolution. There is a 30 MHz overlap between consecutive spectra. At most frequencies, two versions of the same spectrum are shown: one which displays the strong lines, and a magnified version to show the weaker features. Extremely intense lines are displayed in insets. Each emission feature is marked with its corresponding molecular identification. Four short segments of the spectrum, near 220.4 GHz, 228.1 GHz, 234.6 GHz, and 254.0 GHz, were omitted from the figure because of severe image contamination. First order baselines were removed from each spectrum. The frequency scale assumes $V_{\rm LSR} = -26.0$ km s^{-1}. Typical integration time per frequency setting is 7 hr.

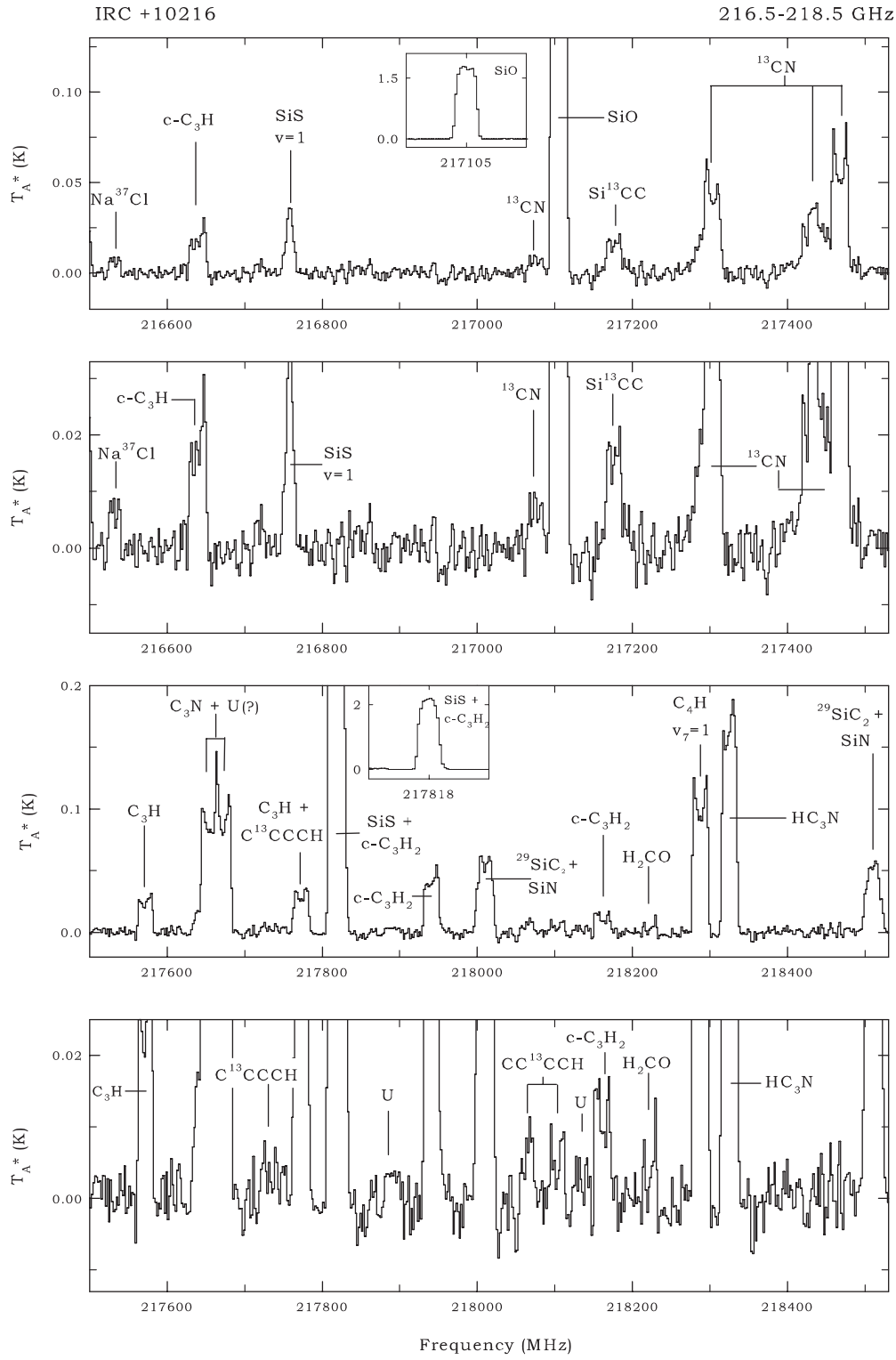

Figure 1. (Continued)

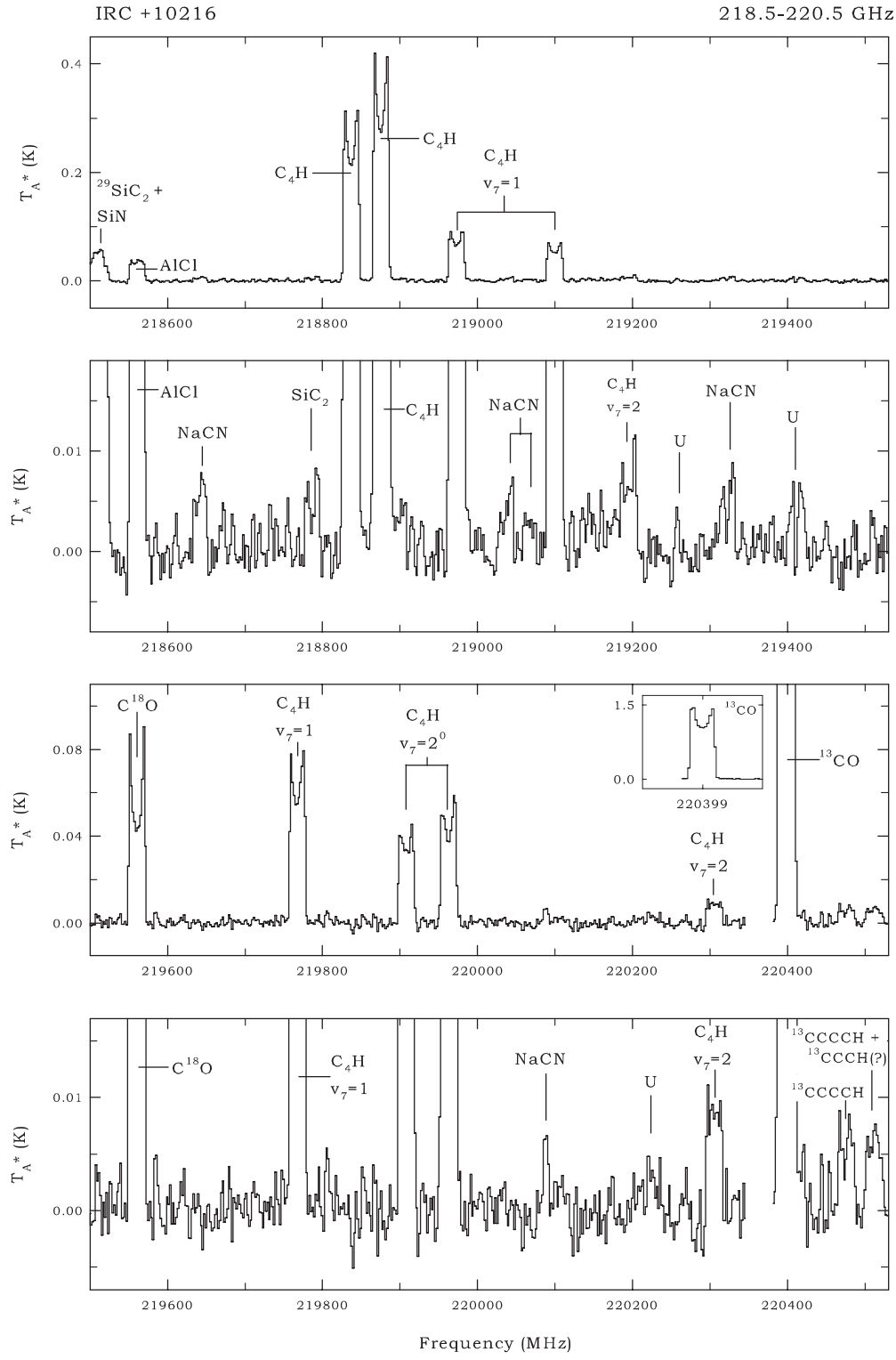

Figure 1. (Continued)

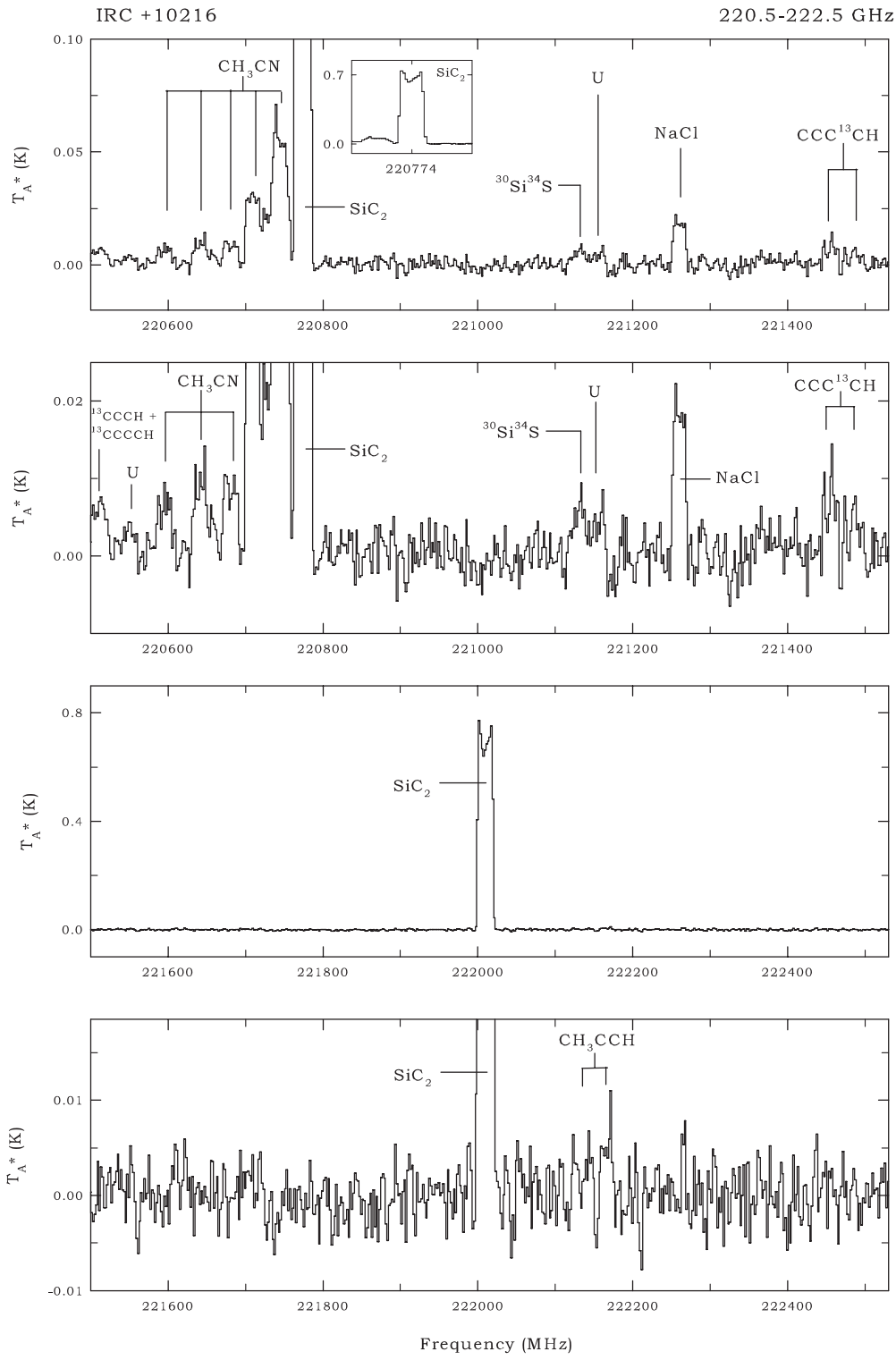

Figure 1. (Continued)

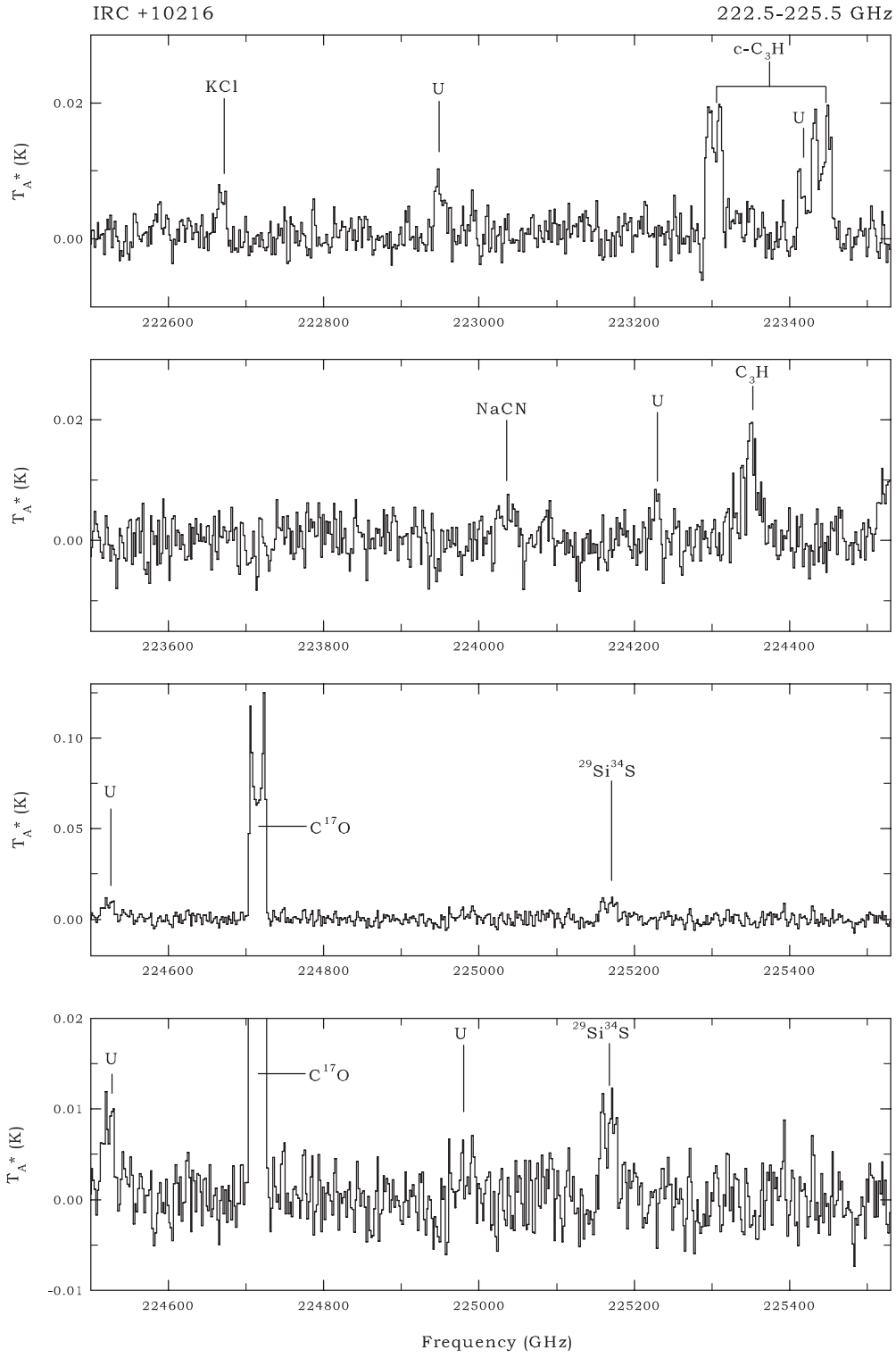

Figure 1. (Continued)

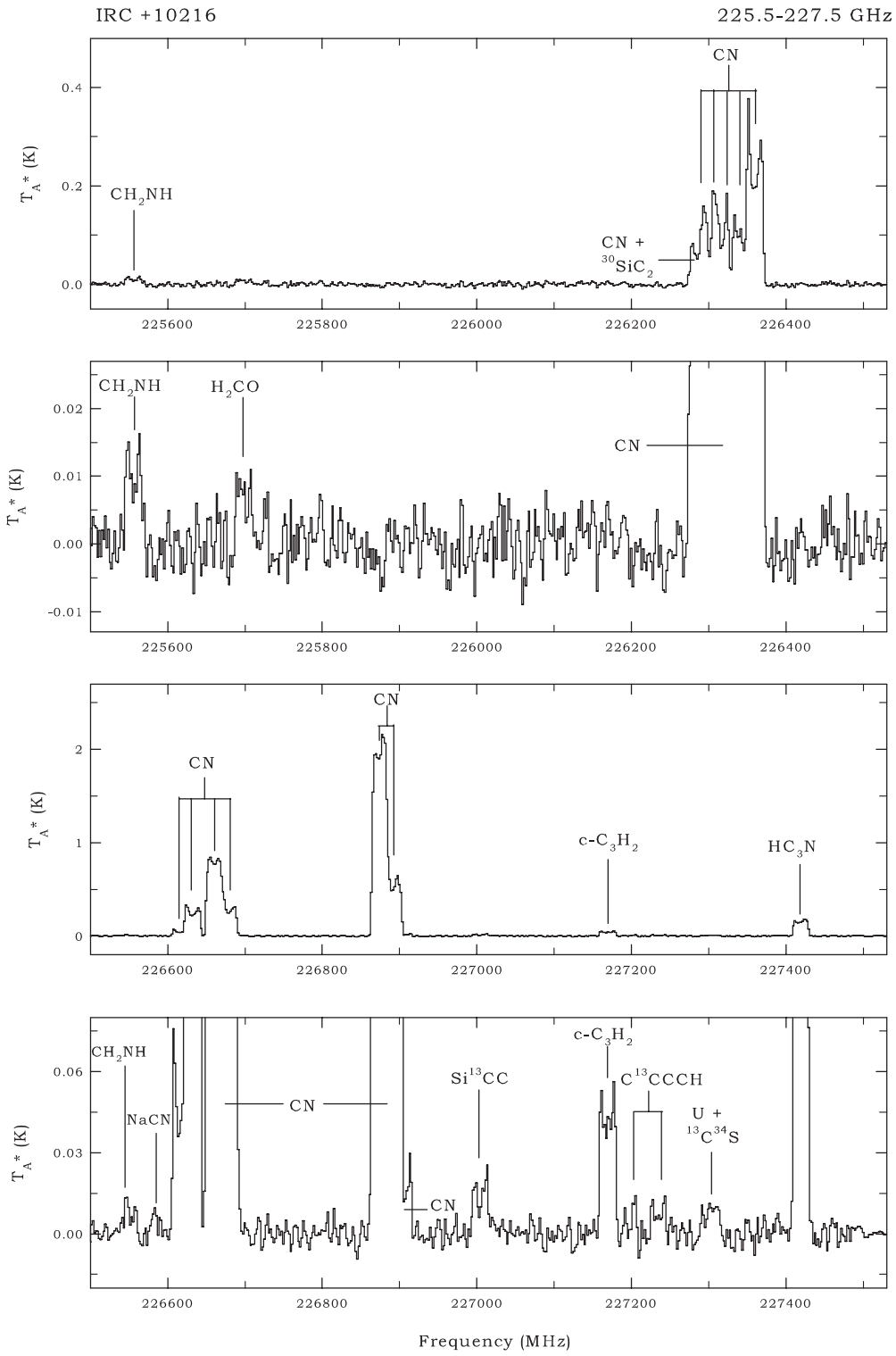

Figure 1. (Continued)

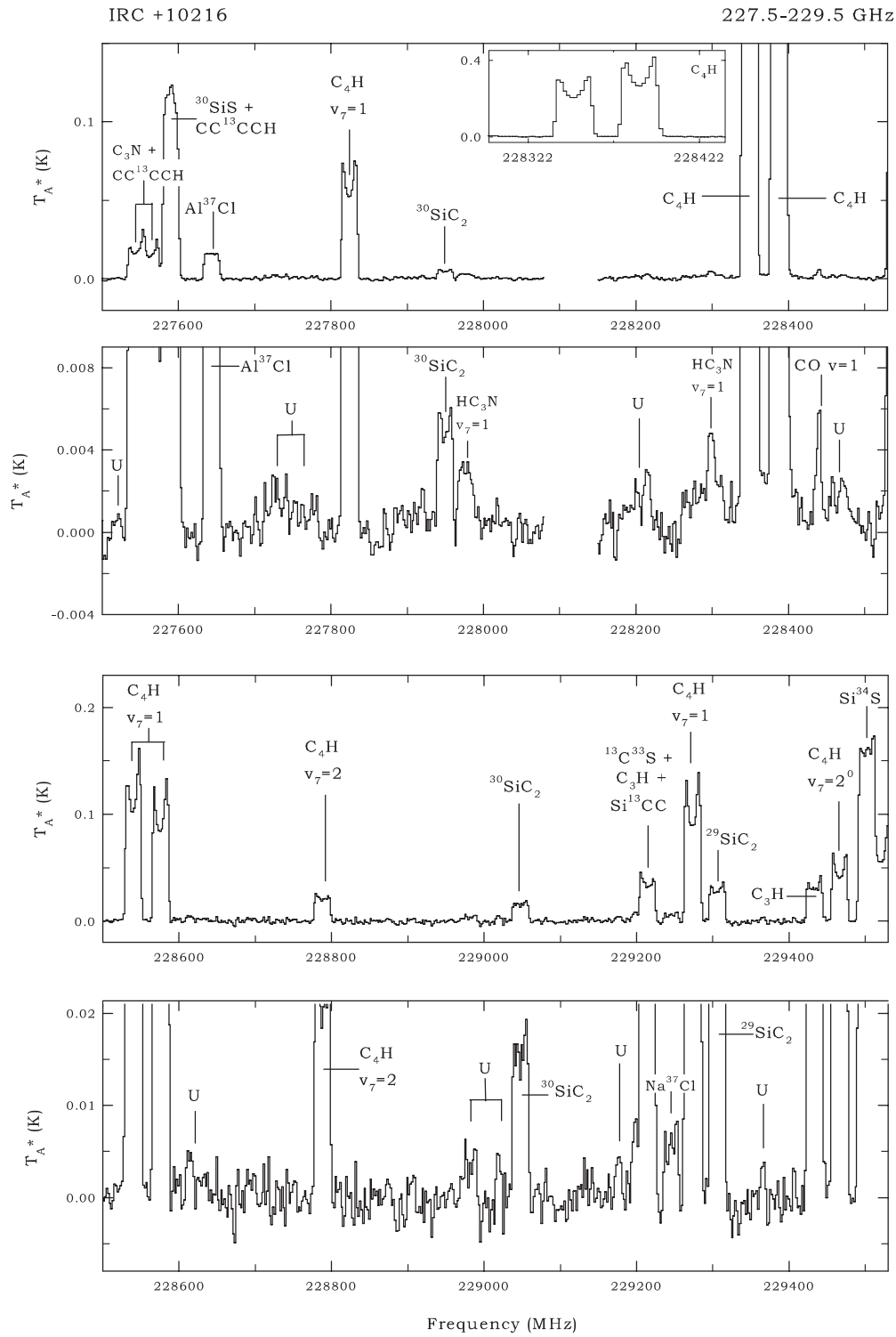

Figure 1. (Continued)

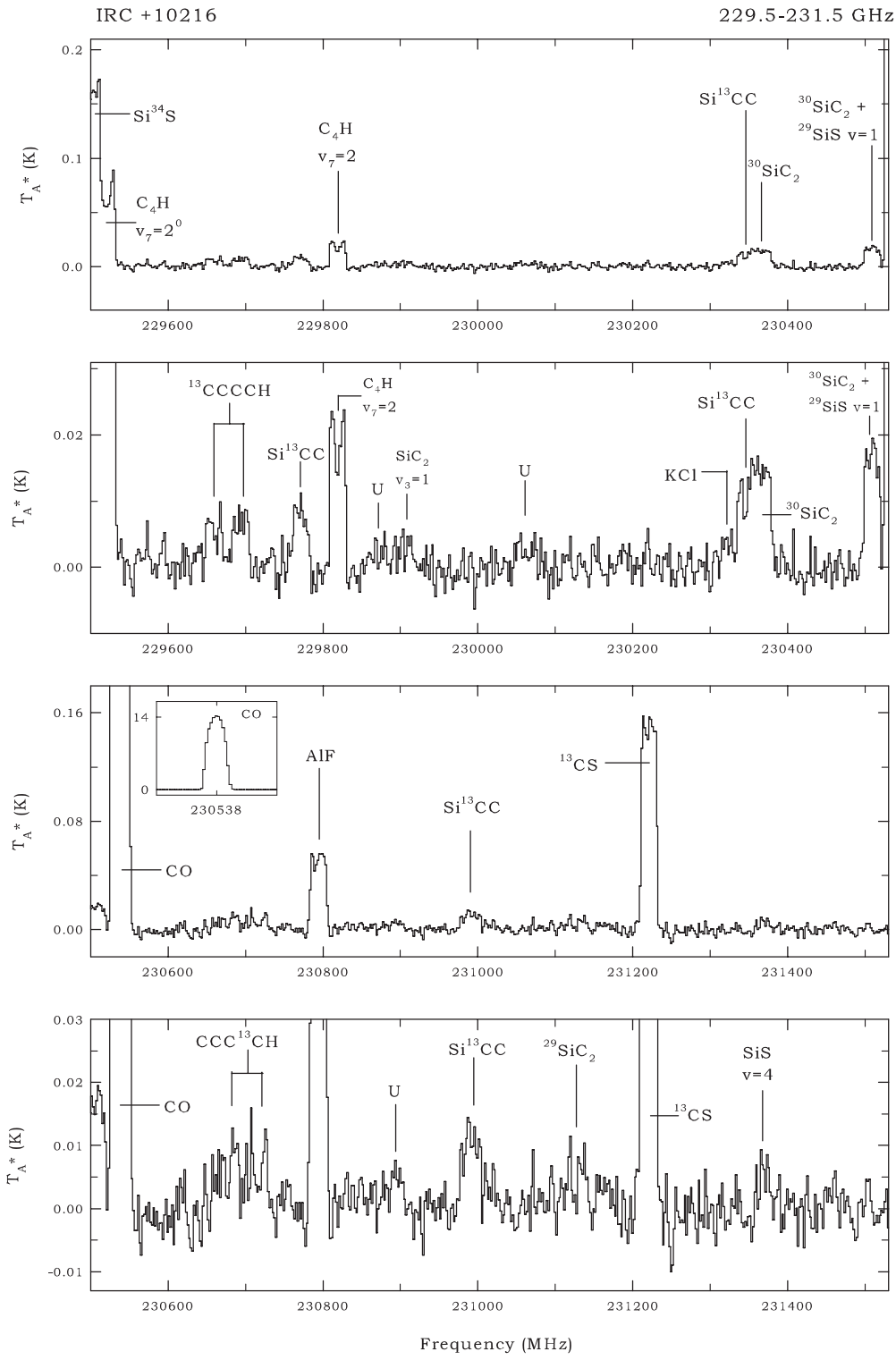

Figure 1. (Continued)

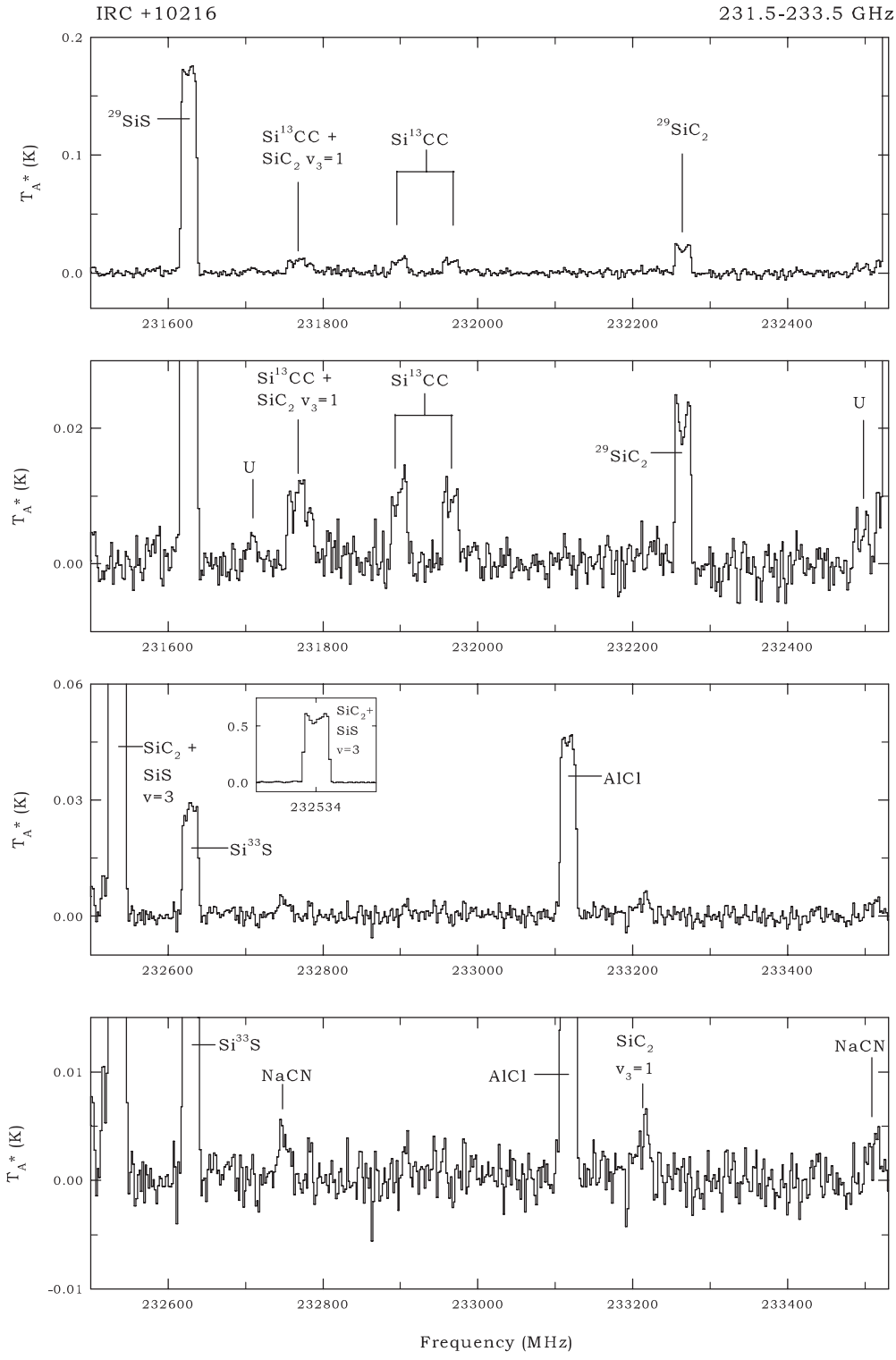

Figure 1. (Continued)

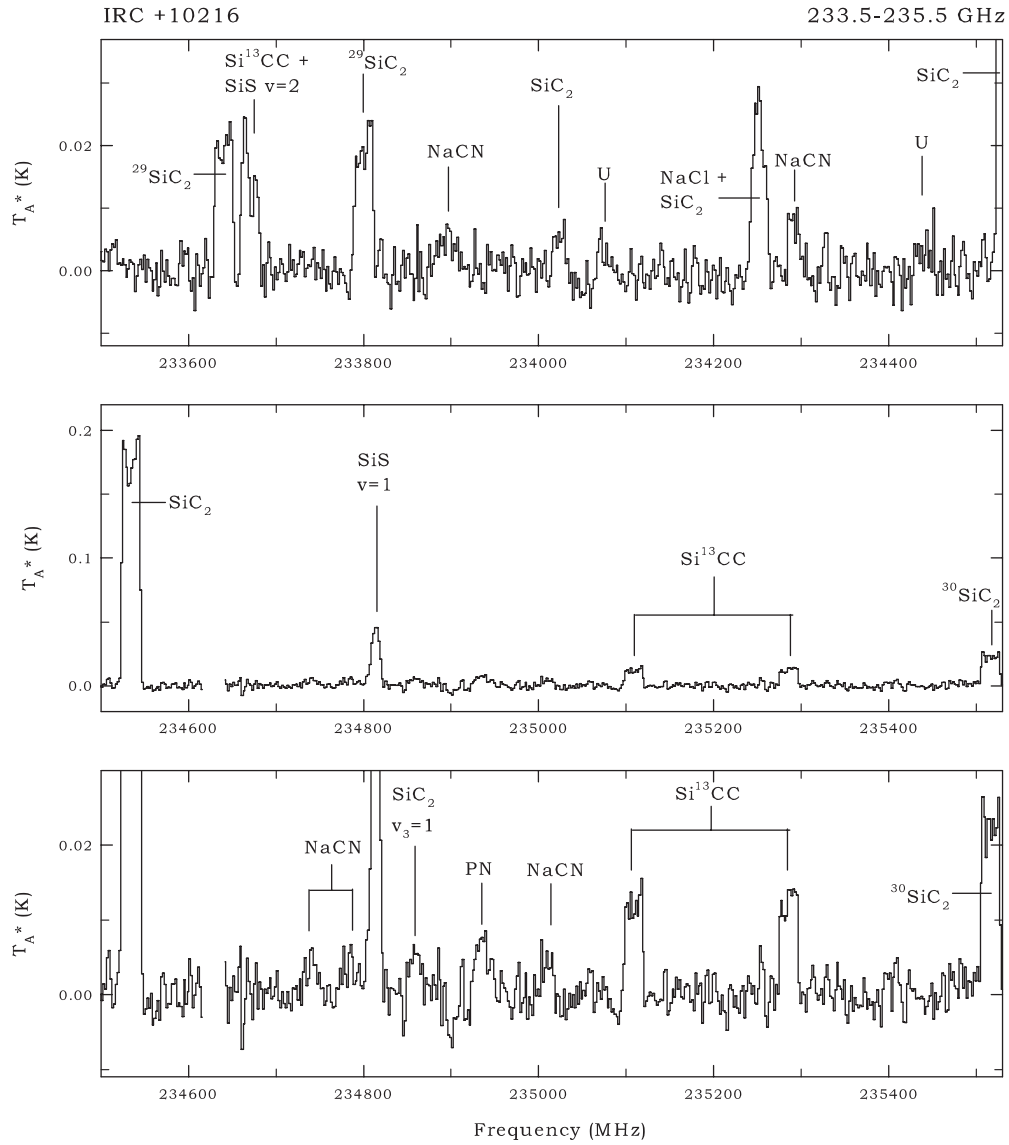

Figure 1. (Continued)

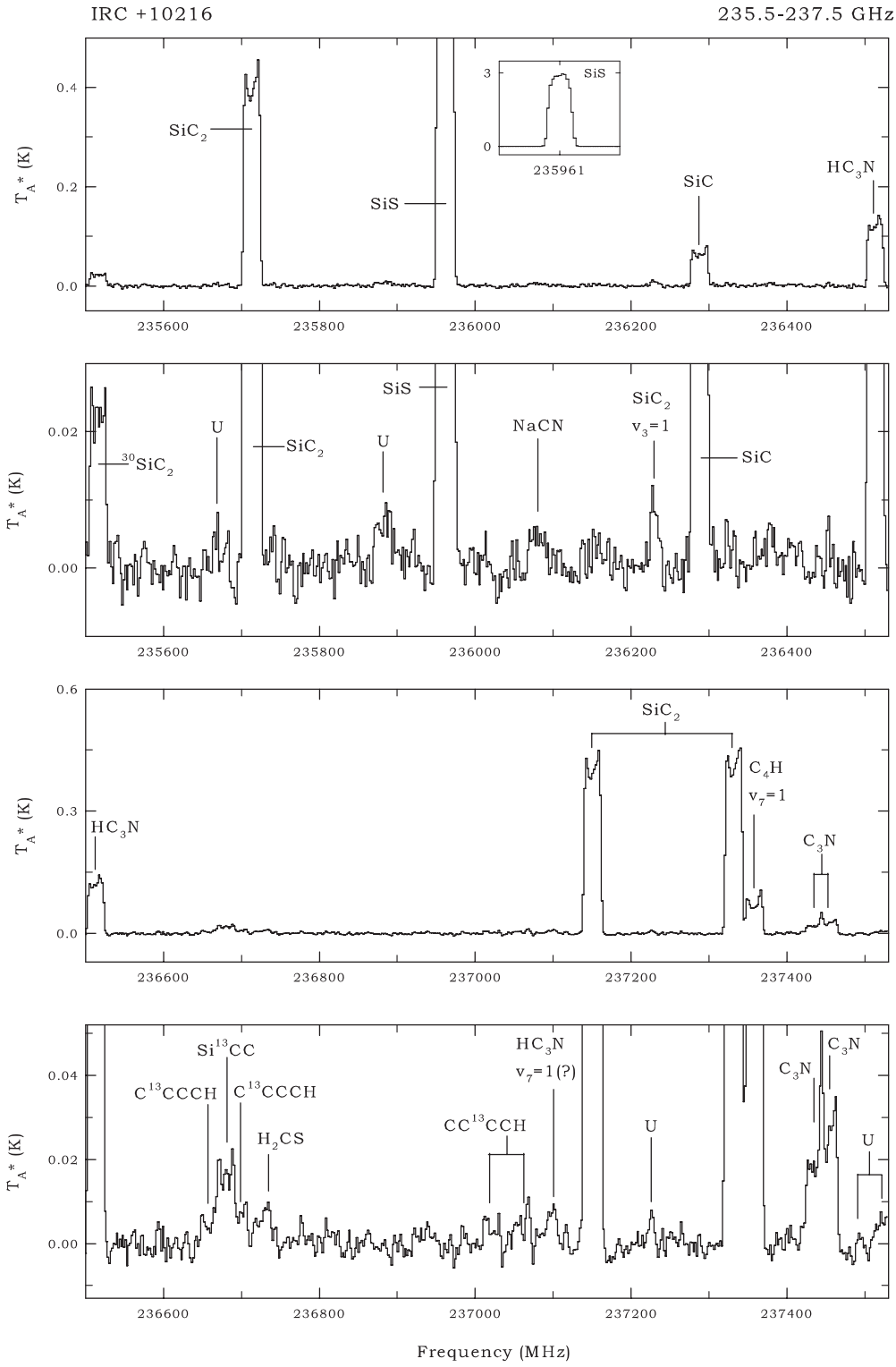

Figure 1. (Continued)

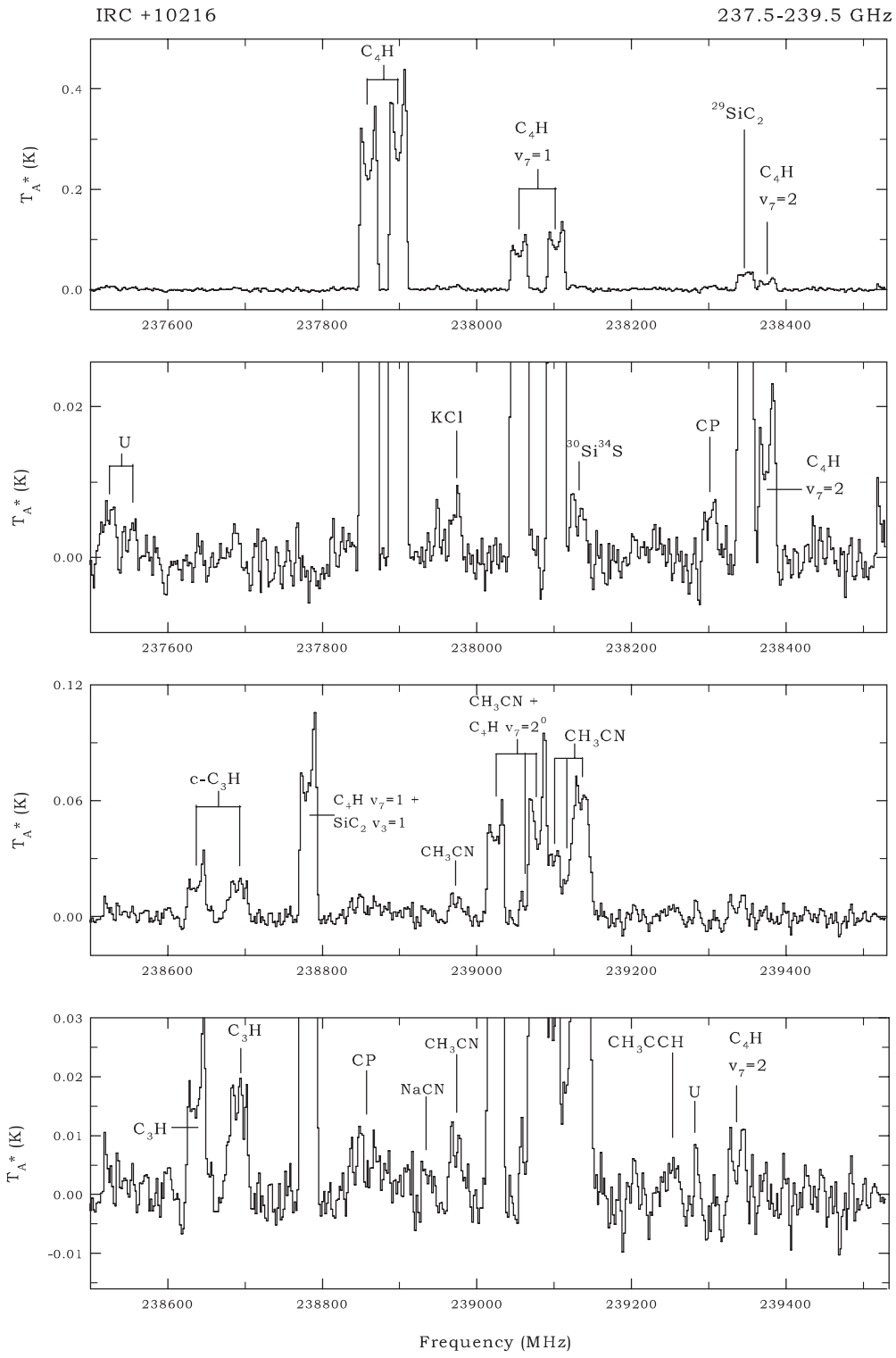

Figure 1. (Continued)

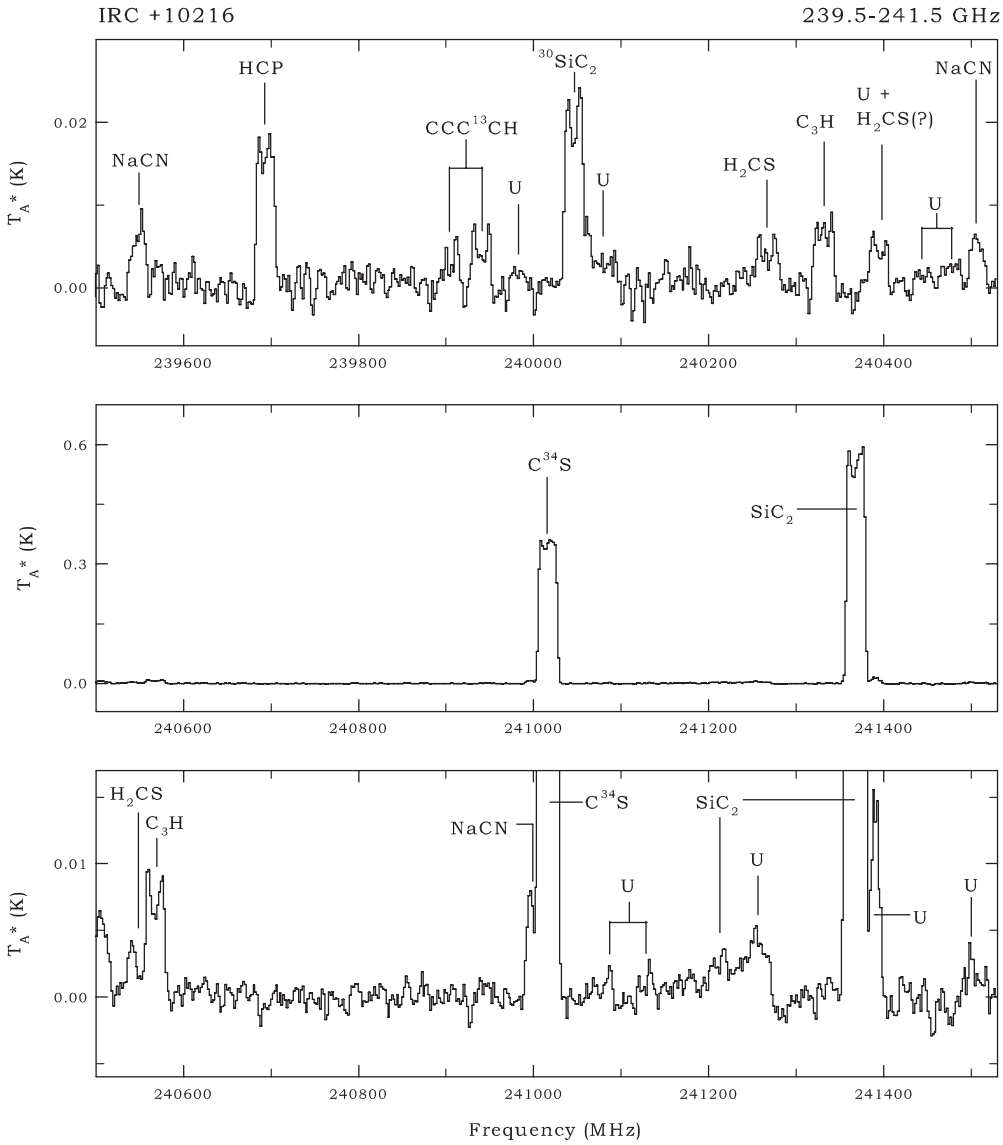

Figure 1. (Continued)

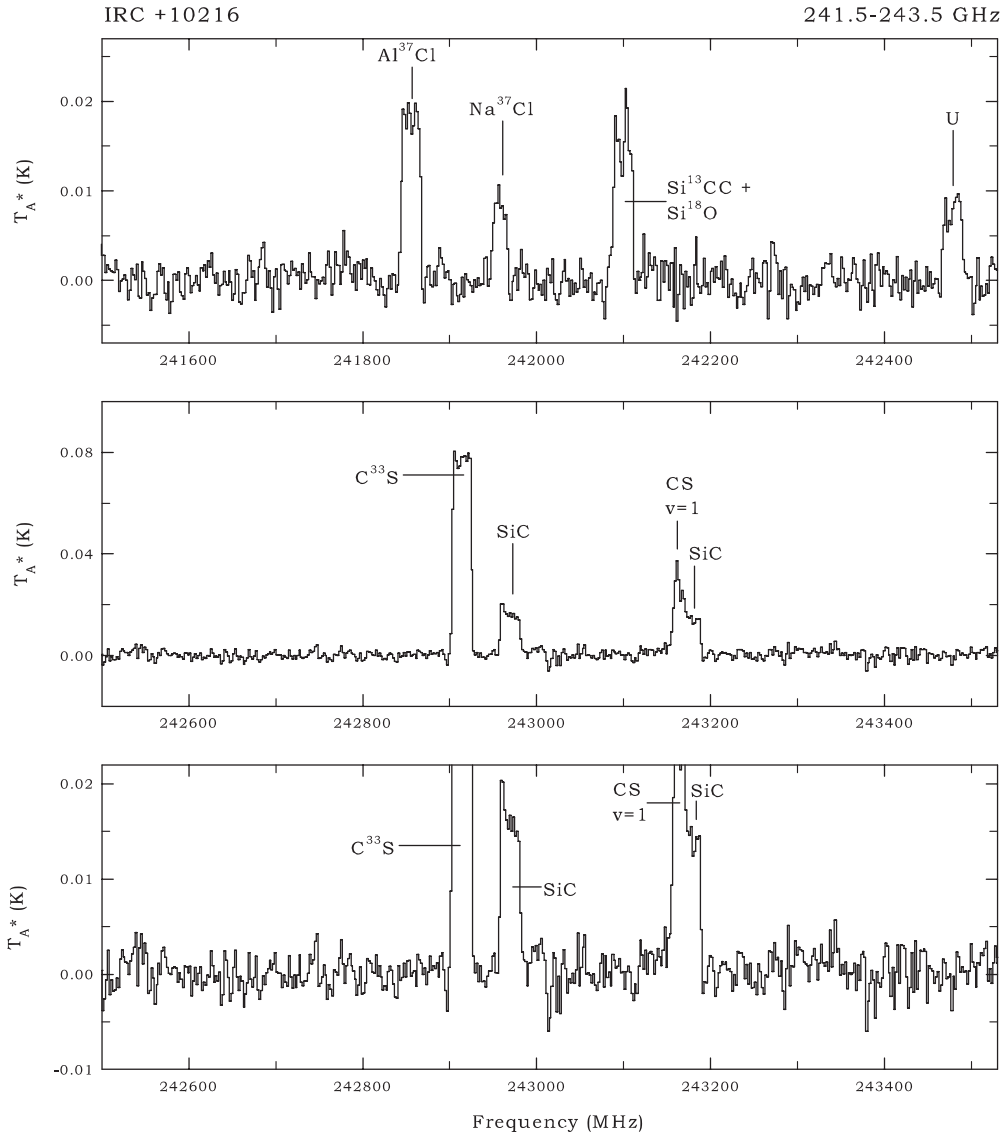

Figure 1. (Continued)

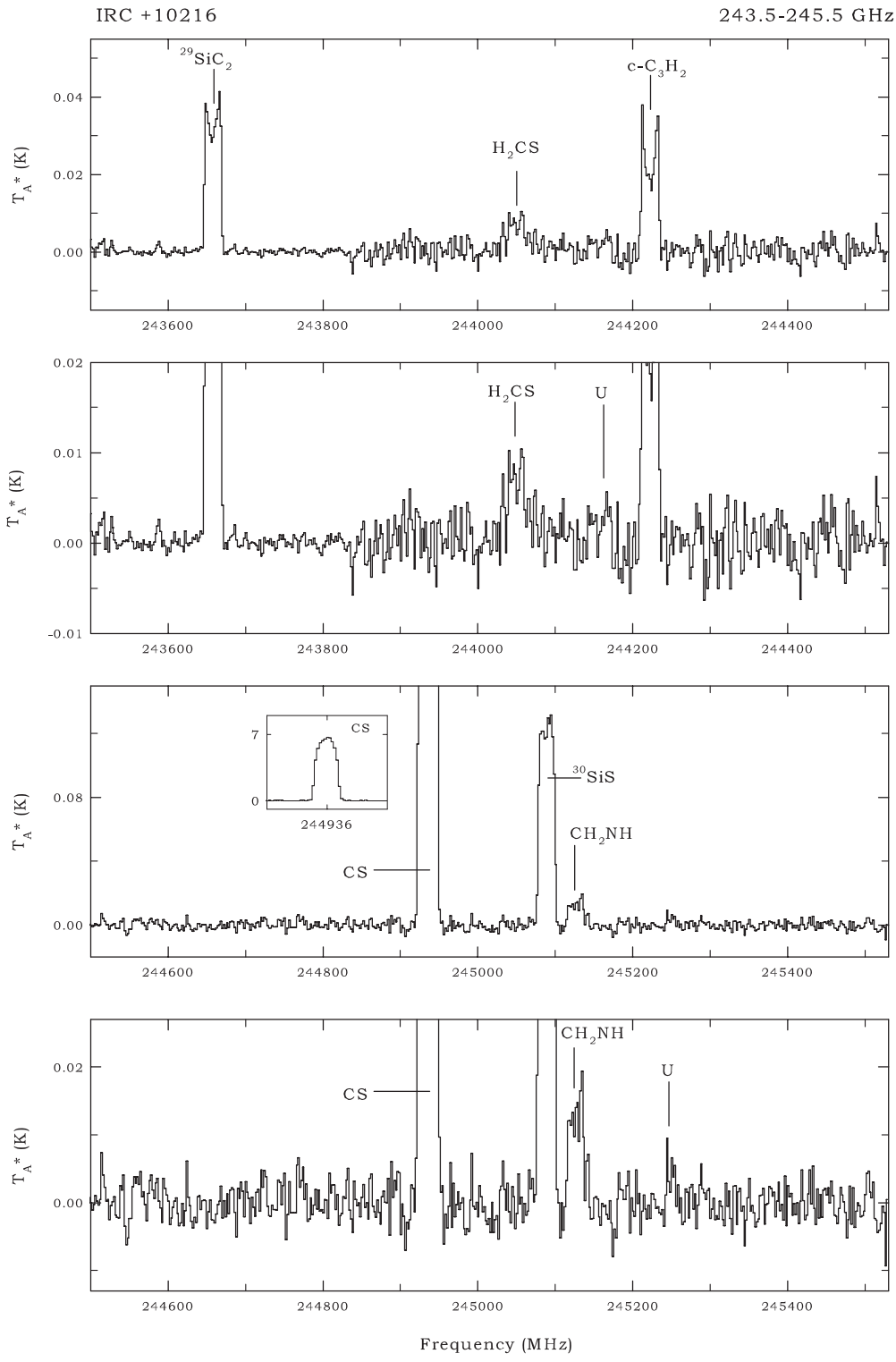

Figure 1. (Continued)

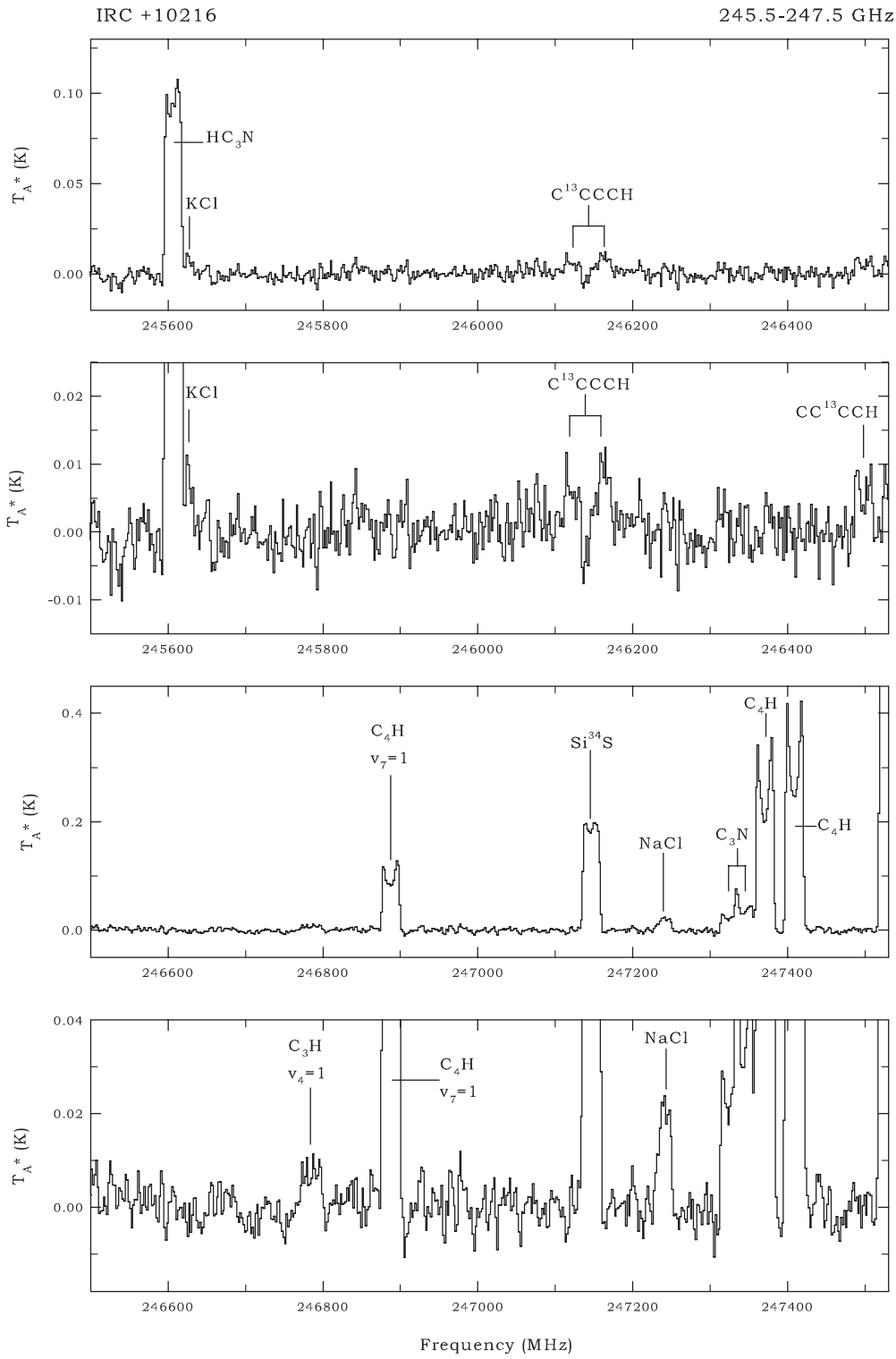

Figure 1. (Continued)

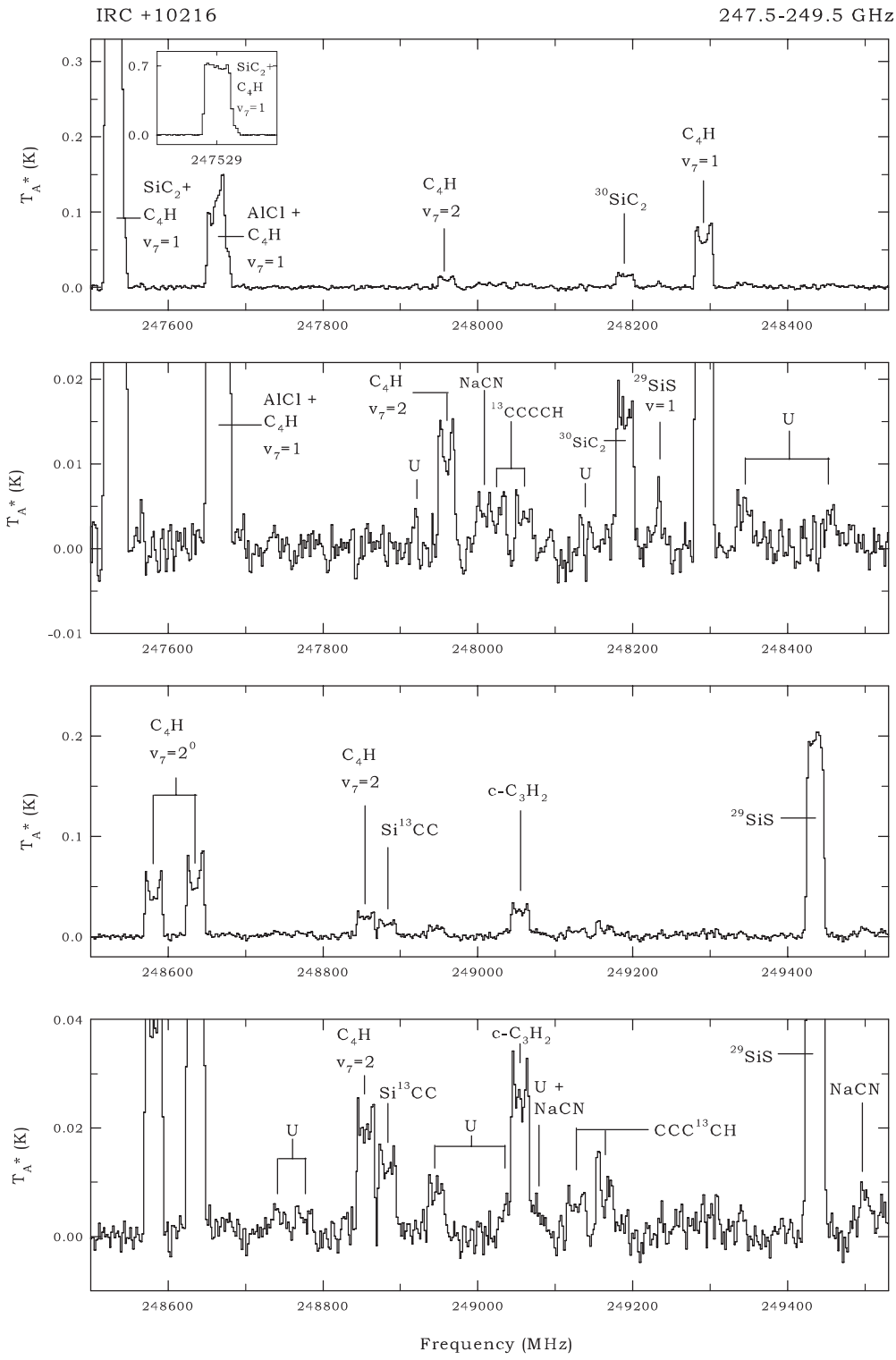

Figure 1. (Continued)

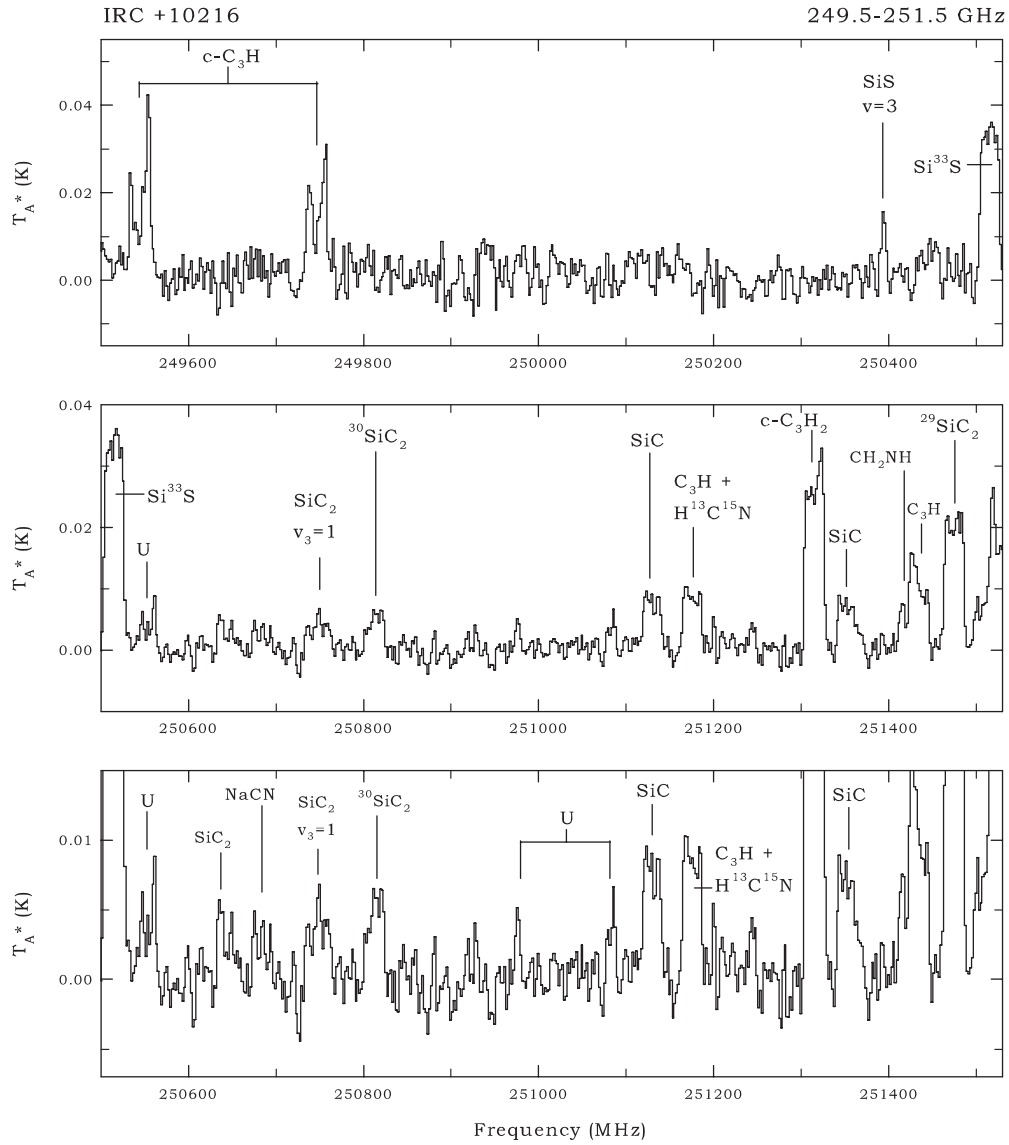

Figure 1. (Continued)

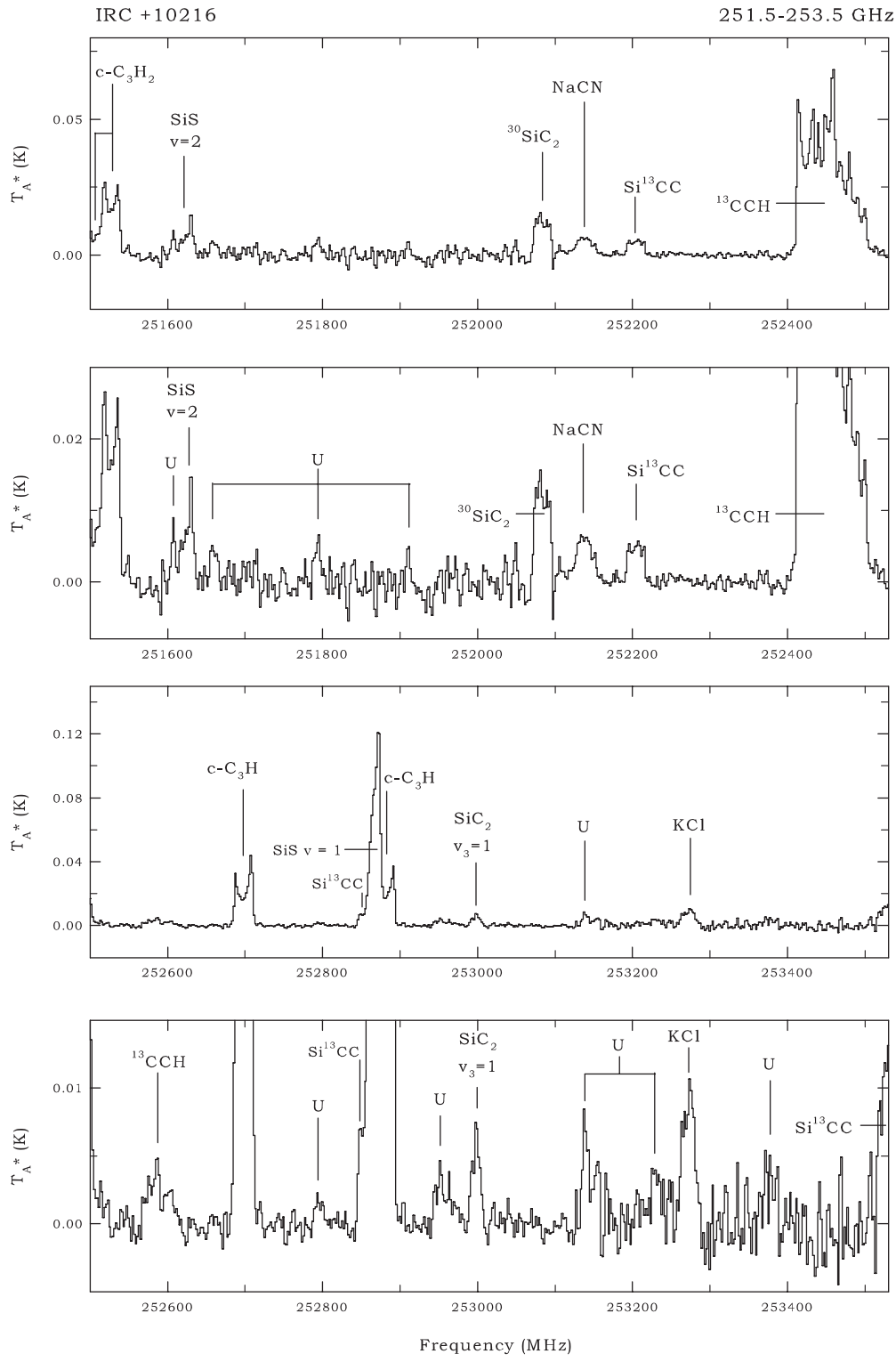

Figure 1. (Continued)

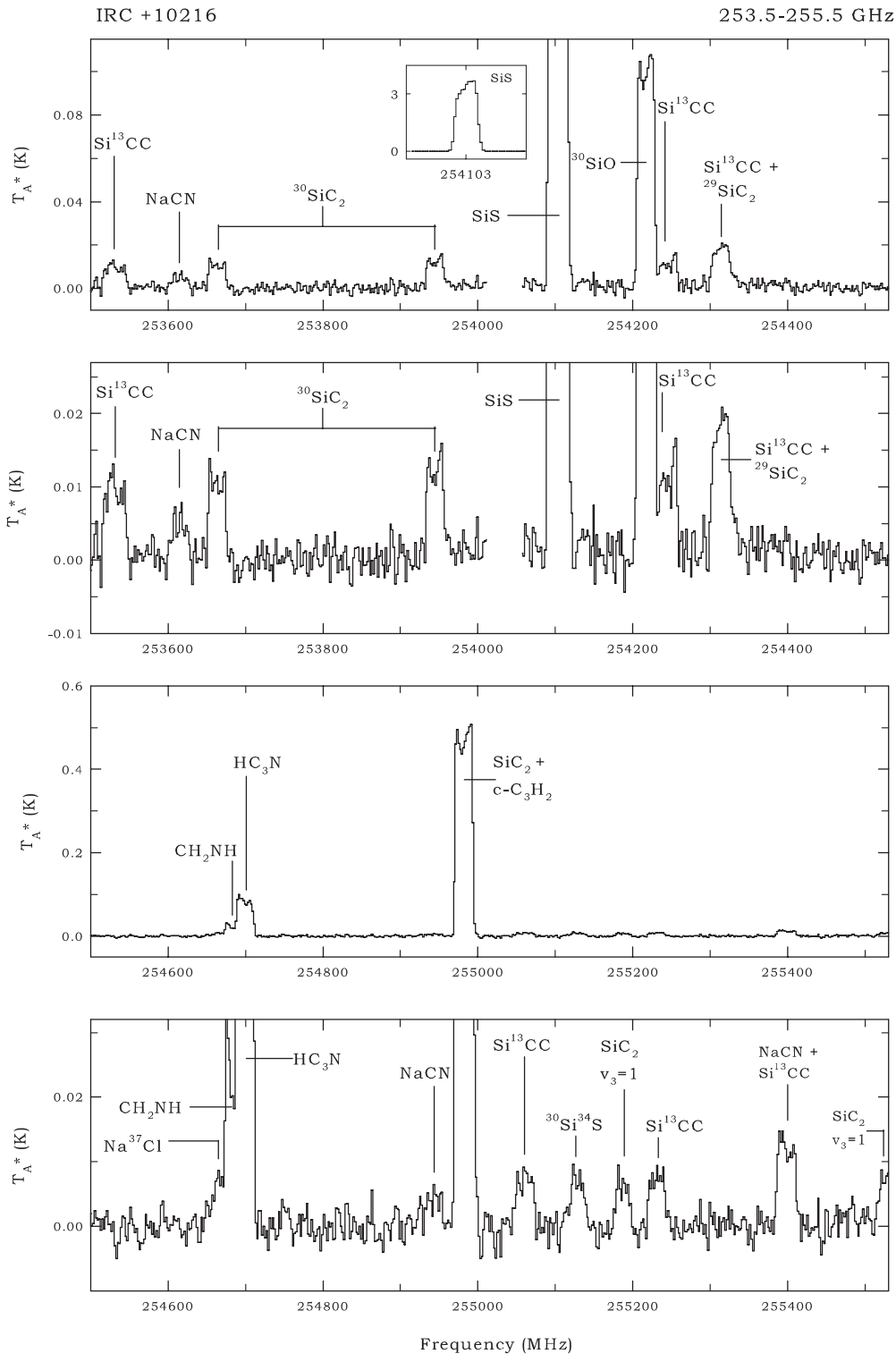

Figure 1. (Continued)

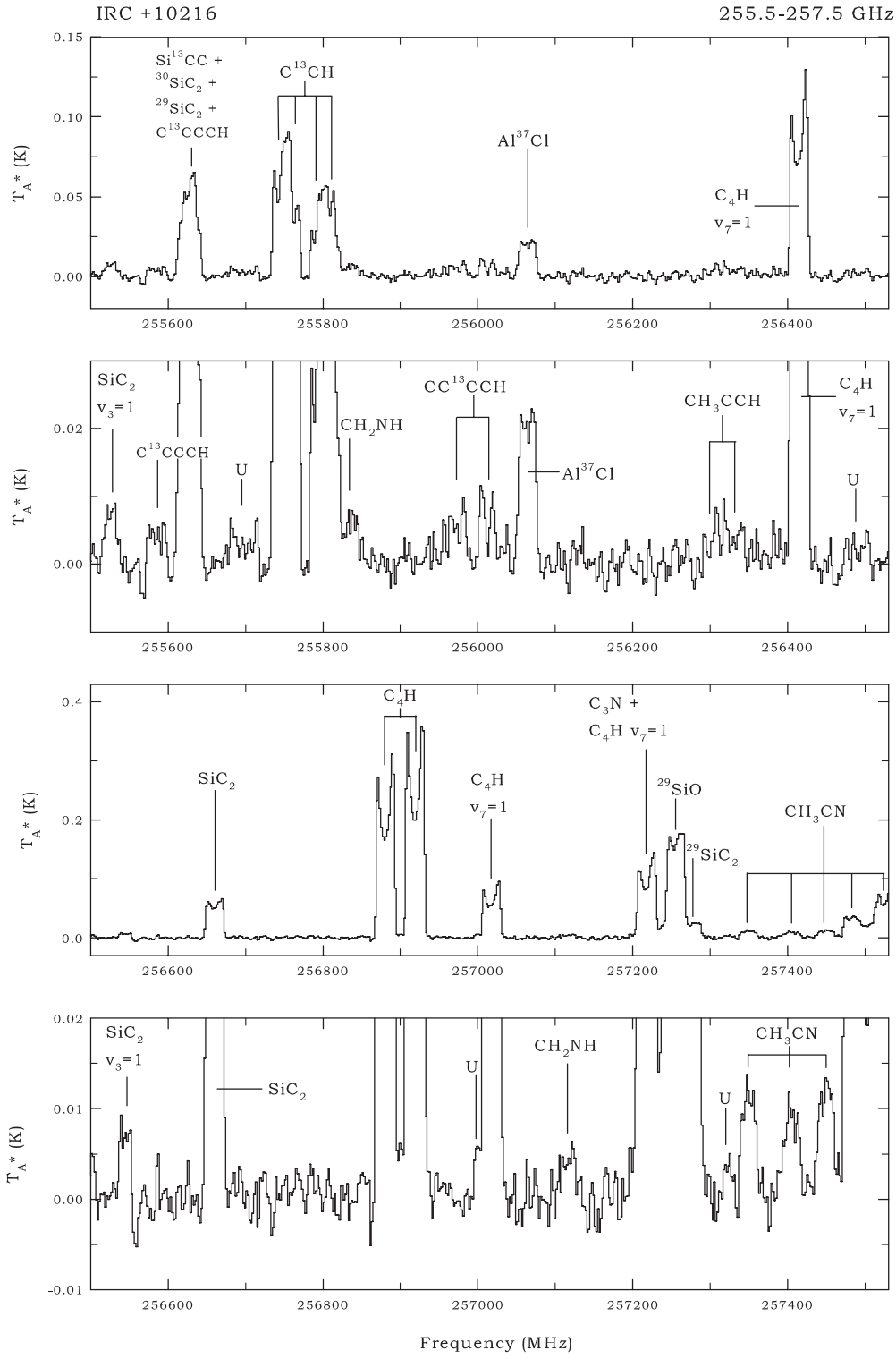

Figure 1. (Continued)

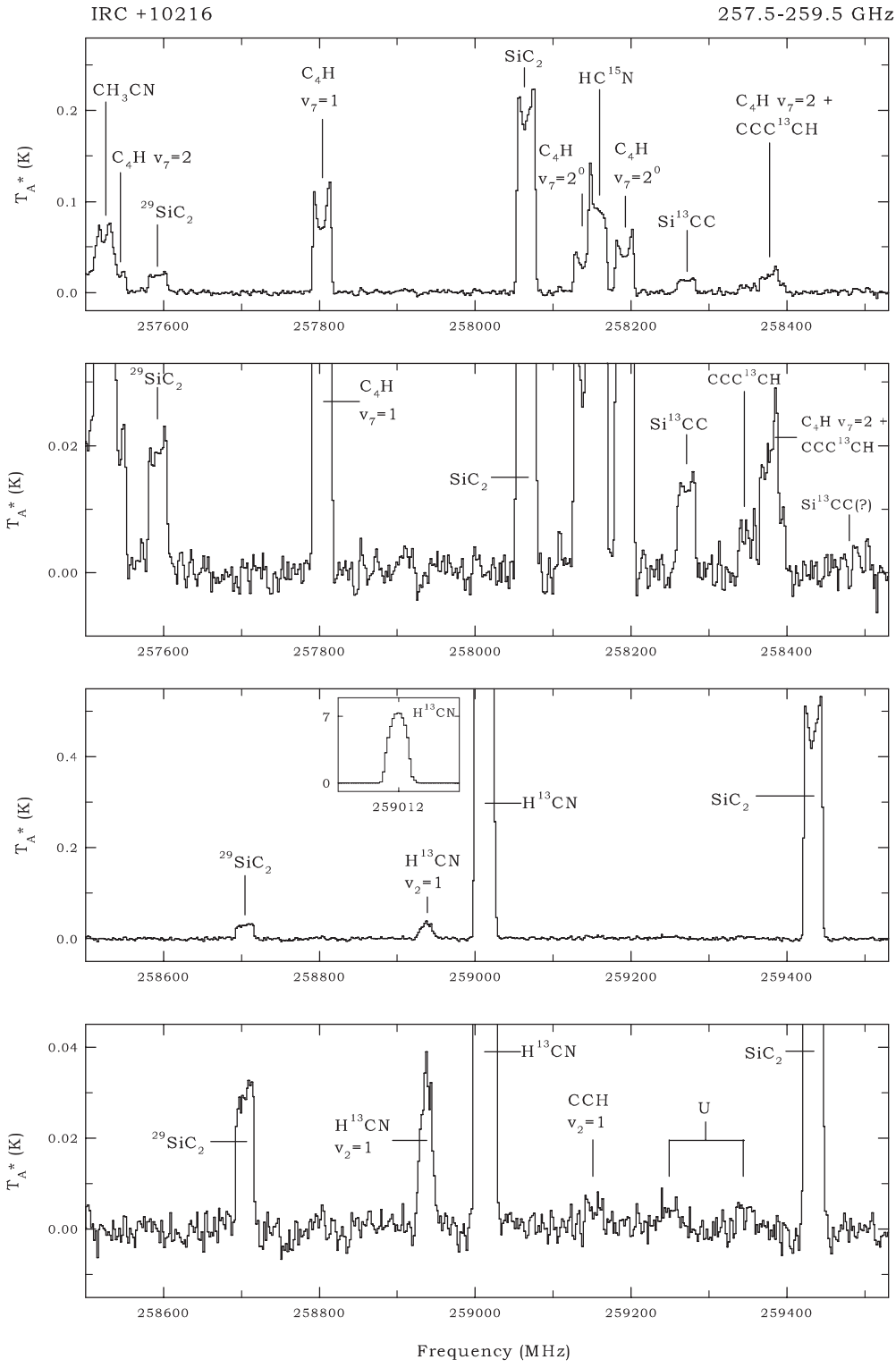

Figure 1. (Continued)

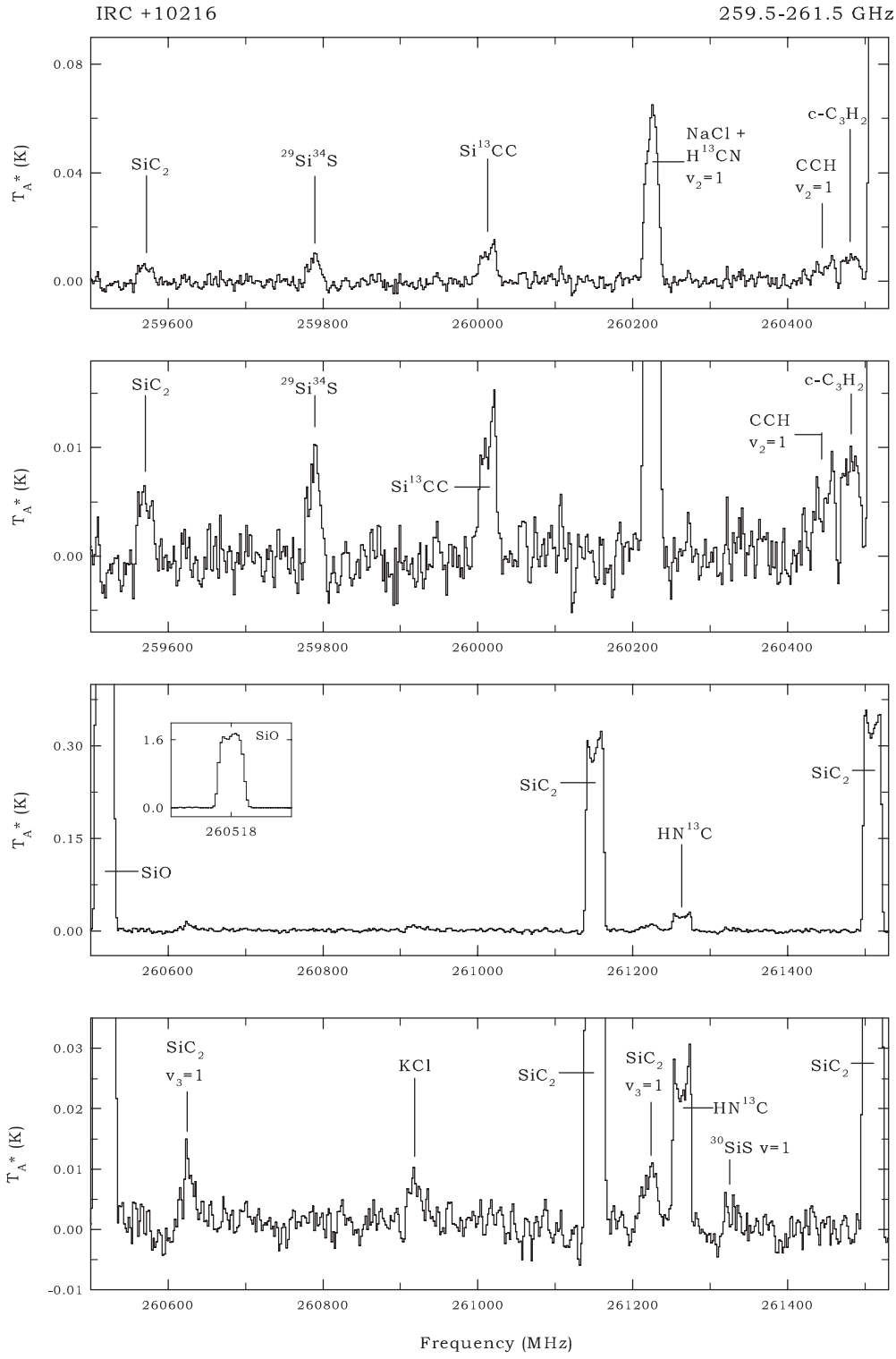

Figure 1. (Continued)

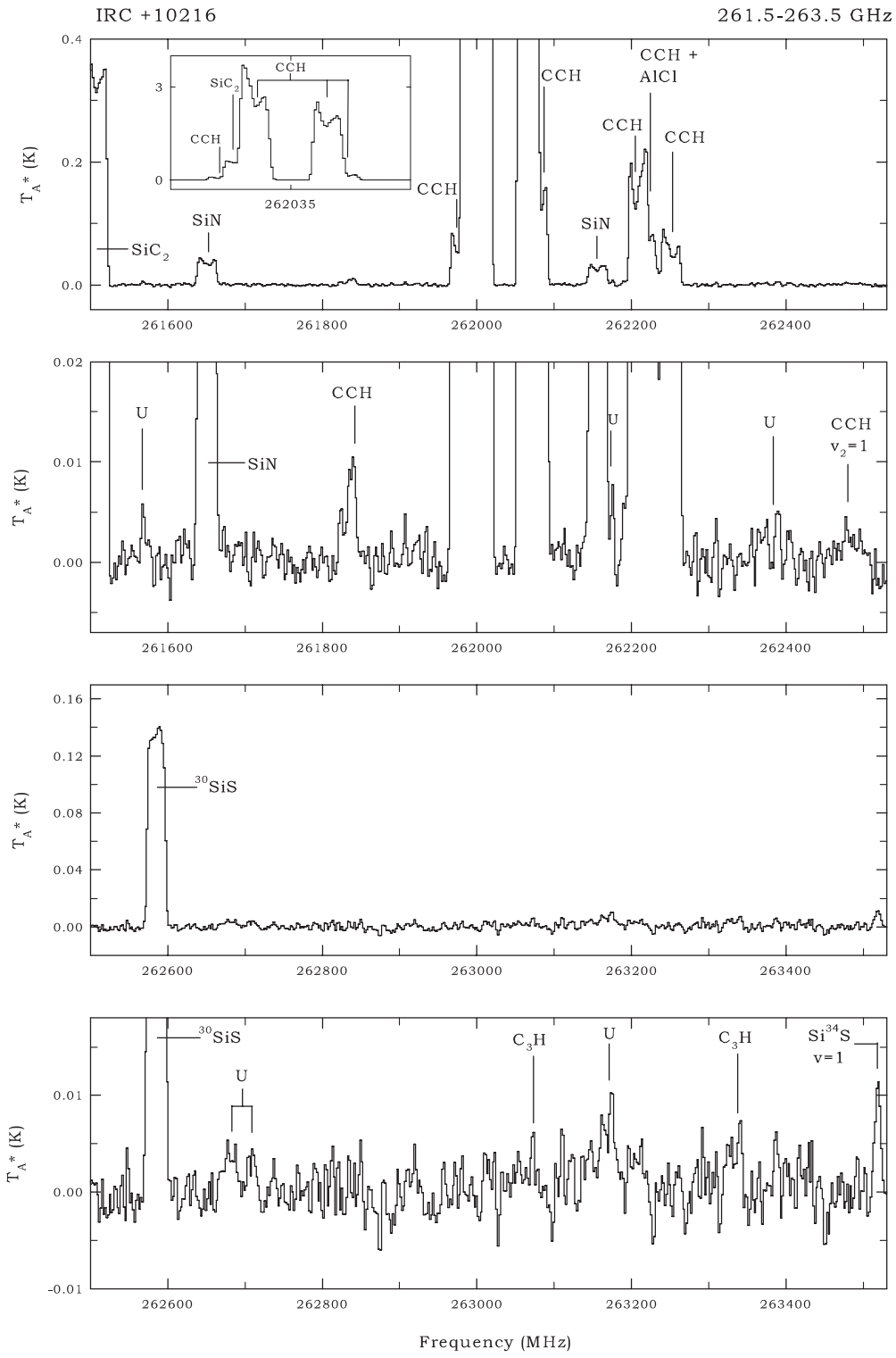

Figure 1. (Continued)

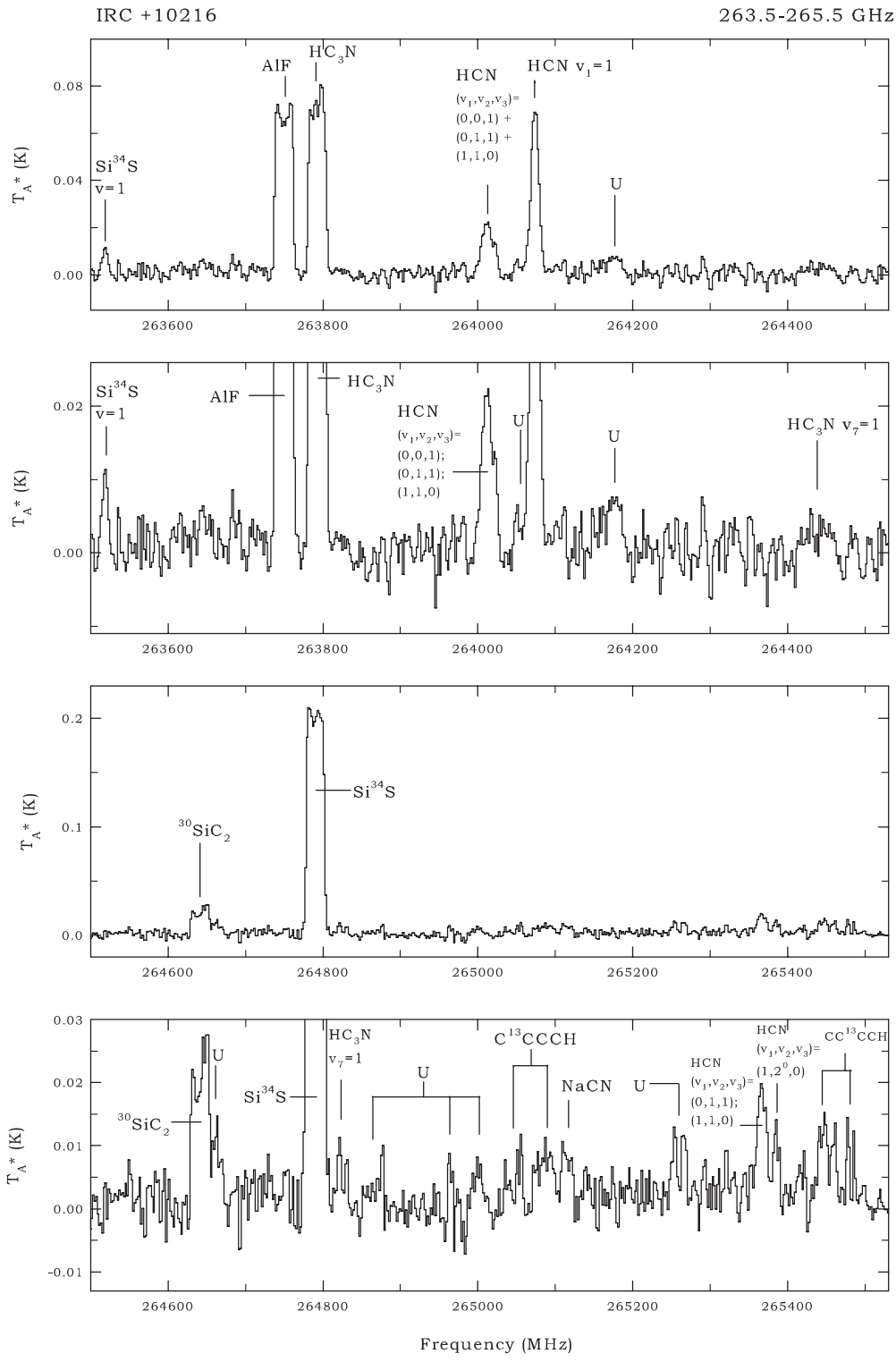

Figure 1. (Continued)

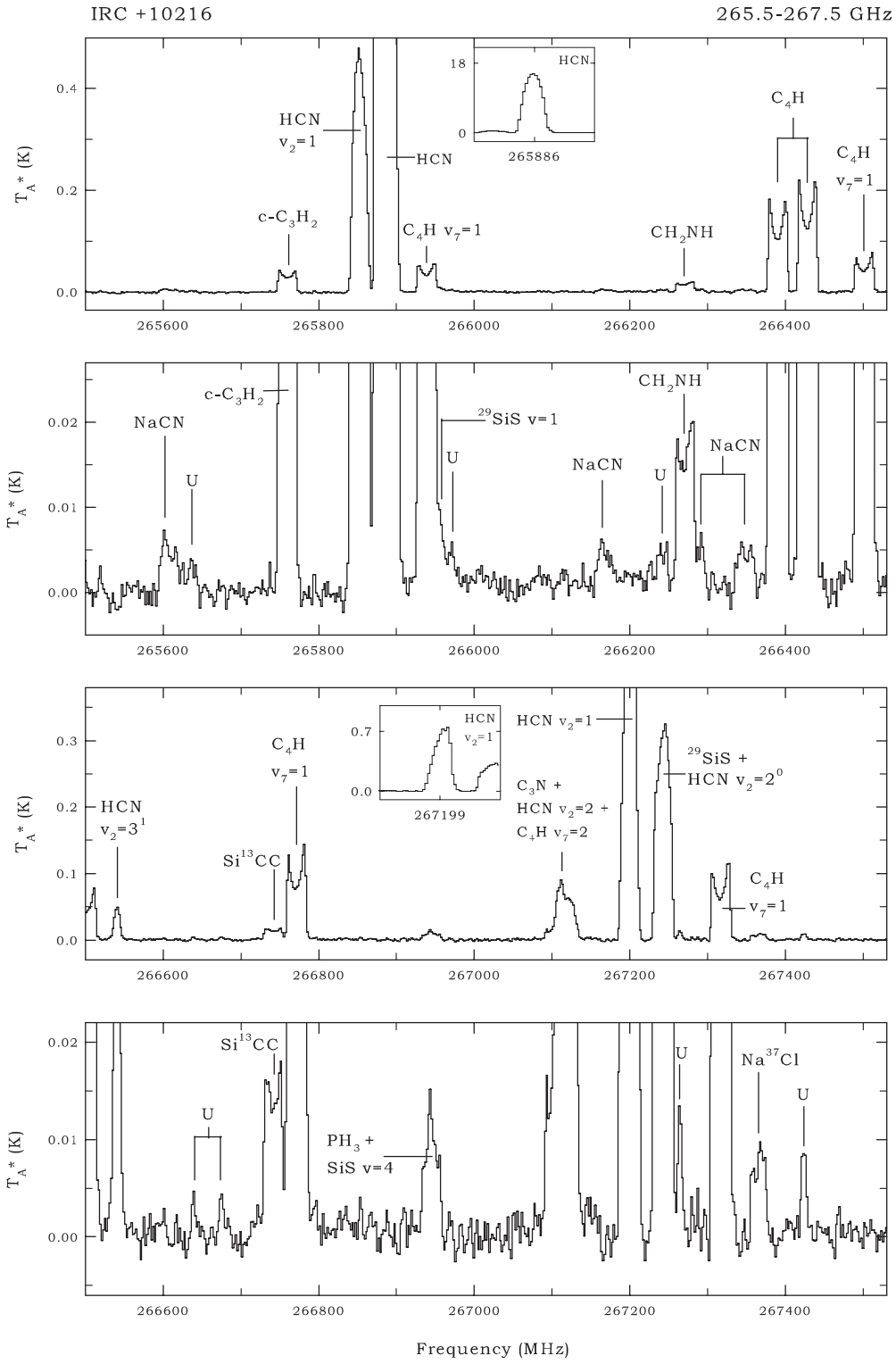

Figure 1. (Continued)

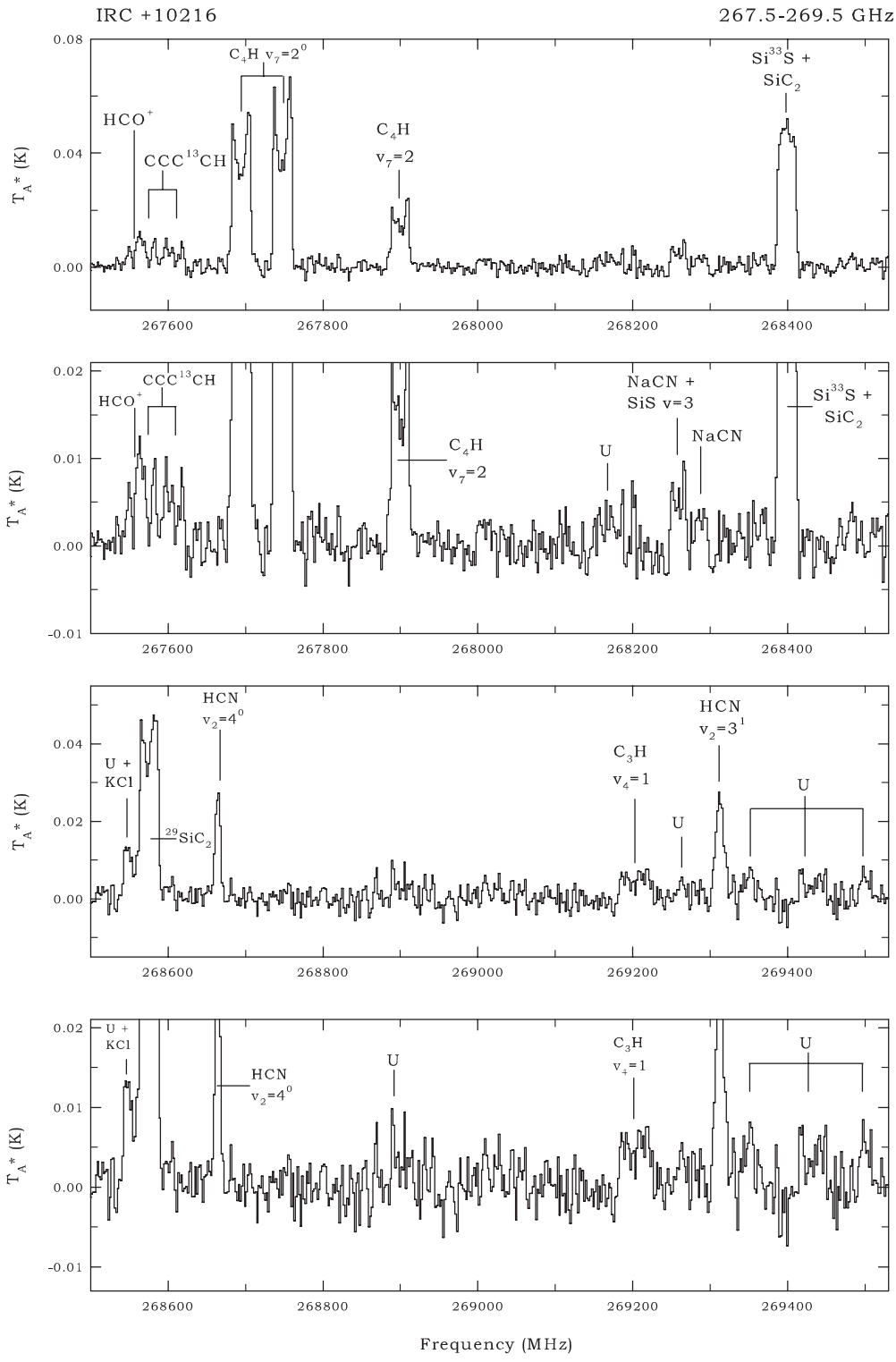

Figure 1. (Continued)

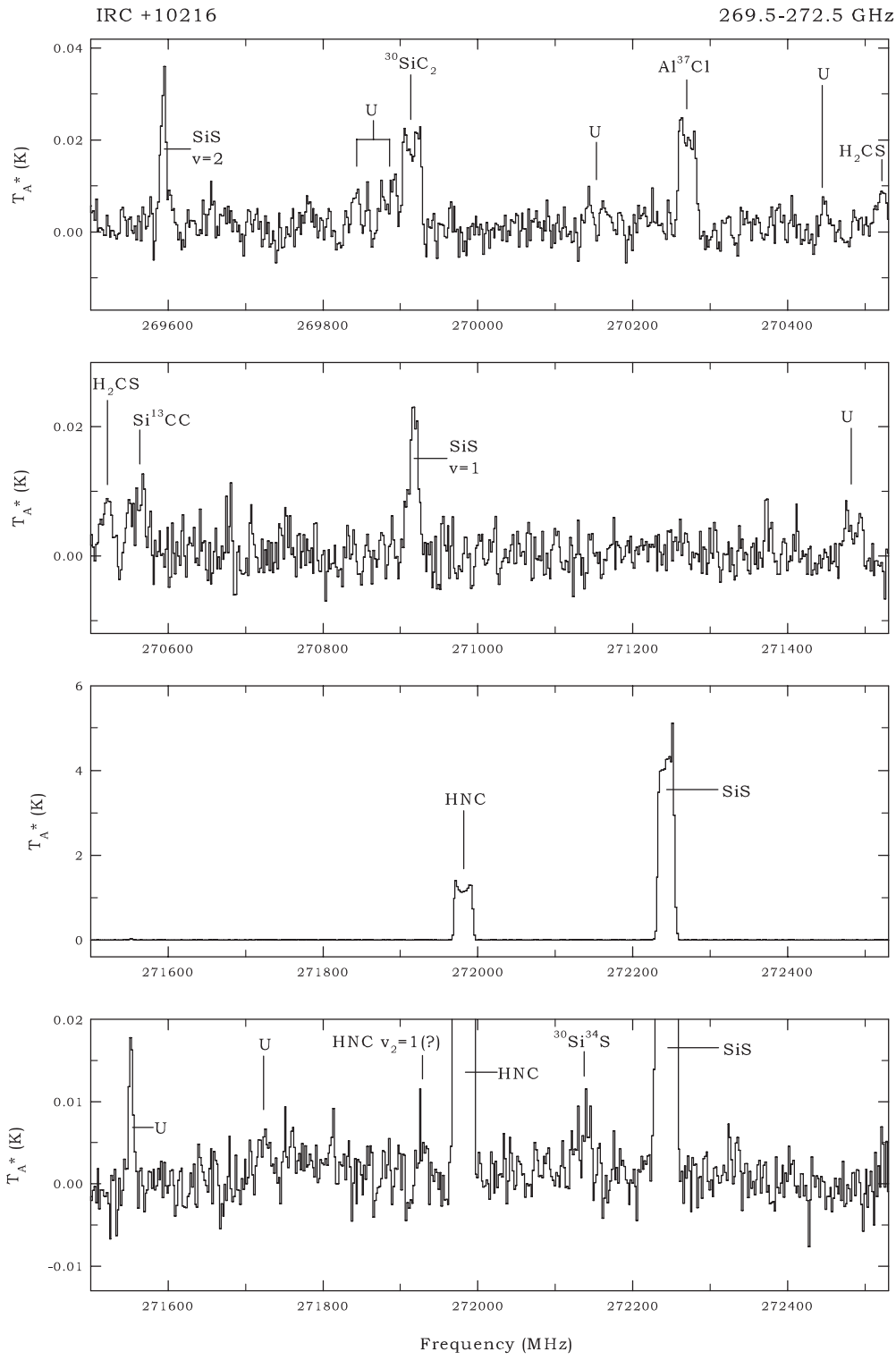

Figure 1. (Continued)

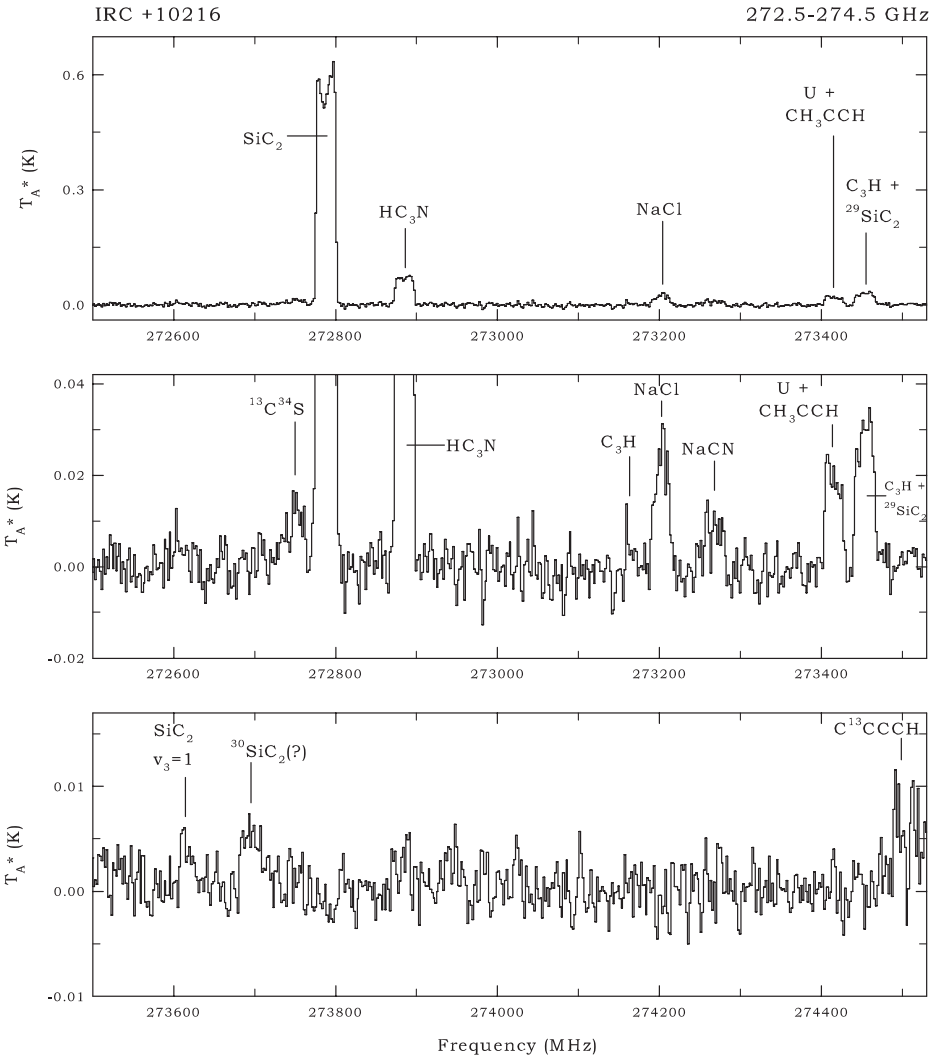

Figure 1. (Continued)

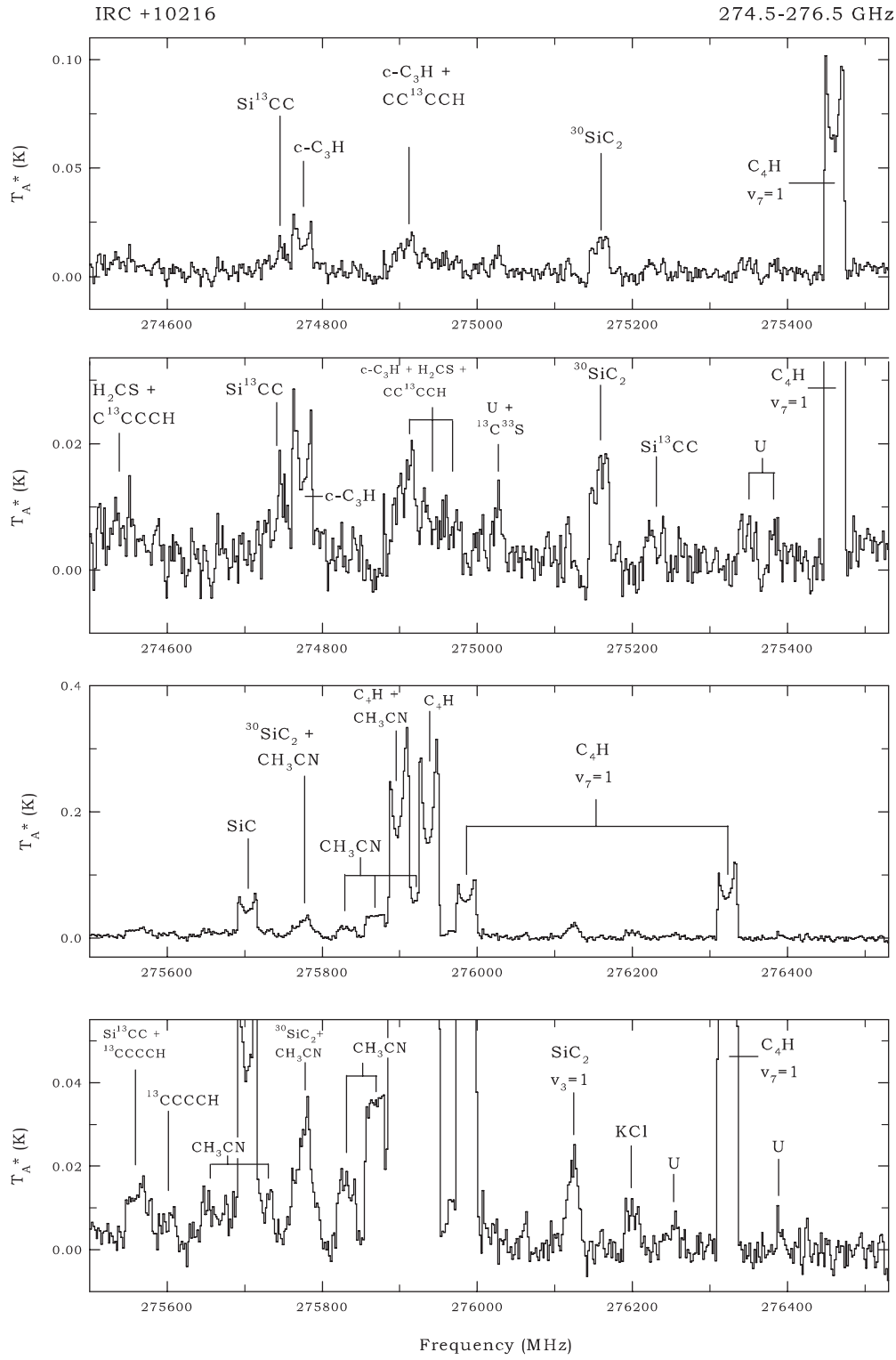

Figure 1. (Continued)

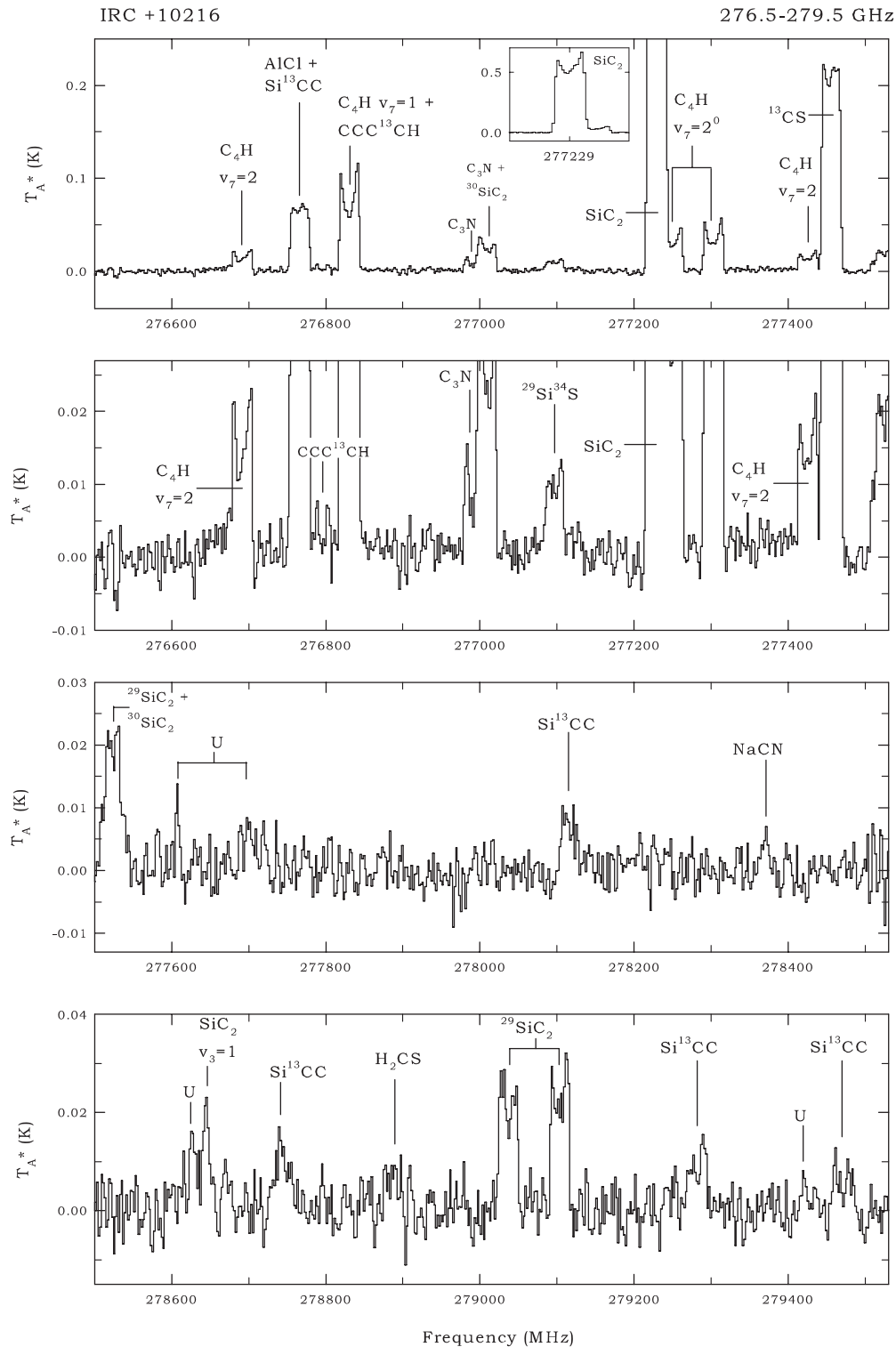

Figure 1. (Continued)

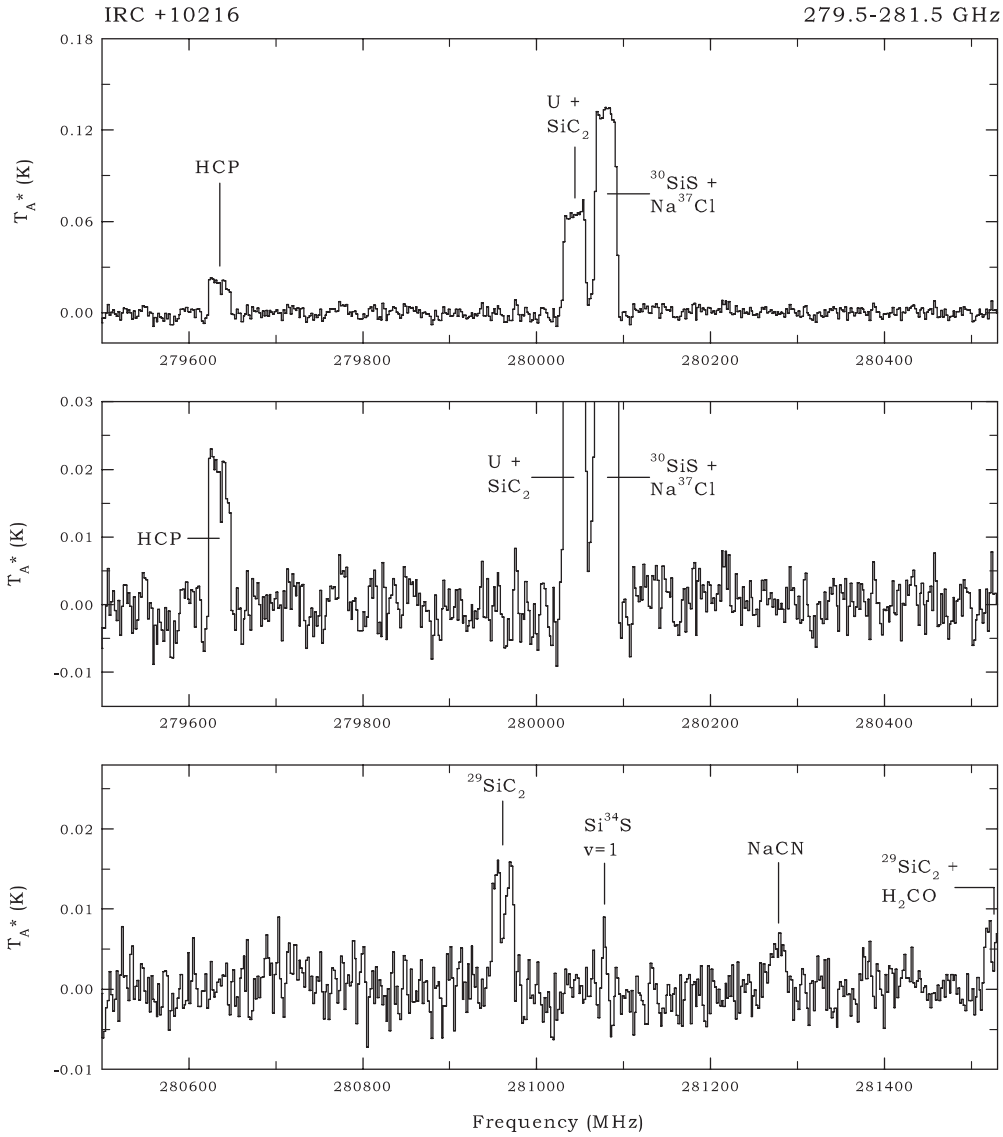

Figure 1. (Continued)

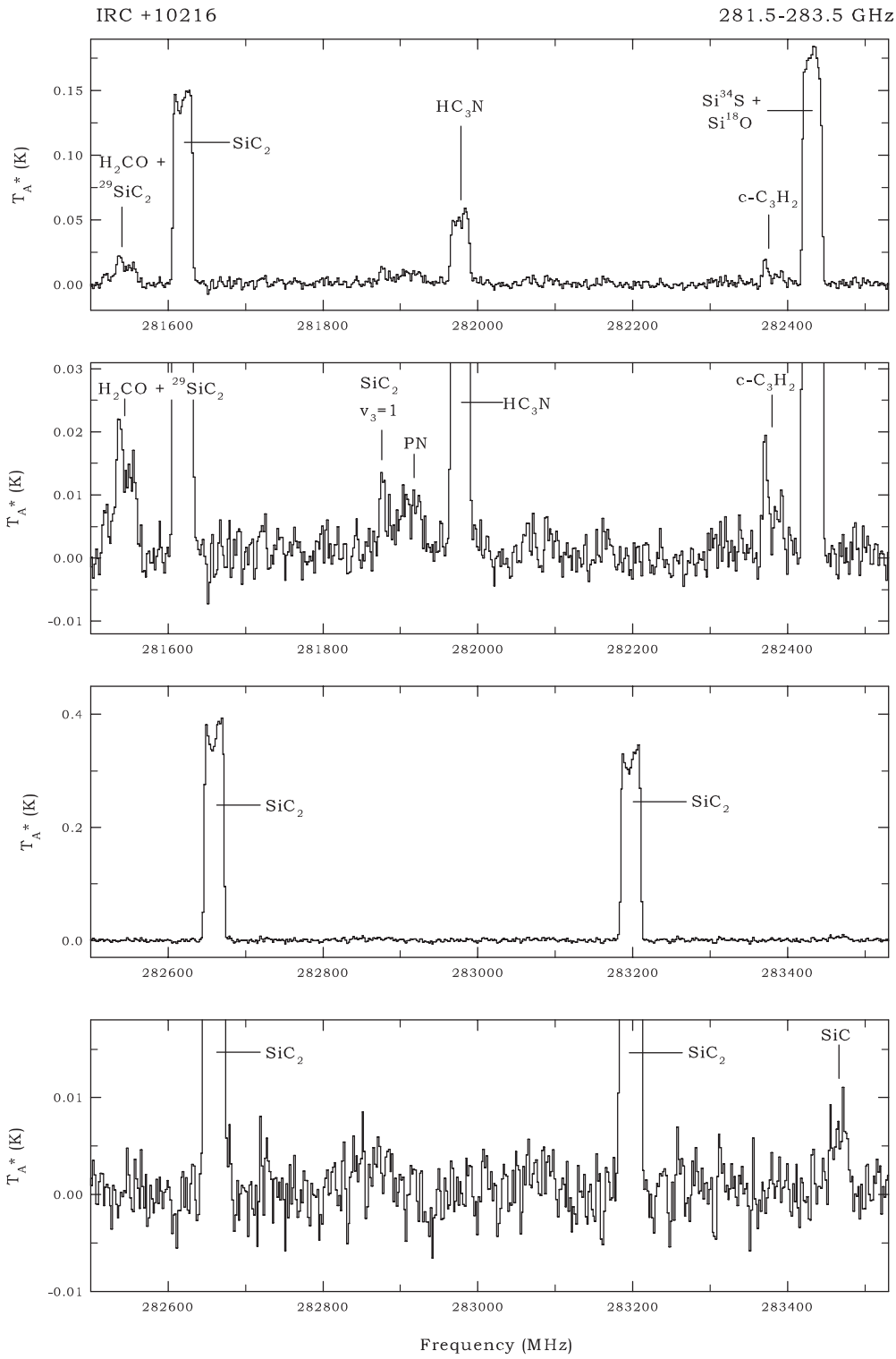

Figure 1. (Continued)

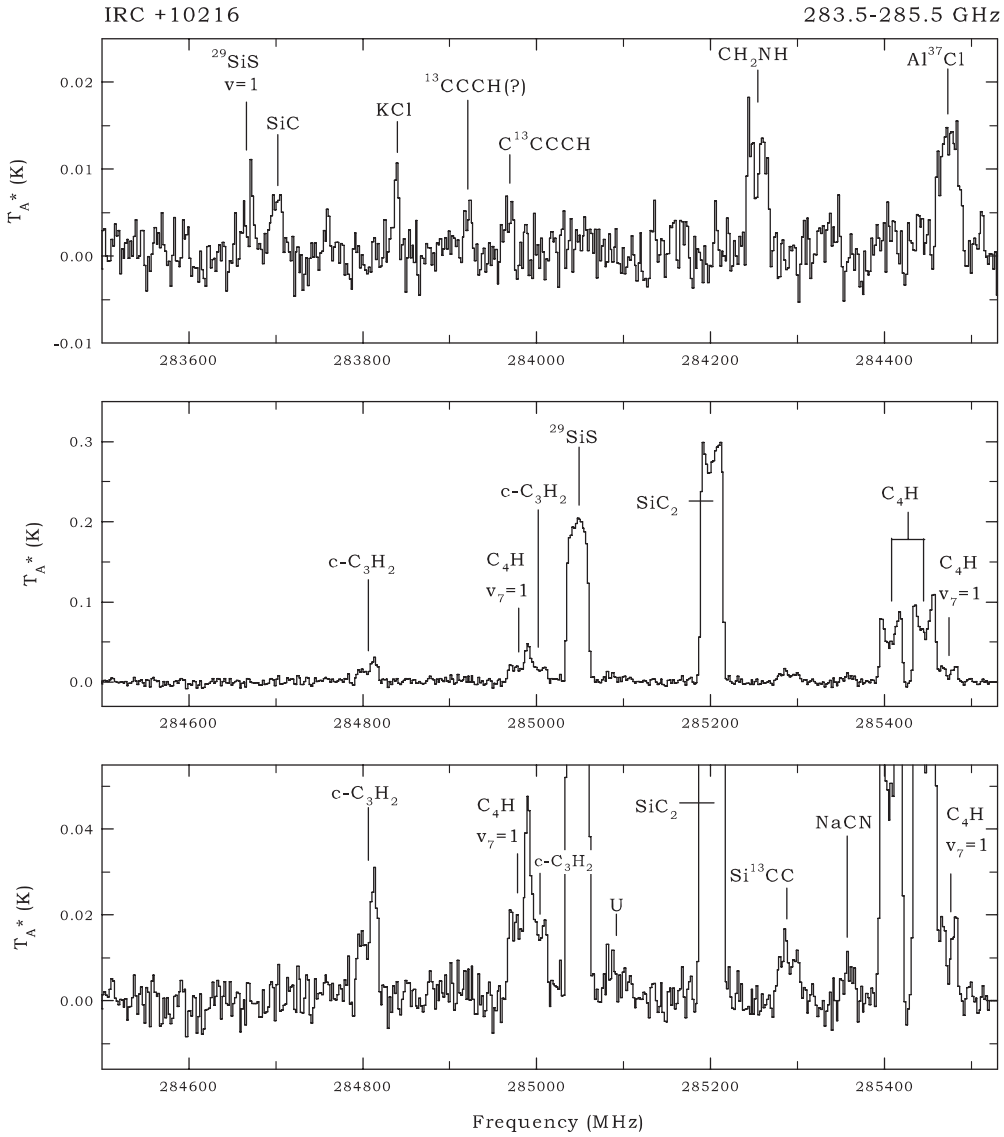

Figure 1. (Continued)

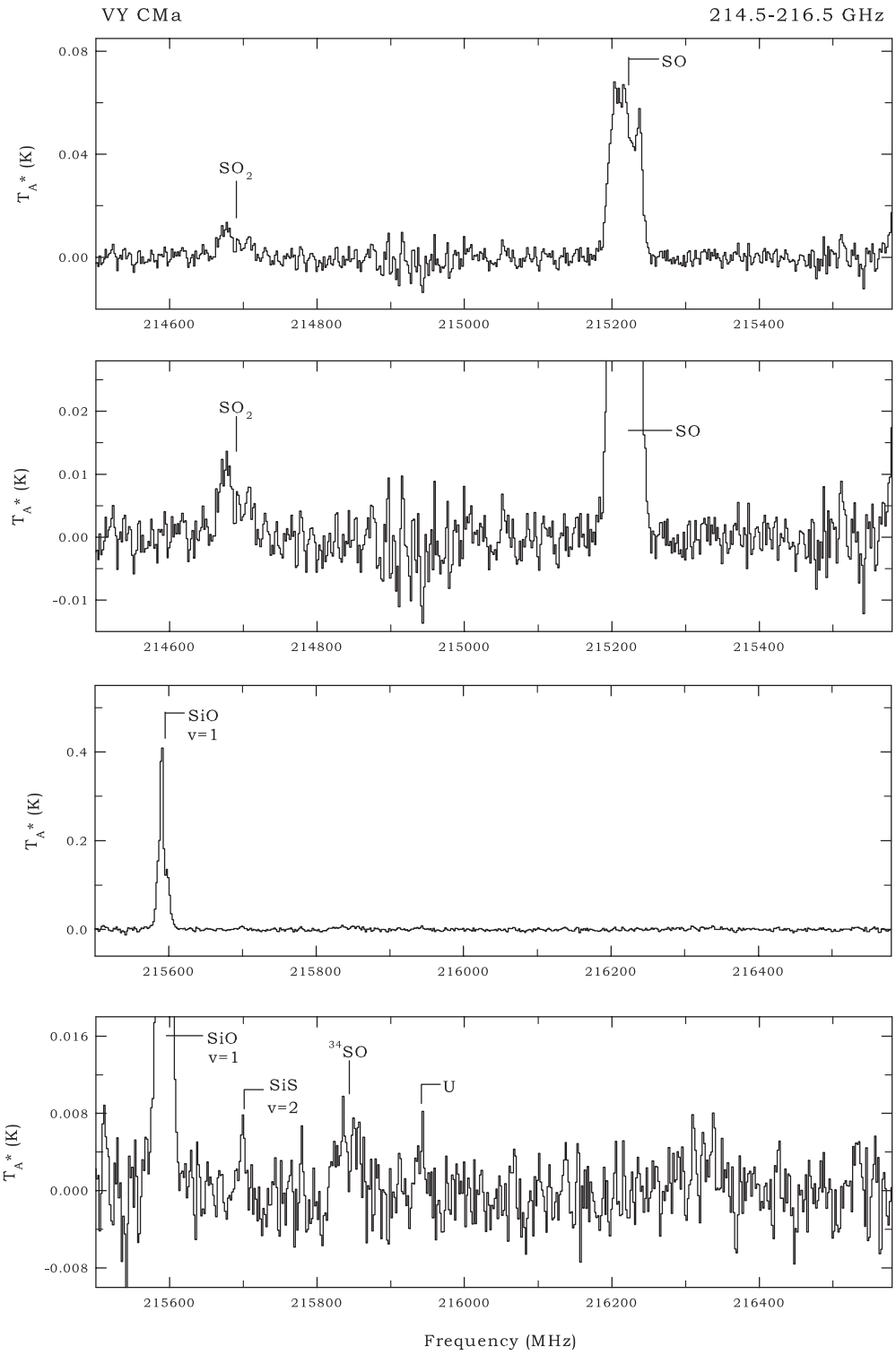

Figure 2. 214.5–285.5 GHz spectrum of VY CMa displayed in consecutive 1.08 GHz frequency segments with 2 MHz spectral resolution. There is an 80 MHz overlap between consecutive spectra. At many frequencies, two versions of the same spectrum are shown: one which displays the strong lines and a magnified version to show the weaker features. Extremely intense lines are displayed in insets. Each emission feature is marked with its corresponding molecular identification. One short segment of the spectrum, near 219.6 GHz, was omitted from the figure because of severe image contamination. First order baselines were removed from each spectrum. The frequency scale assumes $V_{\rm LSR} = 19.0$ km s^{-1}. Typical integration time per frequency setting is 10 hr.

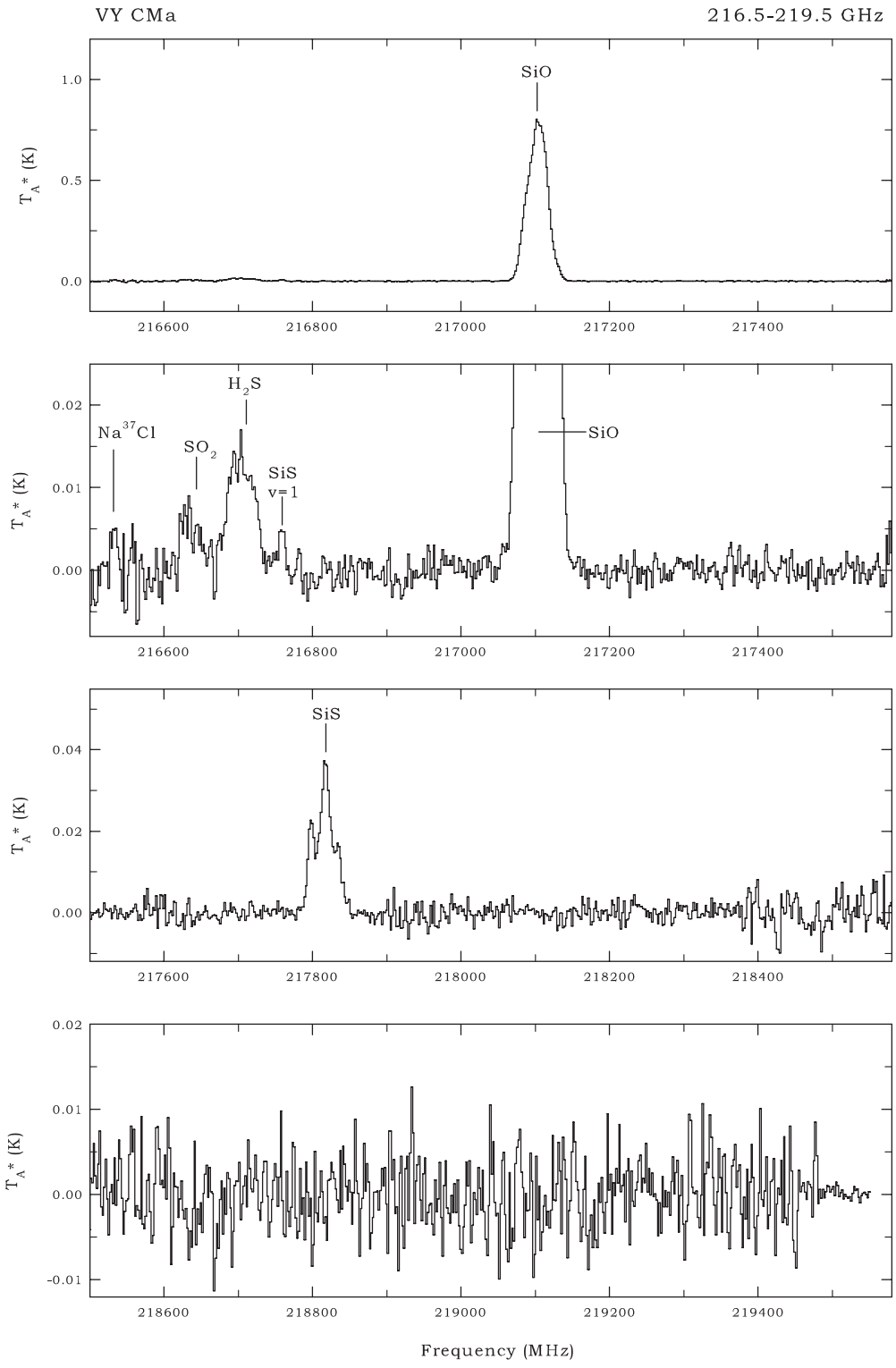

Figure 2. (Continued)

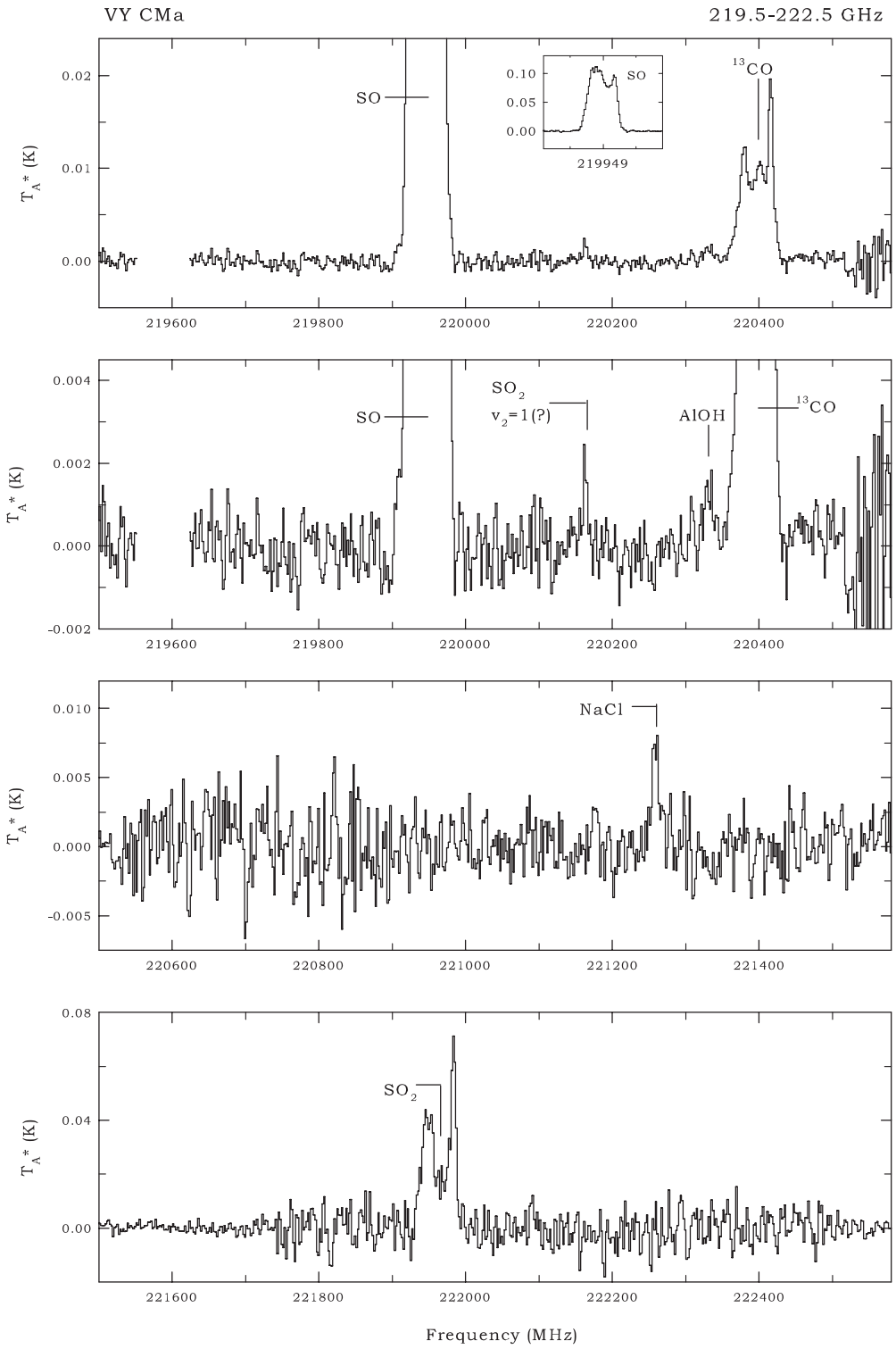

Figure 2. (Continued)

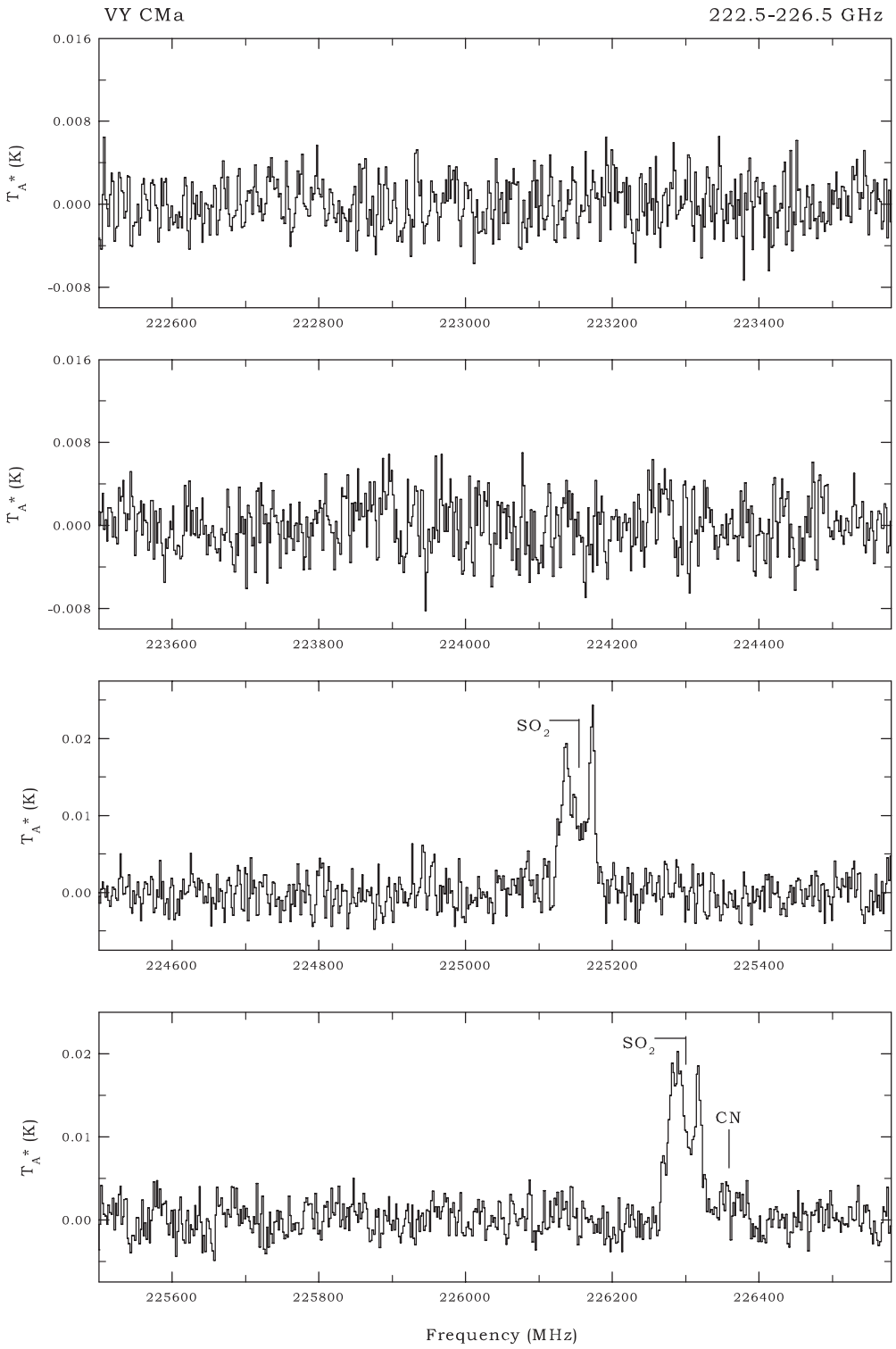

Figure 2. (Continued)

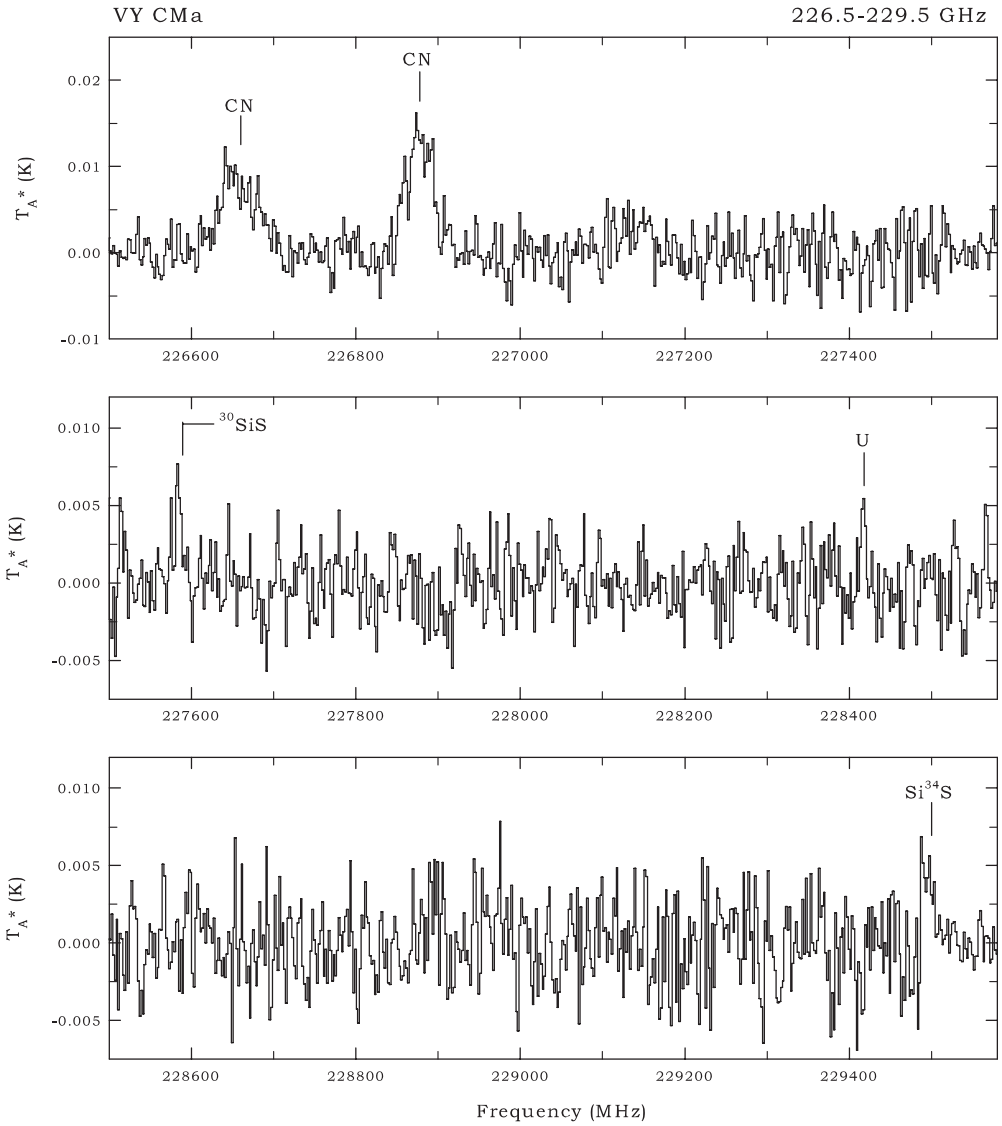

Figure 2. (Continued)

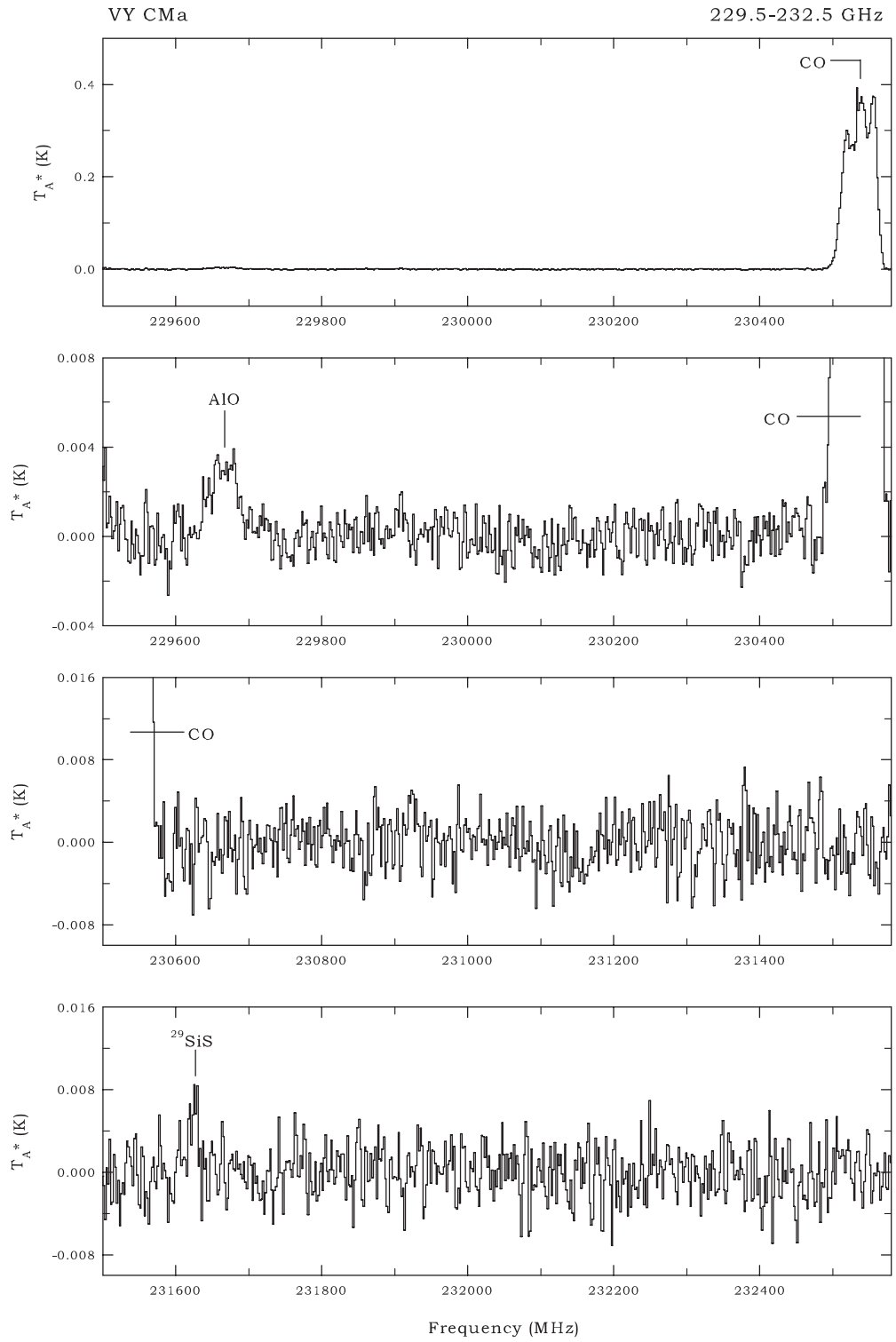

Figure 2. (Continued)

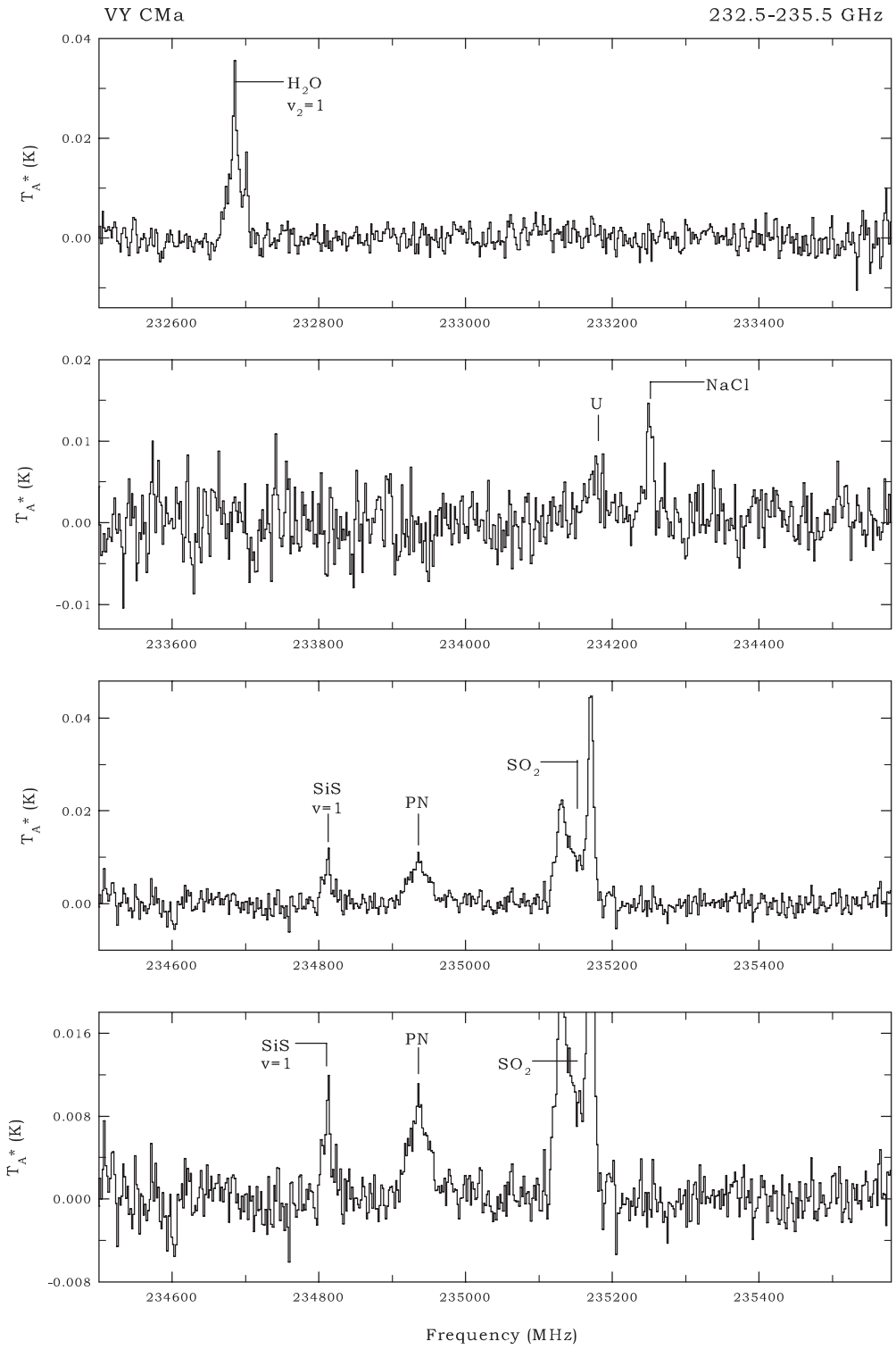

Figure 2. (Continued)

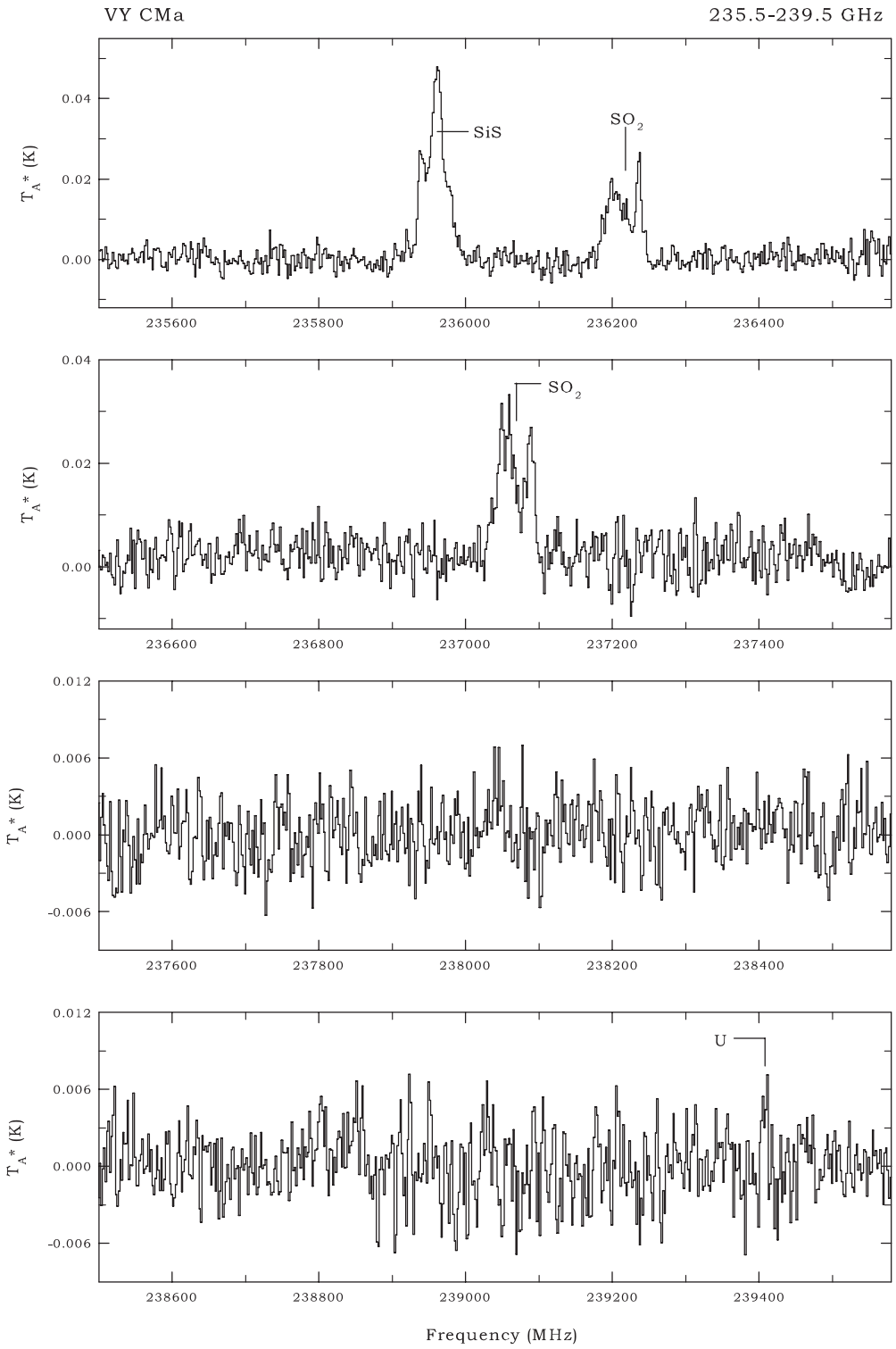

Figure 2. (Continued)

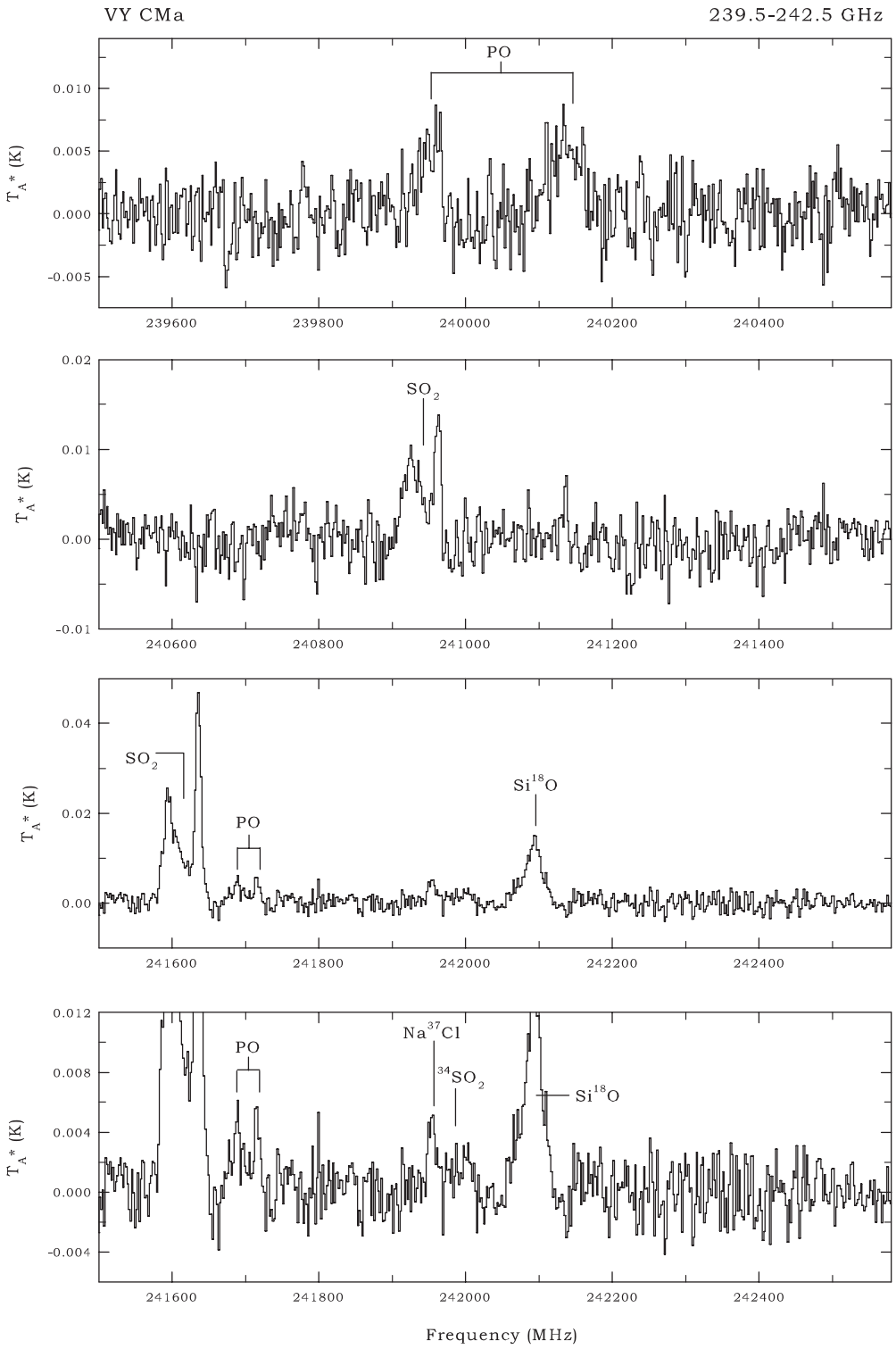

Figure 2. (Continued)

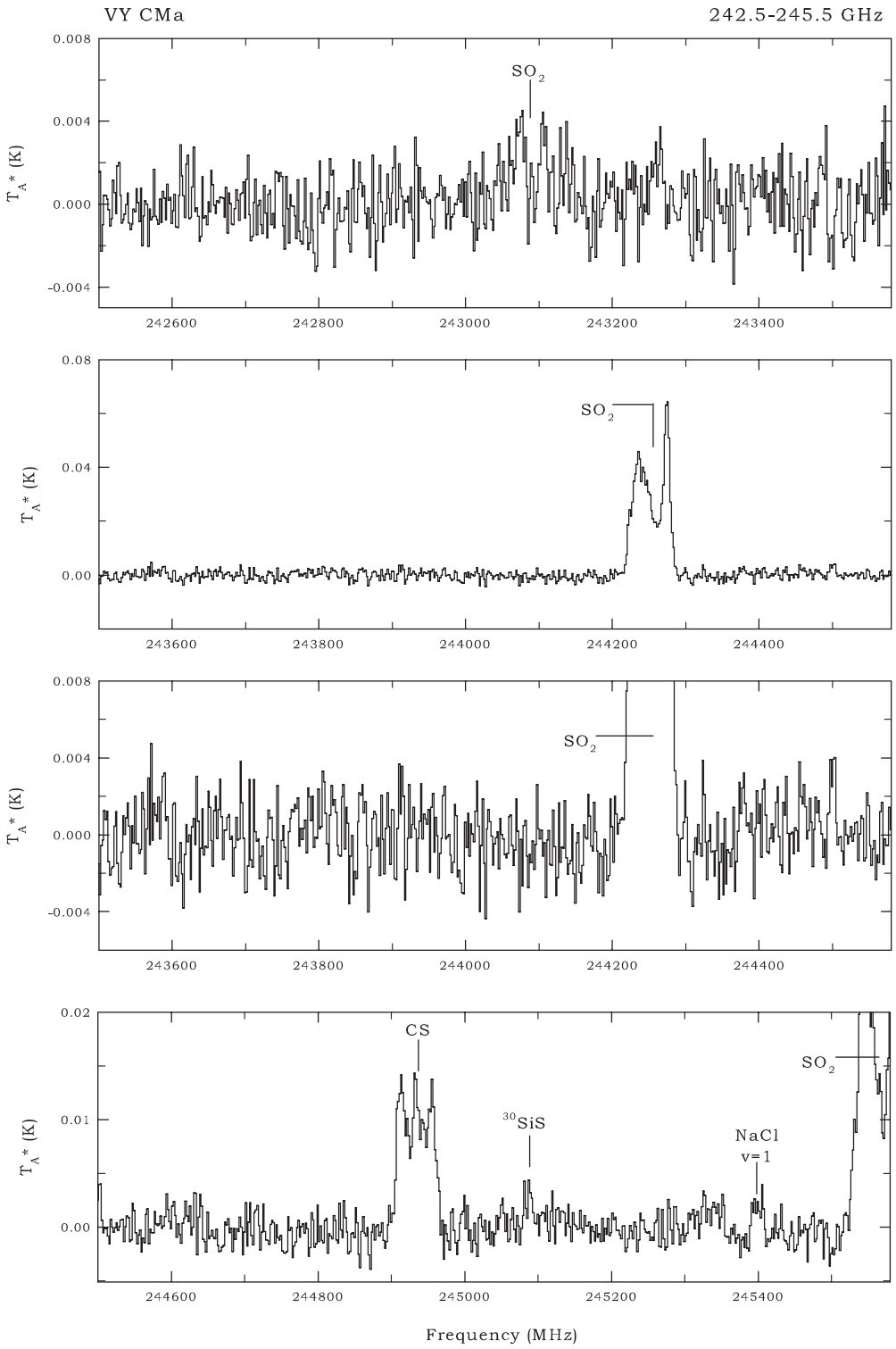

Figure 2. (Continued)

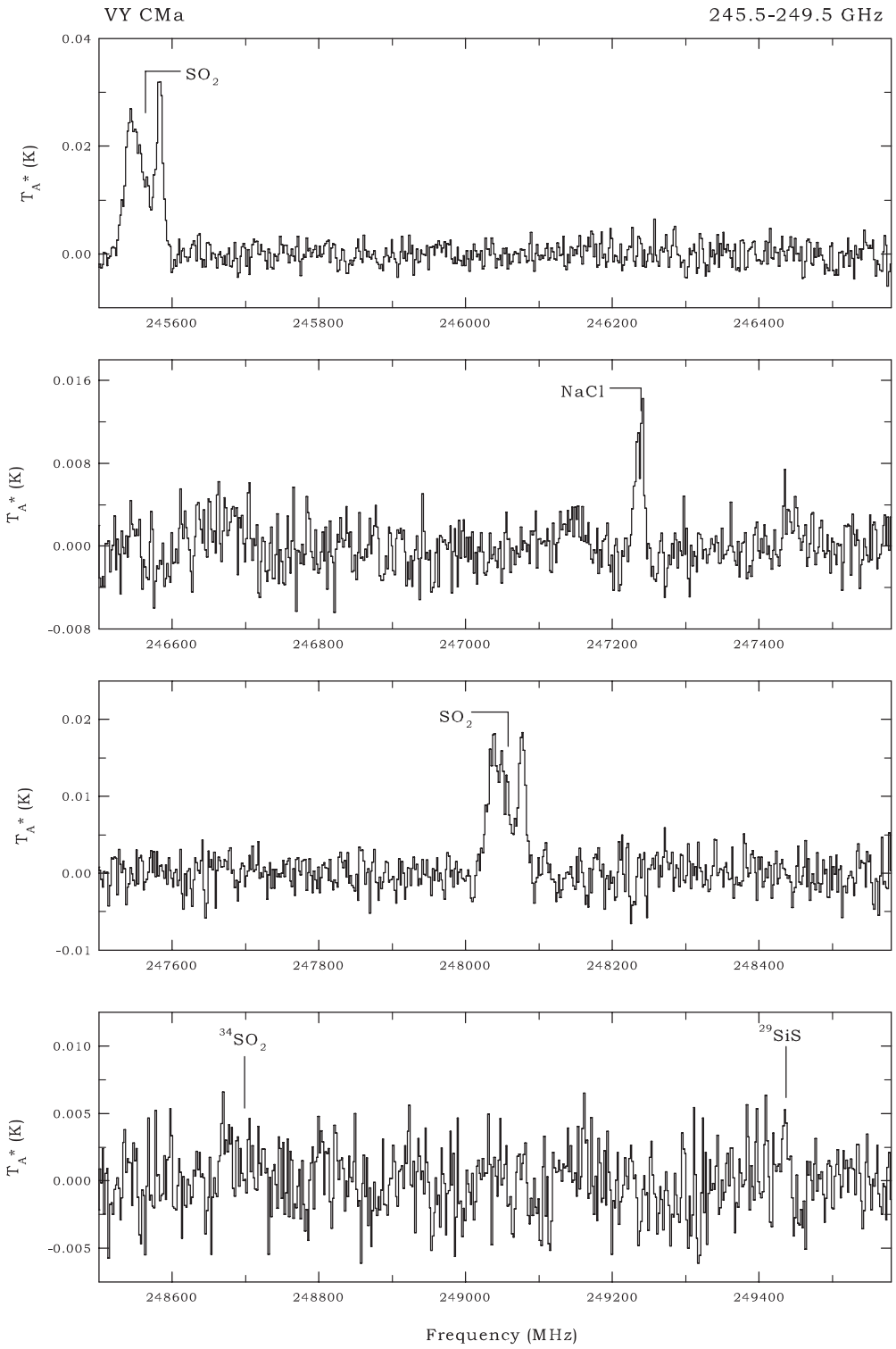

Figure 2. (Continued)

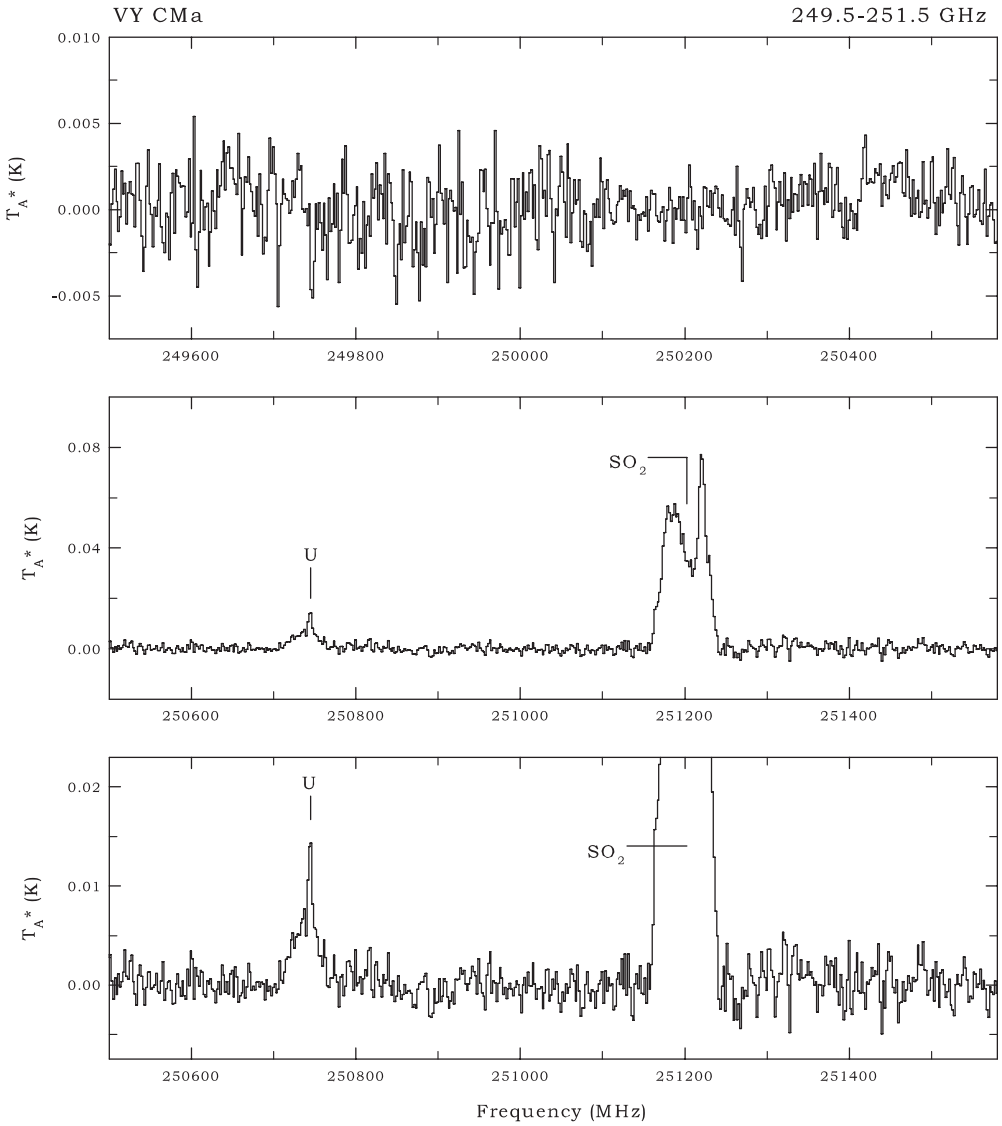

Figure 2. (Continued)

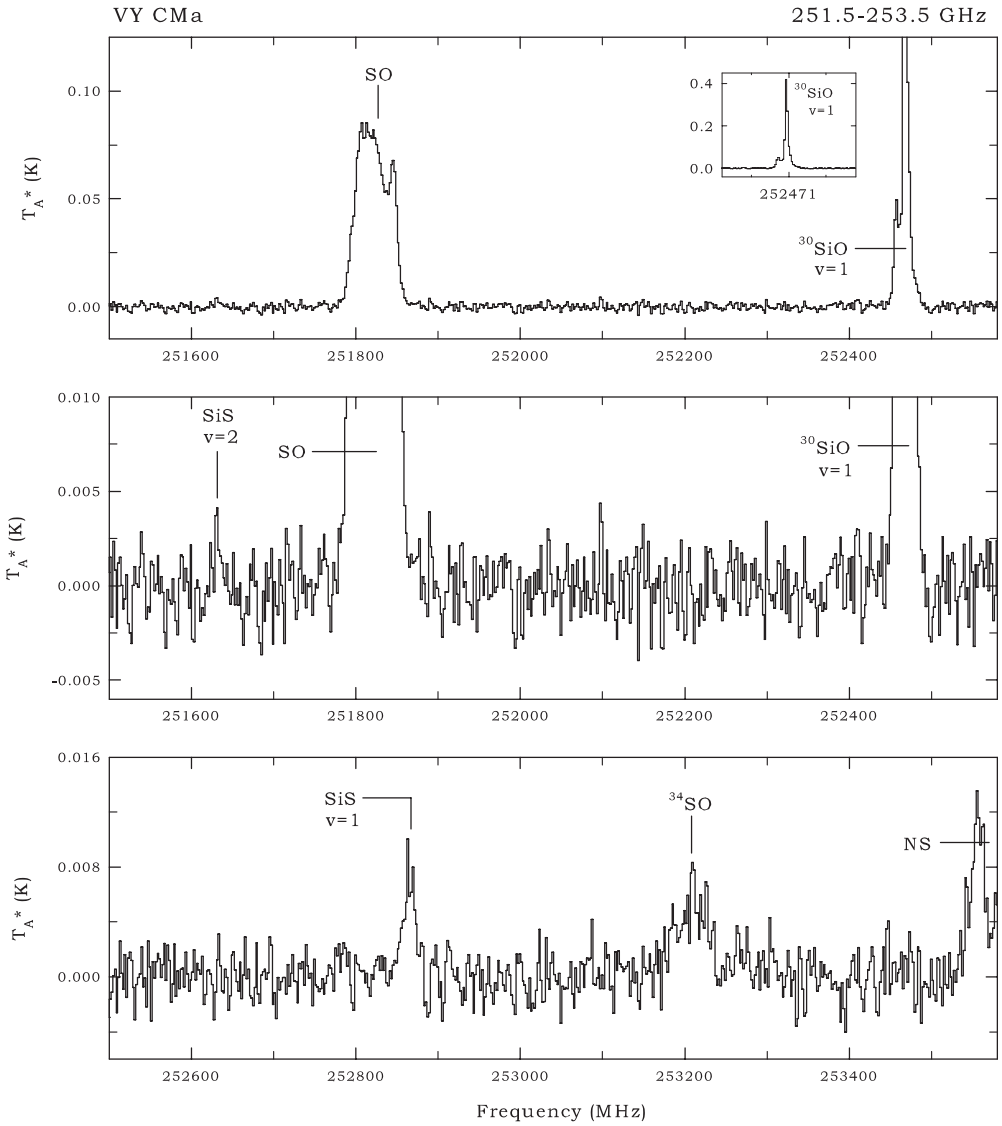

Figure 2. (Continued)

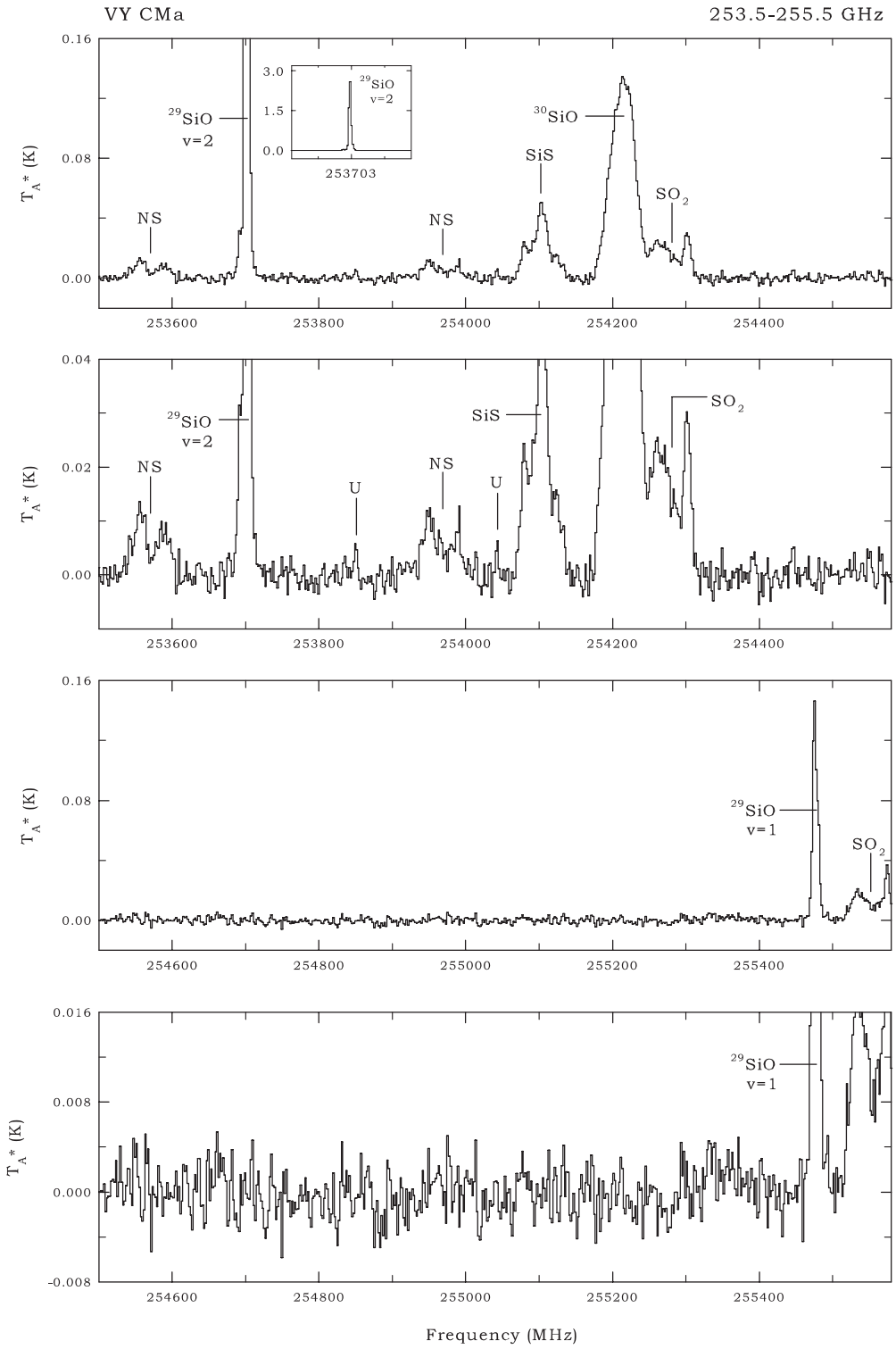

Figure 2. (Continued)

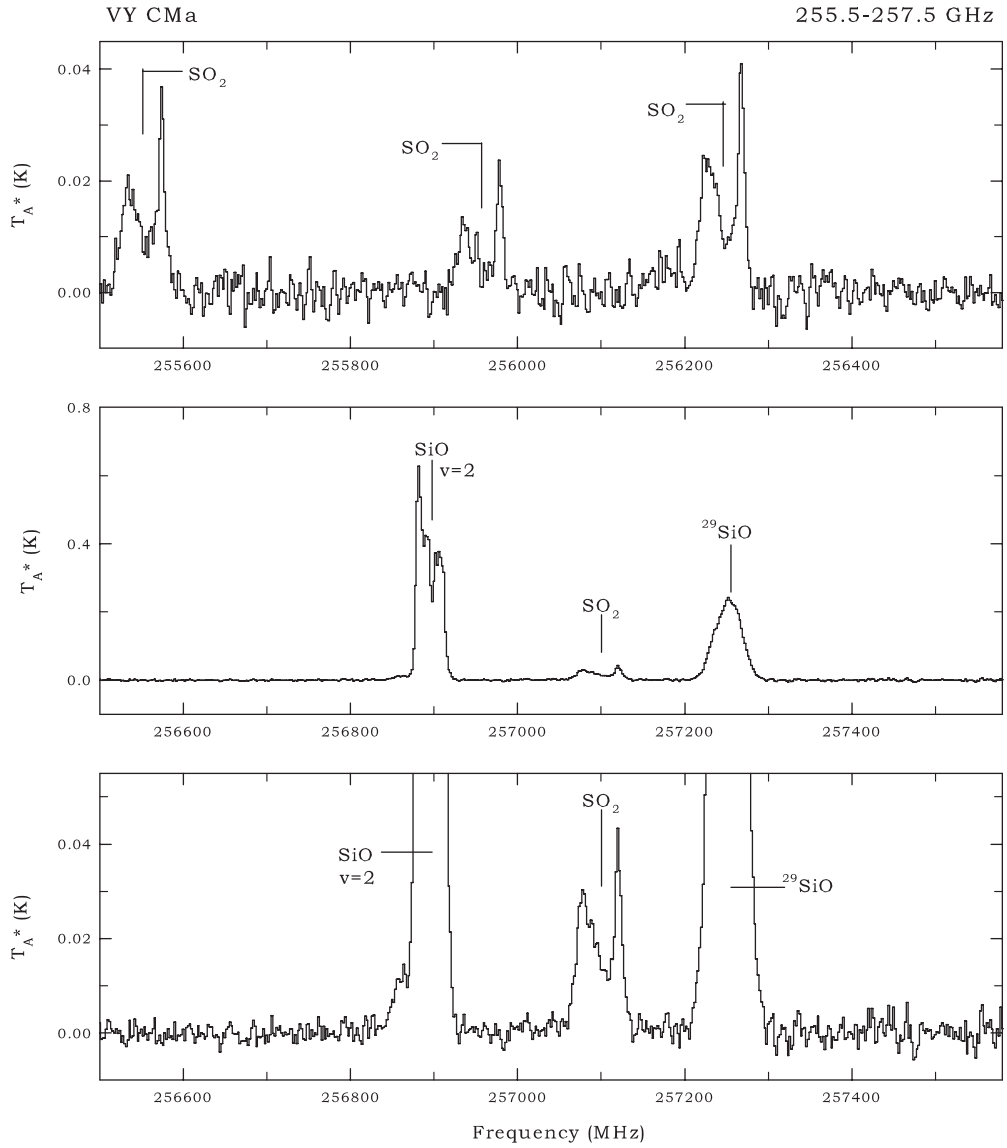

Figure 2. (Continued)

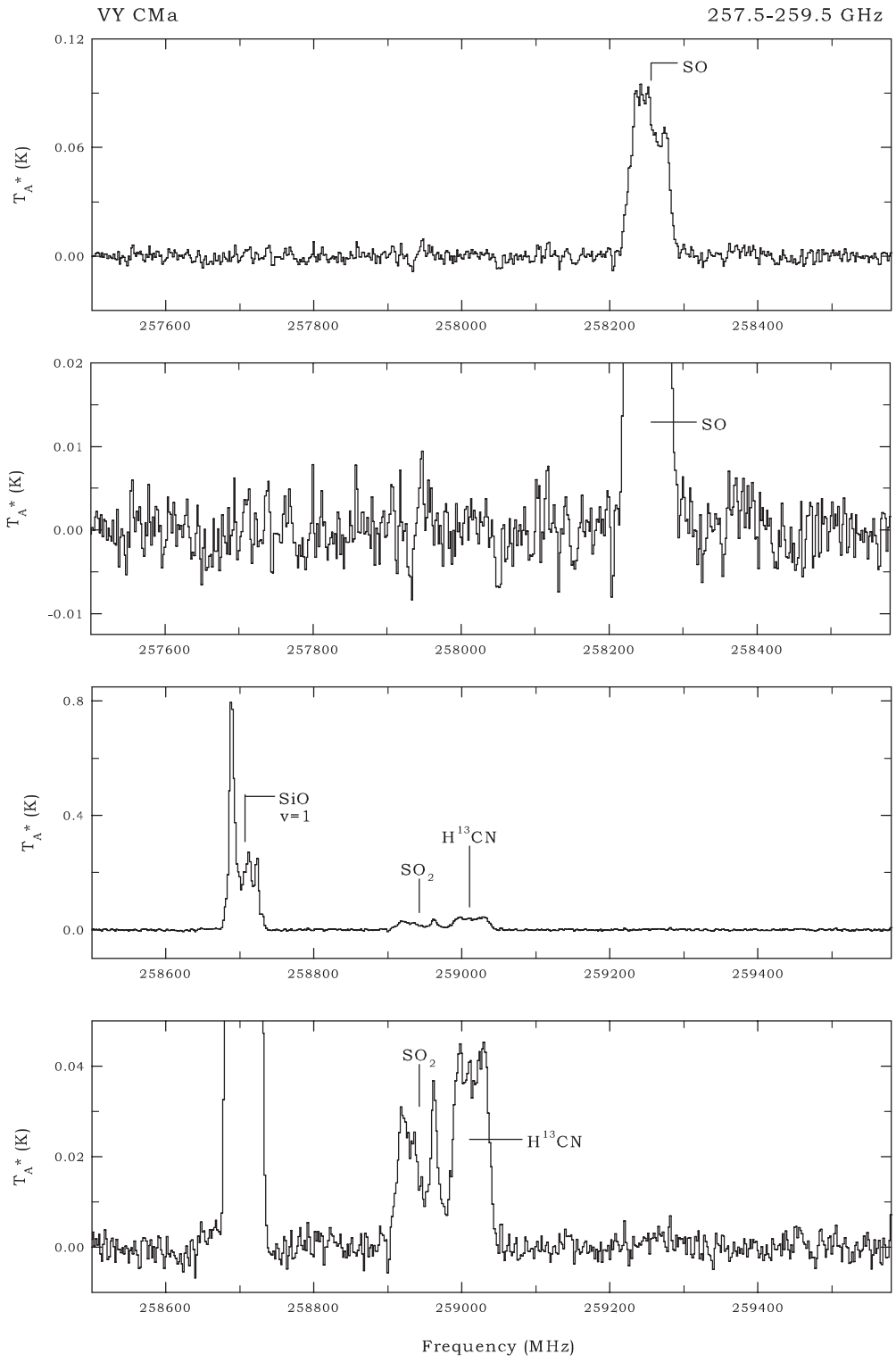

Figure 2. (Continued)

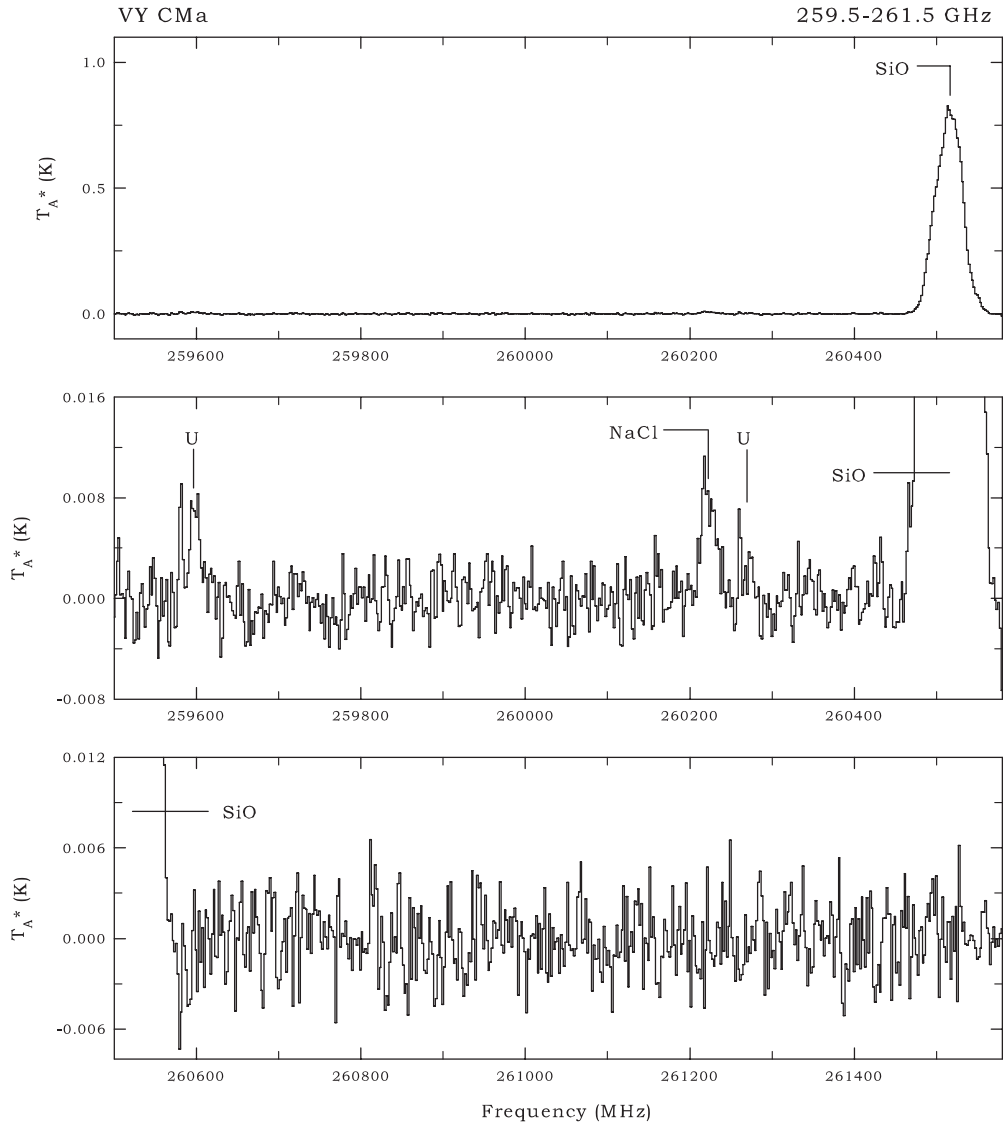

Figure 2. (Continued)

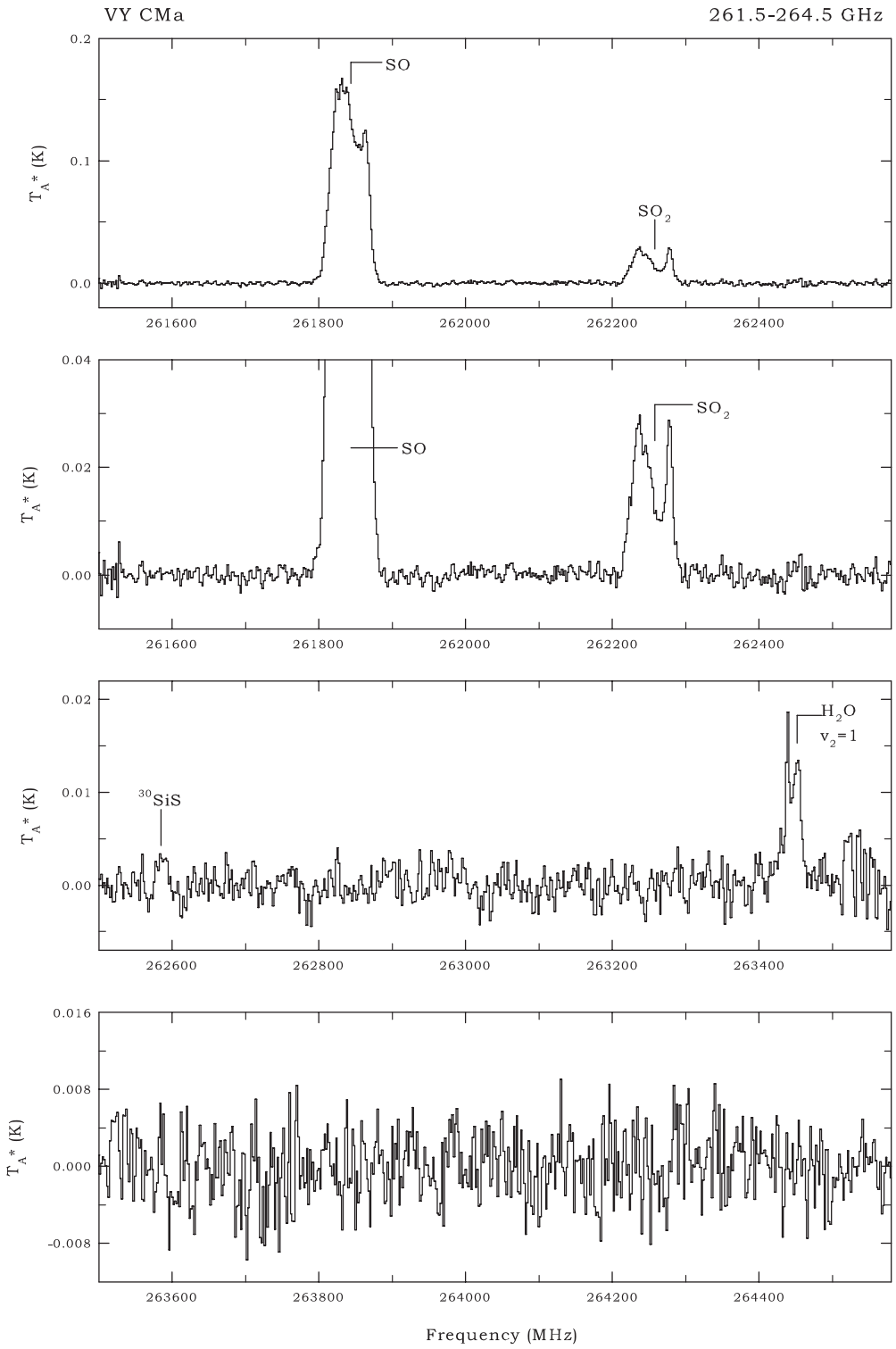

Figure 2. (Continued)

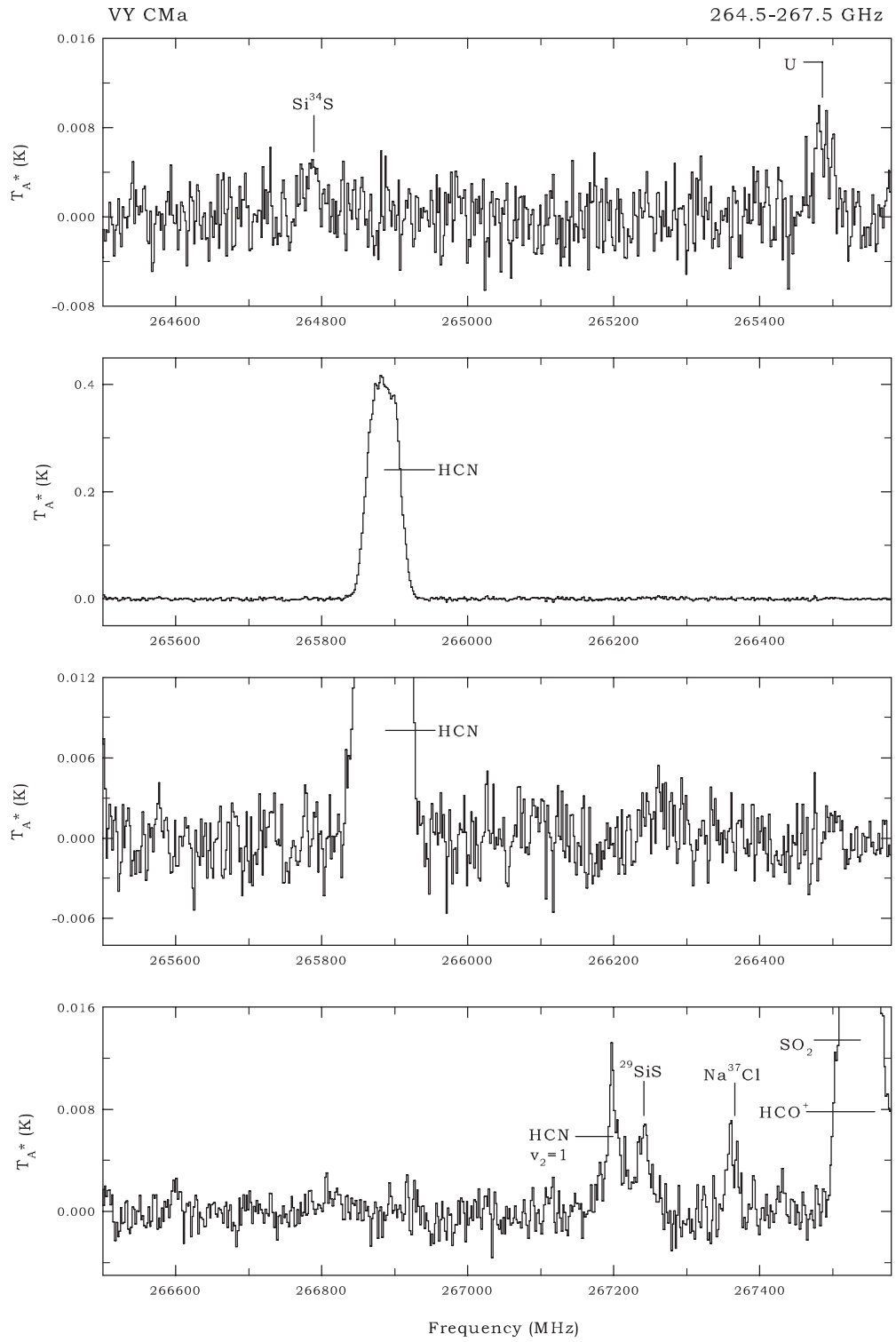

Figure 2. (Continued)

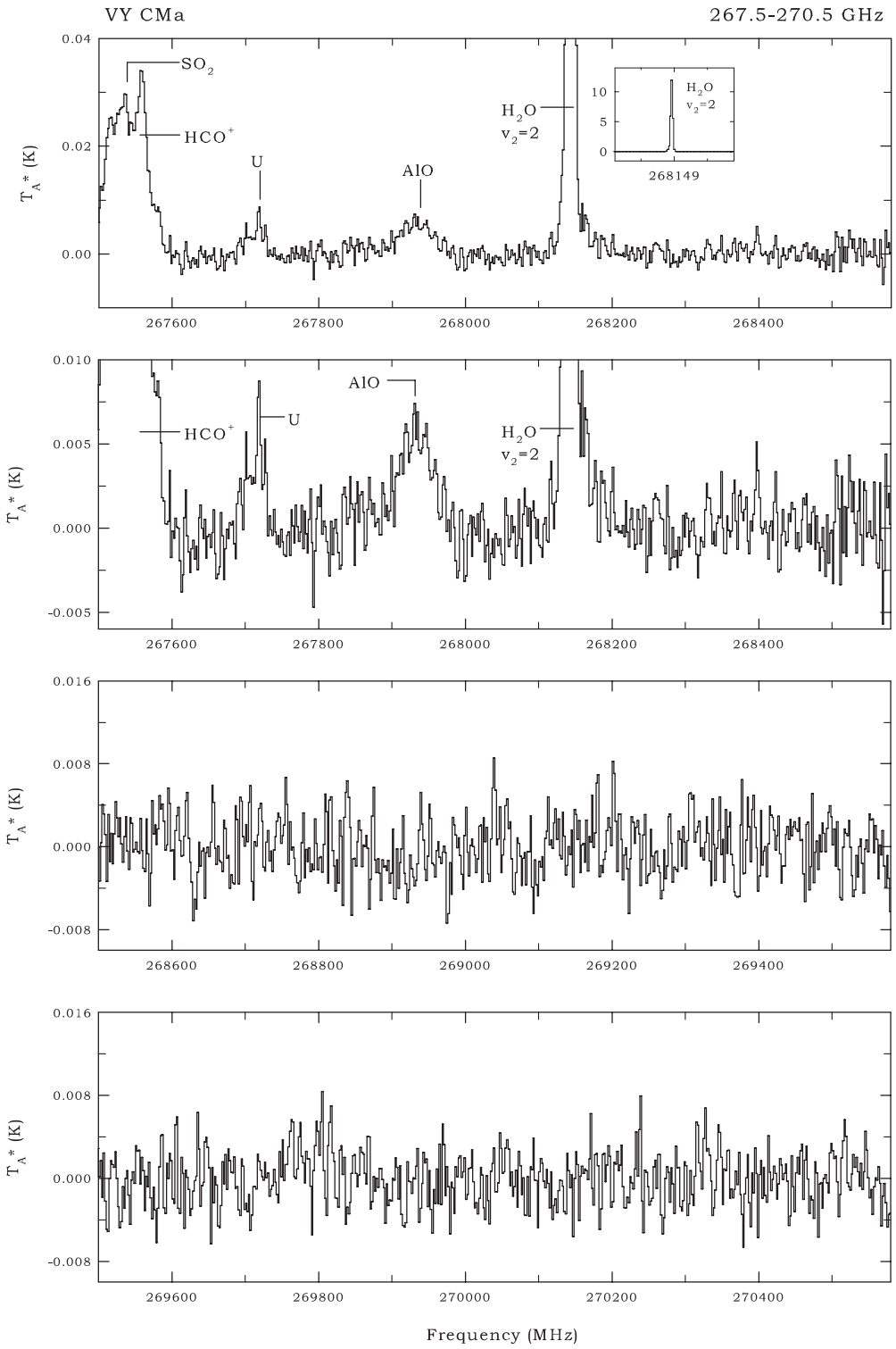

Figure 2. (Continued)

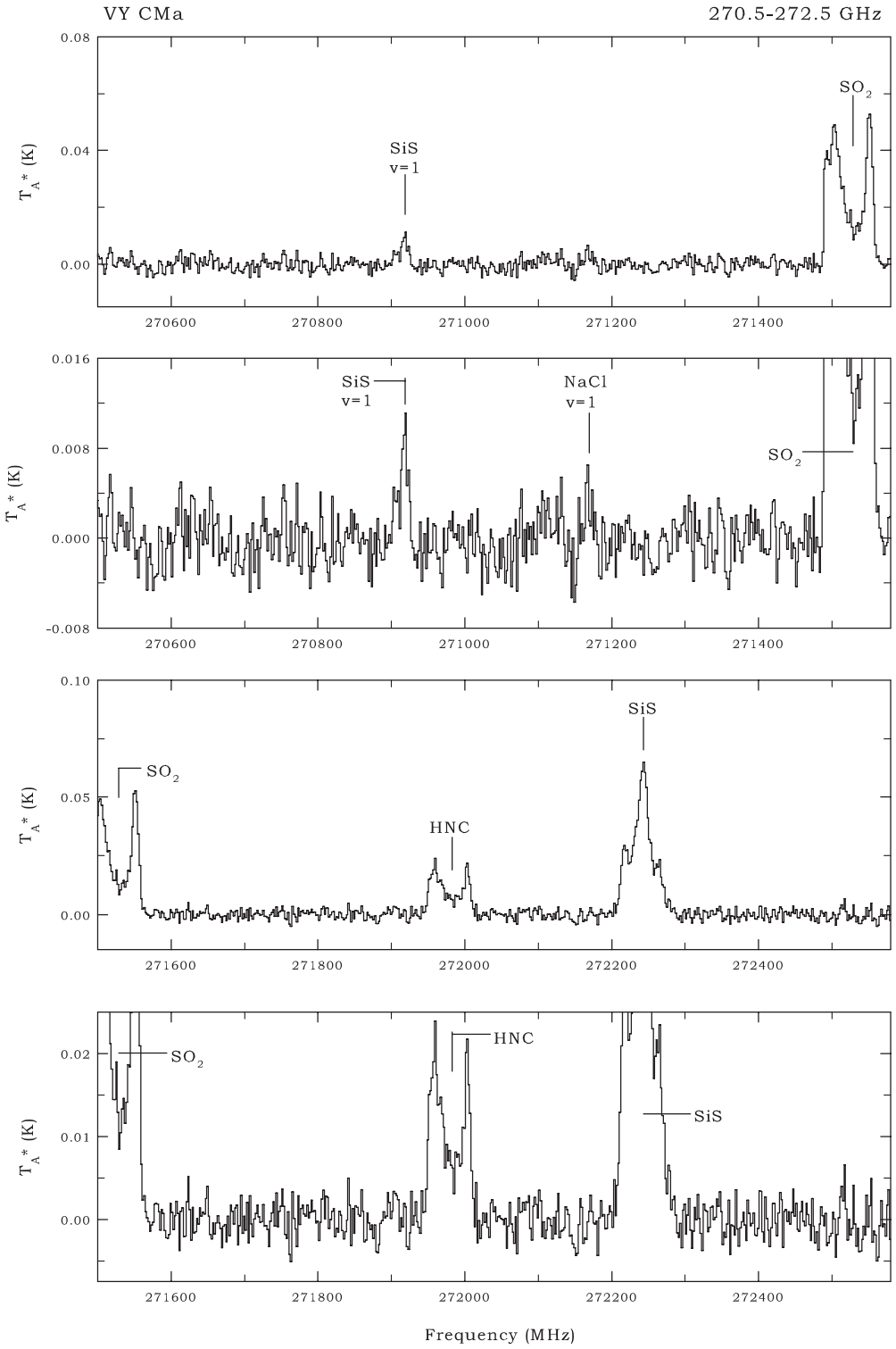

Figure 2. (Continued)

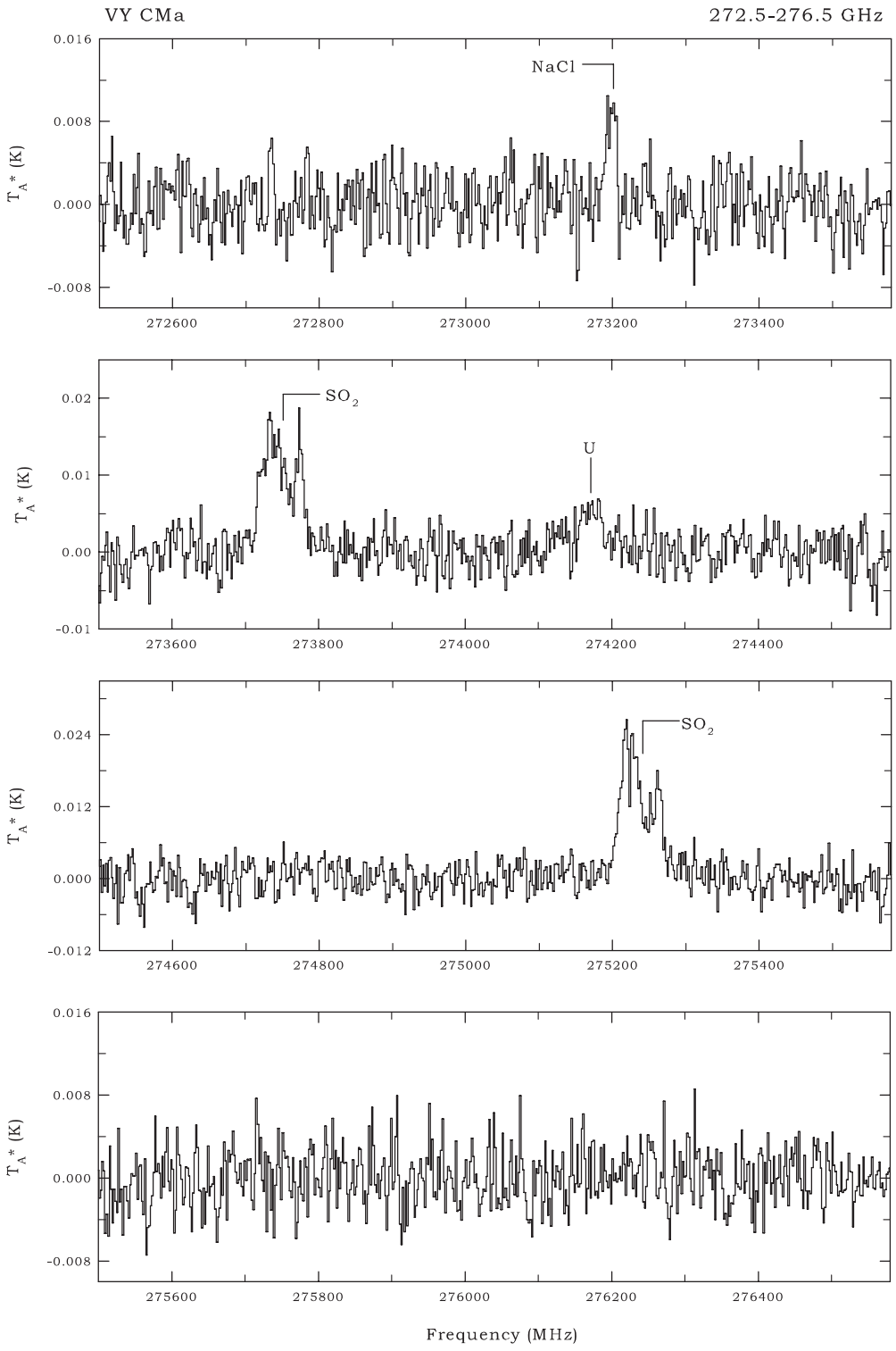

Figure 2. (Continued)

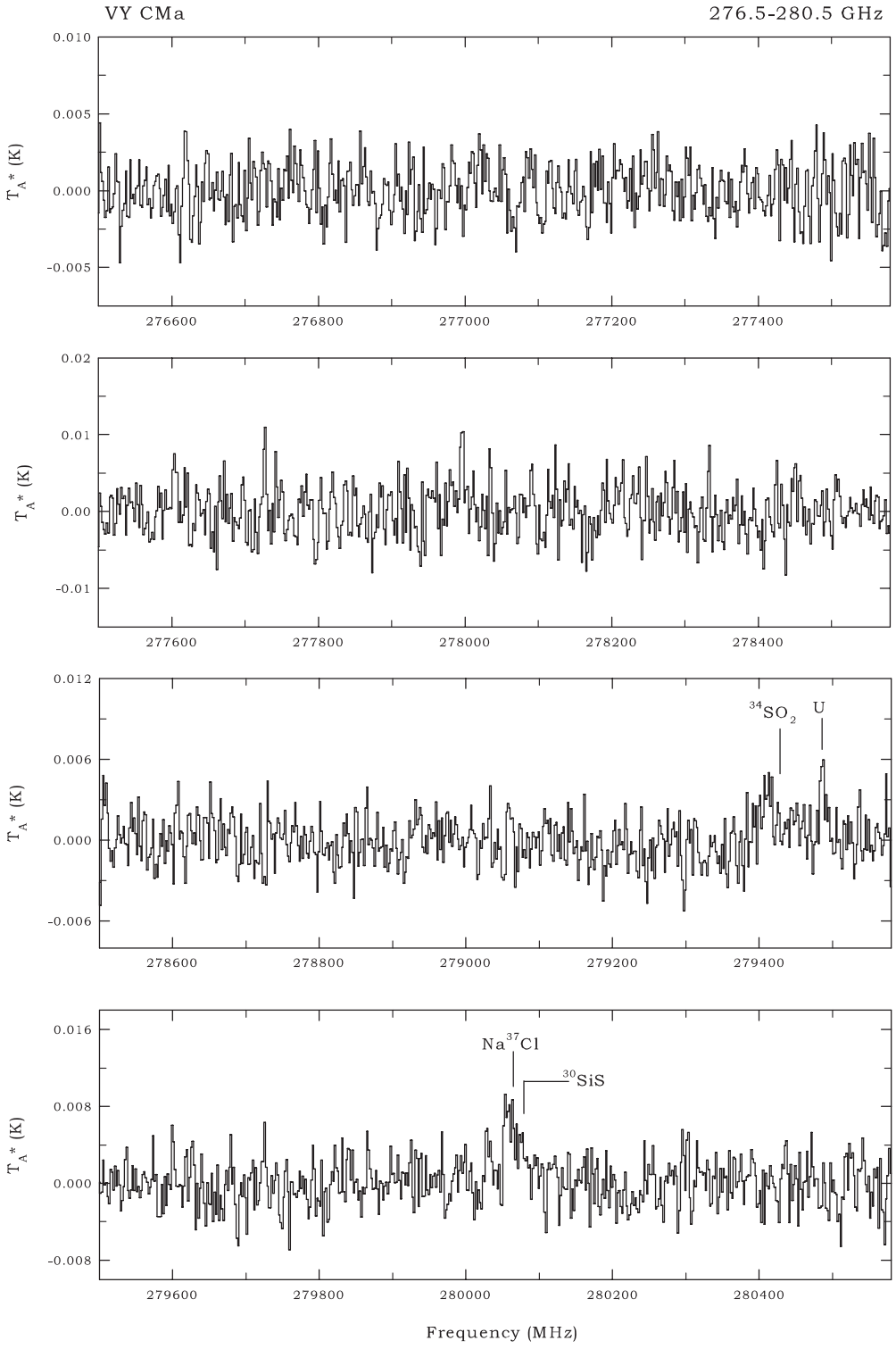

Figure 2. (Continued)

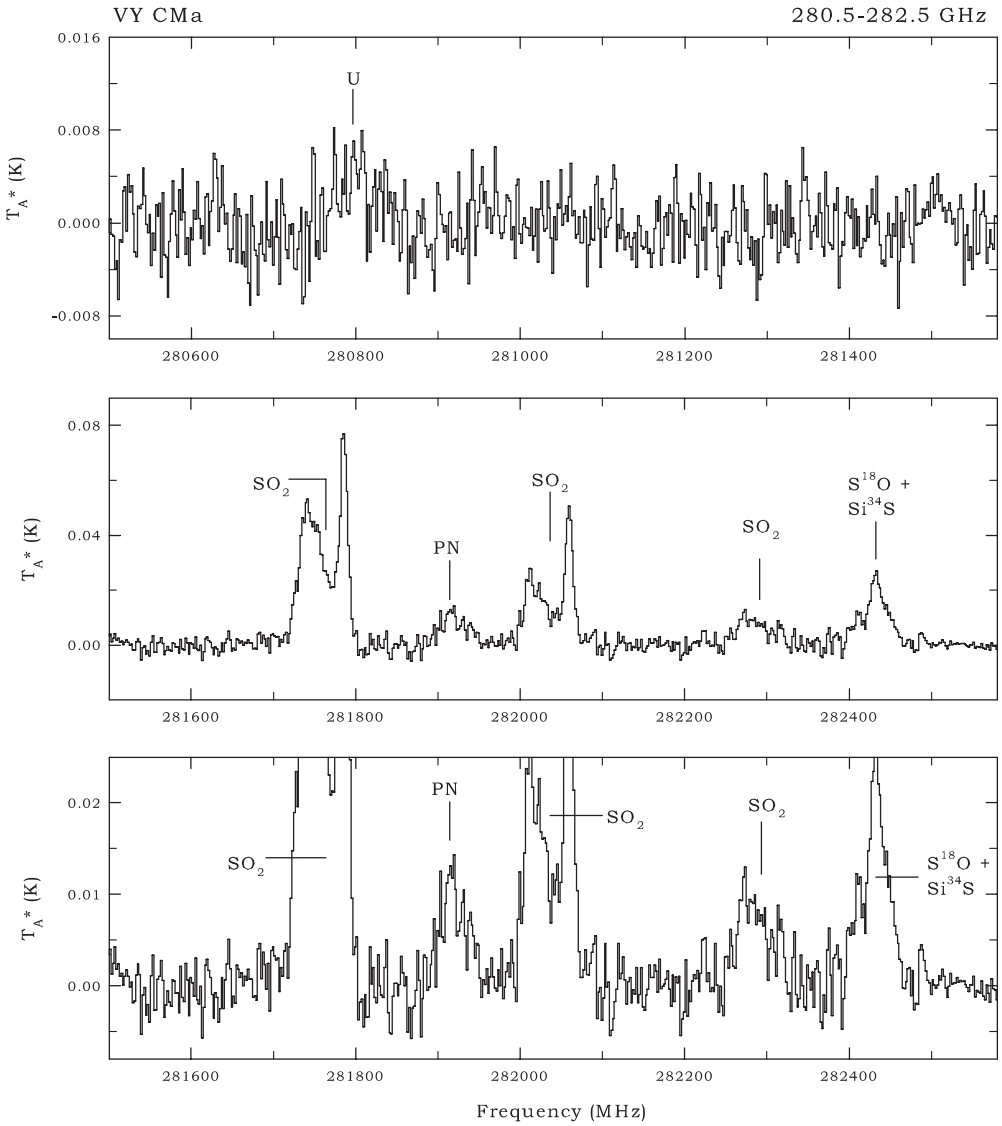

Figure 2. (Continued)

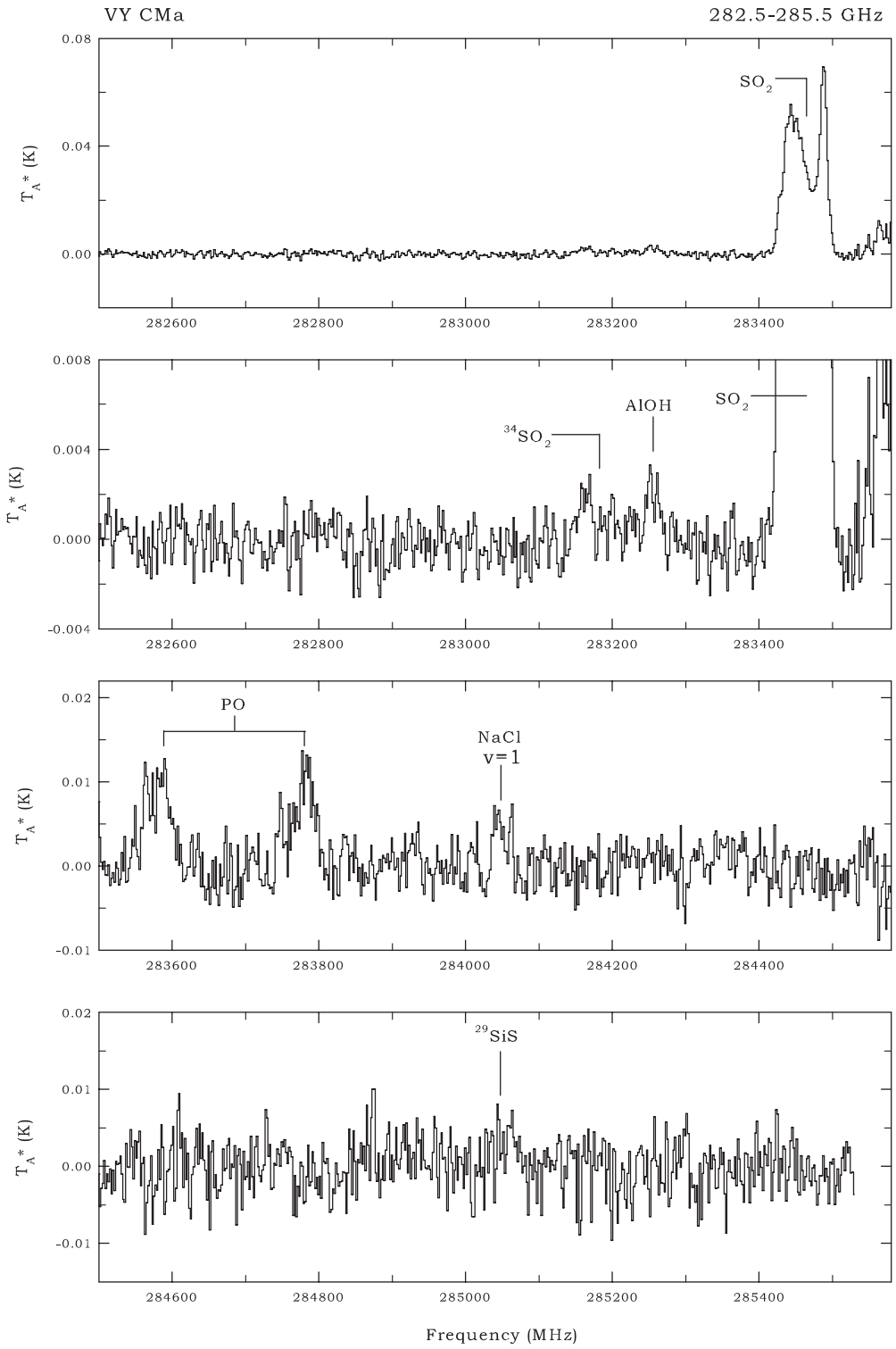

Figure 2. (Continued)

ground state), the vibrational quantum number is displayed as well. For bending modes, the l quantum number is only displayed if $l \neq v$.

All observed spectral lines from the survey are listed in Tables 1 (IRC +10216) and 2 (VY CMa). In these tables, the rest frequency, the assigned transition, and spectral parameters are given for each line. Unidentified features are labeled "U" and assigned a frequency based on $V_{\rm LSR} = -26.0$ km s^{-1} for IRC +10216 and $V_{\rm LSR} = 19.0$ km s^{-1} for VY CMa. Lines were identified using the online catalogs of JPL[6] (Pickett et al. 1998), CDMS[7] (Müller et al. 2005), and SPLATALOGUE[8], in addition to specific articles from the spectroscopic literature. To identify a given spectral feature, all corresponding viable molecular transitions were found in the aforementioned catalogs. Next, line assignments were checked for consistency by comparing intensities of different transitions of the same species. In cases where an emission feature appears to have significantly more intensity than warranted, the feature is assigned to be blended with a U-line. In addition, U-lines were assigned to emission peaks that did not correspond to any viable and internally consistent molecular transitions in the spectroscopic catalogs and literature. For example, some features that were coincident with lines of SiC_2 in the $v_3 = 2$ state ultimately were labeled as "U" because other favorable transitions in this level were "missing."

For each emission feature in IRC +10216, the following line parameters were established using the SHELL fitting routine in CLASS: center frequency, intensity at line center in T_A^*, integrated intensity, and expansion velocity, which is defined as the half-width at zero power, $\Delta V_{\rm HWZP}$ (see Table 1). For weak or blended features where SHELL fitting was not possible, the center frequency, peak intensity, and sometimes expansion velocity were estimated directly from the spectra.

In VY CMa, multiple velocity components exist in molecular line profiles. Emission lines appear to exhibit one to three distinct velocity components—a central component at the LSR velocity of the star (19 km s^{-1}), a red-shifted component at $V_{\rm LSR} \sim 35$ to 45 km s^{-1}, and a blue-shifted component at $V_{\rm LSR} \sim -1$ to -6 km s^{-1} (see Section 3 of this paper and Ziurys et al. 2009). Because of the large distance to VY CMa ($d = 1.14$ kpc), all molecular emission from this object ($\theta_s \leqslant 15$) inch is fully contained in the SMT beam ($\theta_b \sim 30''$). The multiple peaks in the line profiles, which sometime appear as an asymmetric "U" shape (see Figure 2: 235 GHz), are clearly a result of different molecular outflows in the CSE. The "U" shapes are not caused by resolved shell emission, as is the case in IRC +10216. Because of this difference, line parameters in VY CMa were measured using the GAUSS routine in CLASS. Individual Gaussian curves were simultaneously fit to the central, red-shifted, and/or blue-shifted components of each emission feature, when present. Examples of the types of fits to the line profiles are shown in Figure 3. In the lowest panel, the $J = 6 \rightarrow 5$ transition of ^{29}SiO at 257 GHz is shown, which exhibits only the central component and hence is fit with one Gaussian, shown in the dotted line. The middle panel displays the SO_2: $J_{\rm Ka,Kc} = 11_{3,9} \rightarrow 11_{2,10}$ transition at 262 GHz, composed of the red-shifted and blue-shifted components (no central one) and hence fit with two separate Gaussian profiles. The $J = 15 \rightarrow 14$ line of SiS at 272 GHz, shown in the top panel, contains emission from all three velocity features and is modeled

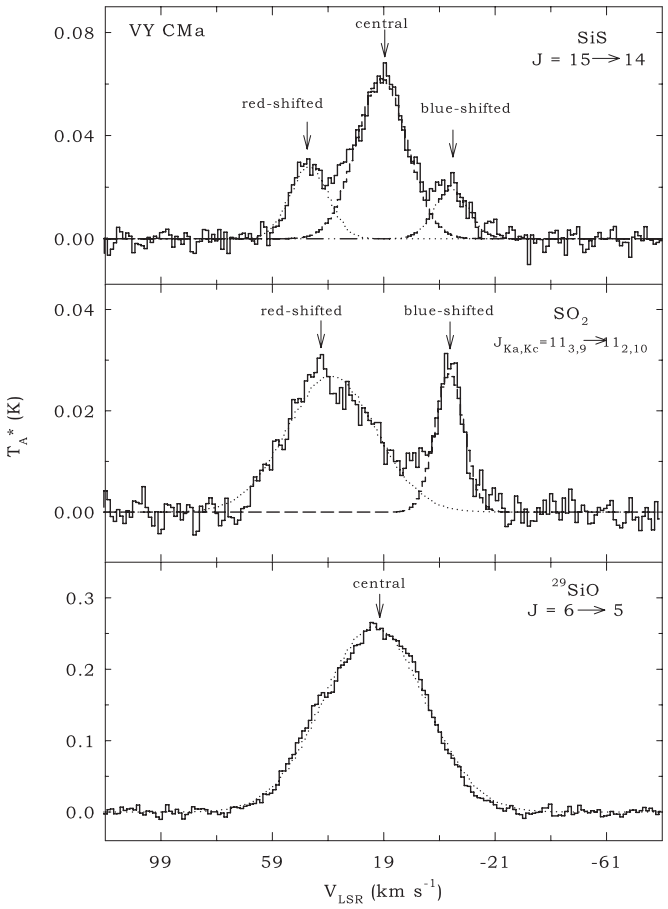

Figure 3. Emission lines of SiS, SO_2, and ^{29}SiO observed toward VY CMa, showing the contrasting line shapes in this object resulting from different kinematic outflows. The ^{29}SiO line profile (lowest panel) shows one central peak near $V_{\rm LSR} \sim 22$ km s^{-1}, with a broad line width of $\Delta V_{1/2} = 43$ km s^{-1}, which arises from a central, spherical wind. SO_2 (middle panel) exhibits a broad red-shifted peak ($\Delta V_{1/2} = 38$ km s^{-1}) at $V_{\rm LSR} \sim 38$ km s^{-1}, and a narrow blue-shifted peak ($\Delta V_{1/2} = 13$ km s^{-1}) at $V_{\rm LSR} \sim -5$ km s^{-1}; these two components are tracing independent blue- and red-shifted outflows. The SiS profile (top panel) shows a combination of the red-shifted and blue-shifted components plus the central spherical wind, with peaks at $V_{\rm LSR} \sim 46$ km s^{-1}, -5 km s^{-1}, and 20 km s^{-1}. Line parameters were measured by fitting Gaussian functions, marked by the dotted lines, to each appropriate velocity component (see Table 2). Spectral resolution is 1 MHz per channel.

with three Gaussians. Line parameters in Table 2 for VY CMa therefore are given for each respective velocity component: peak intensity in T_A^*, full width at half-maximum ($\Delta V_{1/2}$), integrated intensity, and $V_{\rm LSR}$. For very weak features, the profile was modeled only for the central component.

In the last column of Tables 1 and 2, notes are listed for each line, as appropriate. The note "S" indicates a U-shaped "shell" line profile in IRC +10216, "B" indicates an unresolved blend of emission from different species, and "P" denotes a partial blend of emission features where it was possible to estimate line parameters. "R," "F," and "H" respectively indicate that the listed frequency is an average of several rotational transitions (quantum numbers given), several fine structure components, or hyperfine components of the same molecule. "V" denotes a situation where the $\nu_{\rm rest}$ is an average of the same rotational transition of different vibrationally excited states of the same molecule, whereas "L" indicates when the rest frequency is unreliable due to insufficient laboratory data. Finally, "?" is listed when the assignment of a specific molecular transition to the given line is uncertain.

[6] http://spec.jpl.nasa.gov
[7] http://www.astro.uni-koeln.de/cdms/catalog
[8] http://www.splatalogue.net

Table 1
Parameters for Emission Lines in IRC +10216

$\nu_{\rm rest}$ (MHz)	Molecule	Transition	Center T_A^* [a] (K)	$\Delta V_{\rm HWZP}$ [b] (km s^{-1})	$\int T_A^* dV$ (K km s^{-1})	$V_{\rm LSR}$ (km s^{-1})	Notes
214509.4	$Si^{13}CC$	$J_{\rm Ka,Kc} = 9_{1,8} \rightarrow 8_{1,7}$	0.016 ± 0.003	14.1 ± 1.4	0.470 ± 0.024	−26.9 ± 1.4	S
214704.4	U		0.005 ± 0.003	12.0 ± 1.5	0.119 ± 0.059	−26.0	
214741.0	$Si^{33}S$	$J = 12 \rightarrow 11$	0.027 ± 0.003	13.7 ± 0.3	0.659 ± 0.039	−26.6 ± 1.4	
215163.0	U		0.004 ± 0.003			−26.0	
215205.9	$Si^{13}CC$	$J_{\rm Ka,Kc} = 10_{0,10} \rightarrow 9_{0,9}$	0.013 ± 0.003	12.5 ± 0.7	0.378 ± 0.054	−27.2 ± 1.4	S
215246.9	$^{30}SiC_2$	$J_{\rm Ka,Kc} = 9_{2,7} \rightarrow 8_{2,6}$	0.016 ± 0.003	12.5 ± 0.3	0.582 ± 0.045	−23.4 ± 1.4	S
215423.1	$^{30}SiC_2$	$J_{\rm Ka,Kc} = 10_{0,10} \rightarrow 9_{0,9}$	0.018 ± 0.003	13.3 ± 0.5	0.548 ± 0.061	−26.1 ± 1.4	S
215697.5	SiS, $v = 2$	$J = 12 \rightarrow 11$	0.009 ± 0.002	7.6 ± 1.4	0.121 ± 0.056	−25.1 ± 1.4	
216278.8	c-C_3H_2	$J_{\rm Ka,Kc} = 3_{3,0} \rightarrow 2_{2,1}$	0.060 ± 0.002	14.0 ± 1.4	2.078 ± 0.025	−26.6 ± 1.4	S
216358.7	SiC_2, $v_3 = 1$	$J_{\rm Ka,Kc} = 9_{1,8} \rightarrow 8_{1,7}$	0.004 ± 0.002			∼ −26	B
216373.1	CCD	$N, J = 3, 7/2 \rightarrow 2, 5/2$	0.004 ± 0.002			∼ −26	B, H
216490.2	c-C_3H	$N_{\rm Ka,Kc}, J = 4_{1,3}, 9/2 \rightarrow 3_{1,2}, 7/2$	0.025 ± 0.002	17.2 ± 2.8	0.856 ± 0.028	−25.3 ± 5.5	S, H
216531.4	$Na^{37}Cl$	$J = 17 \rightarrow 16$	0.005 ± 0.002	12.0 ± 1.4	0.151 ± 0.014	−27.6 ± 1.4	
216639.5	c-C_3H	$N_{\rm Ka,Kc}, J = 4_{1,3}, 7/2 \rightarrow 3_{1,2}, 5/2$	0.017 ± 0.002	16.1 ± 1.4	0.603 ± 0.014	−25.7 ± 1.4	H
216757.6	SiS, $v = 1$	$J = 12 \rightarrow 11$	0.033 ± 0.002	12.0 ± 1.4	0.524 ± 0.014	−27.1 ± 1.4	

Notes.
[a] Uncertainty range is $\pm 1\sigma$, measured from 2 MHz resolution data.
[b] Half-width at zero power, also referred to as expansion velocity ($V_{\rm exp}$).
S: double-peaked line profile.
B: unresolvable blend of emission lines from different molecules.
P: partial blend of resolvable emission features.
R: $\nu_{\rm rest}$ is average of rotational transition frequencies.
F: $\nu_{\rm rest}$ is average of fine-structure transition frequencies.
H: $\nu_{\rm rest}$ is average of hyperfine-structure transition frequencies.
V: $\nu_{\rm rest}$ is average of rotational transition frequencies of different vibrational states of the same molecule.
L: $\nu_{\rm rest}$ is unreliable (see Section 4.4).
?: uncertain line assignment.

(This table is available in its entirety in a machine-readable form in the online journal. A portion is shown here for guidance regarding its form and content.)

Table 2
Parameters for Emission Lines in VY CMa

$\nu_{\rm rest}$ (MHz)	Molecule	Transition	Outflow	T_A^*[a] (K)	$\Delta V_{1/2}$ [b] (km s^{-1})	$\int T_A^* dV$ (K km s^{-1})	$V_{\rm LSR}$ (km s^{-1})	Notes
214689.4	SO_2	$J_{\rm Ka,Kc} = 16_{3,13} \rightarrow 16_{2,14}$	Red	0.012 ± 0.002	29.2 ± 5.6	0.360 ± 0.050	37.5 ± 5.6	
			Blue	0.007 ± 0.002	24.4 ± 5.6	0.170 ± 0.040	−6.9 ± 5.6	
215220.7	SO	$N_J = 5_5 \rightarrow 4_4$	Red	0.077 ± 0.002	39.7 ± 5.6	3.266 ± 0.140	33.0 ± 5.6	
			Blue	0.051 ± 0.002	20.9 ± 5.6	1.125 ± 0.130	−5.8 ± 5.6	
215596.0	SiO, $v = 1$	$J = 5 \rightarrow 4$	Central	0.390 ± 0.002	13.9 ± 2.8	5.747 ± 0.060	26.7 ± 2.8	
215697.5	SiS, $v = 2$	$J = 12 \rightarrow 11$	Central	0.006 ± 0.002	11.2 ± 5.9	0.104 ± 0.029	19.8 ± 2.8	
215839.9	^{34}SO	$N_J = 5_6 \rightarrow 4_5$	Central	0.007 ± 0.002	46.7 ± 8.3	0.302 ± 0.044	22.5 ± 8.3	
215939	U		Central	0.005 ± 0.002	22.8 ± 8.3	0.110 ± 0.034	19.0	
216531.4	$Na^{37}Cl$	$J = 17 \rightarrow 16$	Central	0.005 ± 0.002	17.2 ± 5.6	0.054 ± 0.015	15.8 ± 5.6	
216643.3	SO_2	$J_{\rm Ka,Kc} = 22_{2,20} \rightarrow 22_{1,21}$	Red	0.007 ± 0.001	41.4 ± 8.3	0.340 ± 0.060	35.5 ± 8.3	P
216710.4	H_2S	$J_{\rm Ka,Kc} = 2_{2,0} \rightarrow 2_{1,1}$	Central	0.015 ± 0.001	52.4 ± 8.3	0.890 ± 0.070	26.9 ± 8.3	P
216757.6	SiS, $v = 1$	$J = 12 \rightarrow 11$	Central	0.006 ± 0.001	11.4 ± 5.6	0.075 ± 0.040	19.9 ± 5.6	P
217105.0	SiO	$J = 5 \rightarrow 4$	Central	0.796 ± 0.001	43.1 ± 2.8	36.484 ± 0.060	21.5 ± 2.8	
217817.7	SiS	$J = 12 \rightarrow 11$	Central	0.034 ± 0.002	25.0 ± 2.8	0.900 ± 0.050	18.2 ± 2.8	
			Red	0.020 ± 0.002	12.3 ± 2.8	0.362 ± 0.030	44.4 ± 2.8	
			Blue	0.014 ± 0.002	9.2 ± 2.8	0.139 ± 0.039	−3.4 ± 2.8	

Notes.
[a] Uncertainty range is $\pm 1\sigma$, measured from 2 MHz resolution data.
[b] Full width at half-maximum.
B: unresolvable blend of emission lines from different molecules.
P: partial blend of resolvable emission features.
R: $\nu_{\rm rest}$ is average of rotational transition frequencies.
F: $\nu_{\rm rest}$ is average of fine-structure transition frequencies.
H: $\nu_{\rm rest}$ is average of hyperfine-structure transition frequencies.
?: uncertain line assignment.

(This table is available in its entirety in a machine-readable form in the online journal. A portion is shown here for guidance regarding its form and content.)

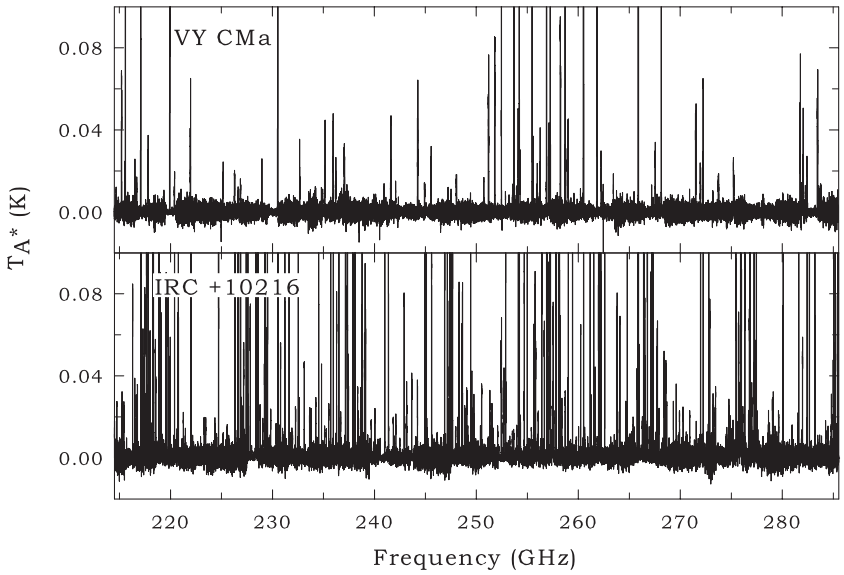

Figure 4. Entire ARO SMT survey of VY CMa and IRC +10216, condensed into one spectrum for the 214.5–285.5 GHz region of each source with identical intensity scales. The temperature scale is truncated at $T_A^* = 0.1$ K to show the weaker lines. It is clear from this figure that IRC +10216 contains many more spectral lines than VY CMa.

4. DISCUSSION

4.1. Overview of the Survey

In Figures 4 and 5, overviews of the survey are presented. Figure 4 displays the survey data from both sources on an antenna temperature scale of 0.1 K, giving a snapshot of the relative complexity of the molecular content of IRC +10216 relative to VY CMa. In Figure 5, the intensity scale is determined by the strongest features in both sources, excluding the water maser line at 267 GHz in VY CMa. Figure 4 clearly illustrates that there are far more spectral lines in IRC +10216 than VY CMa, but the latter source is nonetheless not devoid of molecular emission. In both objects, CO, HCN, and SiO ($v = 0$) are responsible for some of the most intense emission features, as exemplified in Figure 5. In VY CMa, the other strong lines arise from vibrationally excited H_2O and SiO, while in IRC +10216, SiS, CS, CCH, HNC, and CN also cause prominent features.

Tables 3 and 4 summarize the various molecular species identified in the survey in IRC +10216 and VY CMa, respectively. For each chemical compound, the observed isotopologues, vibrationally excited states, and the number of discernable lines are also listed, as well as the total number of lines per source.

In IRC +10216, a total of 717 lines were observed, arising from 32 different molecules, and "U" lines make up 18% of the features, or 126 lines (see Table 3). Of the 32 molecules seen in the 1 mm spectrum of IRC +10216, nine are radicals (CN, CP, SiC, CCH, l-C_3H, c-C_3H, C_3N, SiN, and C_4H) and one is an ion (HCO^+). Two molecules, SiC_2 and C_4H, in their various isotopologues and vibrational states (Table 3), account for 36% of the observed lines in the survey of IRC +10216. SiC_2 accounts for 132 of the emission features and C_4H produces 124 individual lines. SiS contributes a total of 47 spectral features, including its $v = 0$–4 states and the ^{29}SiS, ^{30}SiS, $Si^{34}S$, $Si^{33}S$, $^{30}Si^{34}S$, and $^{29}Si^{34}S$ isotopic variations. The next most prominent species is NaCN in its $v = 0$ state, with 38 emission lines, all with relatively weak intensities ($T_A^* = 2$–11 mK). A number of molecules that are present in lower frequency data are notably absent from the 215–285 GHz spectral region, for example the carbon chains HC_9N, HC_7N, HC_5N, HC_2N, C_6H, C_5H, C_4H_2, C_4Si, C_3S, C_2S, and the refractory-containing molecule MgNC. These heavier molecules have their prominent emission lines at wavelengths of 2 mm or longer (see Cernicharo et al. 2000). Finally, the He et al. (2008) survey assigned a weak line at 258707 MHz to the SiO ($v = 1$) $J = 6 \rightarrow 5$ transition in IRC +10216. We identify this feature instead as the $J_{\mathrm{Ka,Kc}} = 12_{0,12} \rightarrow 11_{0,11}$ transition of $^{29}SiC_2$. The intensity is consistent with other transitions of $^{29}SiC_2$ in the 1 mm band.

In VY CMa, a total of 130 molecular features were detected from 18 different chemical compounds, with 14 lines remaining unidentified (see Table 4). Of the 18 molecules seen the VY CMa data, five are radicals (SO, CN, NS, PO, and AlO), and one is an ion (HCO^+). For molecules that only have one transition at 1 mm (HNC and HCO^+, for example), 2 and 3 mm lines were also observed as confirming data: see Ziurys et al. (2007, 2009). Sulfur dioxide in its main and $^{34}SO_2$ isotopologue accounts for 35 of the observed emission lines, and SiS is the next most prevalent species with 21 lines arising from its main and ^{29}SiS, ^{30}SiS, $Si^{34}S$ isotopologues and $v = 0, 1, 2$ vibrational states. It is notable that only diatomic and triatomic molecules are detected in the 1 mm survey band, and the most common types of species seen are oxides and sulfides. A four-atom polyatomic species, NH_3, has also been observed in VY CMa (Monnier et al. 2000).

Approximately five times more spectral lines were detected in IRC +10216 than in VY CMa. While IRC +10216 is relatively close to earth, at a distance of 150 pc, VY CMa is almost an order of magnitude farther away ($d = 1.14$ kpc). If VY CMa were at the distance of IRC +10216, it is likely that its spectrum would show a comparable number of emission features.

4.2. Variations in Line Profiles

4.2.1. Narrow Lines in IRC +10216

In IRC +10216, widths of the vast majority of lines reflect the well-known terminal expansion velocity of 14 km s^{-1} (Cernicharo et al. 2000). As discussed in many other papers, spectral line shapes in IRC +10216 range from flat topped, arising from optically thin, unresolved emission, to U-shaped, from optically thin, resolved shell emission, to parabolic, from

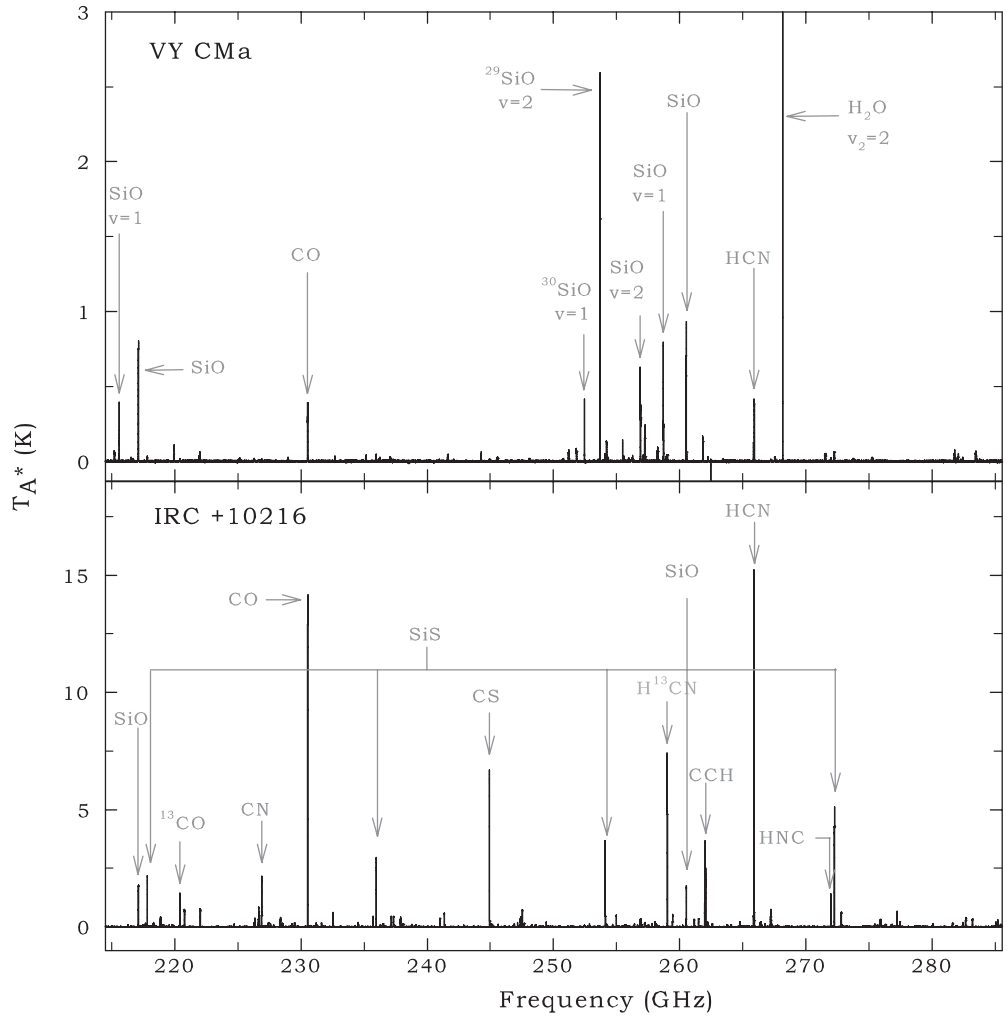

Figure 5. Entire ARO SMT survey of VY CMa and IRC +10216 over the complete frequency range, plotted on a temperature scale set by the strongest features in each source. The most intense line ($T_A^* \sim 14$ K) in the 1 mm band of VY CMa, attributed to a rotational transition of water in its $v_2 = 2$ vibrational state, has been truncated. Strong emission features from CO, HCN, and SiO are common to both envelopes, as the figure shows. VY CMa also exhibits substantial maser lines from minor isotopologues and vibrationally excited states of SiO. In IRC +10216, other prominent lines arise from SiS, CS, CN, HNC, and CCH.

optically thick resolved and unresolved emission (Olofsson et al. 1982).

A number of lines show unusually narrow linewidths ($V_{\rm exp} \leqslant 10$ km s^{-1}), signaling that they arise from the very inner regions of the CSE where gas has not yet reached terminal velocity. These features are listed in Table 5. While some of the narrow lines could not be identified, many can be attributed to vibrationally excited states of SiS, CS, CO, HCN, and SiC_2, as well as KCl in its $v = 0$ state. The lowest value of $V_{\rm exp}$ detected was found to be 3 km s^{-1}, arising from the $v = 1$ levels of CO ($J = 2 \rightarrow 1$) and ^{29}SiS ($J = 14 \rightarrow 13$); CO in its $v = 1$ state had been previously identified by Patel et al. (2009a). Other SiS lines in the $v = 1$, 2, 3, and 4 states exhibit expansion velocities ranging from 3.9 to 7.6 km s^{-1}. Patel et al. (2009b) had observed some of these same states in SiS at 345 GHz. HCN emission from the $(v_1,v_2,v_3) = (1,2,0)$, (0,3,0), and (0,4,0) states also exhibit very narrow lines ($V_{\rm exp} \sim 7$ km s^{-1}). To our knowledge, our measurements are the first detections of the HCN (1,2,0) and (0,3,0) levels. Interestingly, two transitions of KCl in its ground vibrational state were found to have $V_{\rm exp} \sim$ 8–9 km s^{-1}. Cernicharo et al. (2000) reported KCl lines with expansion velocities ranging from 7.8 to 13.5 km s^{-1} at 2 mm, in agreement with these findings.

Recently, Shinnaga et al. (2009) imaged four narrow lines of HCN, KCl, and Si^{34}S at 265 GHz using the eSMA, with a beam size of $0\farcs22 \times 0\farcs46$. The exact same lines were detected in our survey data. Shinnaga et al. assigned one of the lines, at 265265 MHz ($V_{\rm exp} = 4.6$ km s^{-1}), to the $J = 35 \rightarrow 34$ transition of KCl in the $v = 2$ level. However, throughout our survey, no other lines of KCl in either the $v = 1$ or $v = 2$ levels were detected. Upper limits for these transitions were 2–7 mK, much lower than the 11 mK intensity of the feature at 265265 MHz (see Figure 1 and Table 1). Therefore, we assign the feature at 265265 MHz as unidentified until there is further evidence for vibrationally excited KCl.

4.2.2. Multi-component Line Profiles in VY Canis Majoris

The line profiles in VY CMa are decidedly more complex than those from spherical outflows such as that of IRC +10216 and vary between chemical species (see Figure 3). As discussed in Ziurys et al. (2007, 2009), transitions of CO, CS, and SiS exhibit three velocity components (central spherical wind, red-shifted flow, blue-shifted flow) while lines of SO_2 and HNC have only red and blue components and essentially no emission at the central $V_{\rm LSR}$. Conversely, emission from NaCl, PN, vibrationally

Table 3
Molecular Lines Observed in the 1 mm Spectrum of IRC +10216

Molecule	Variation	No. of Lines	Molecule	Variation	No. of Lines
CO	$v = 1$, ^{13}CO, C^{18}O, C^{17}O	5	CCH	$v_2 = 1$, ^{13}CCH, C^{13}CH, CCD	17
CS	$v = 1$, ^{13}CS, C^{33}S, C^{34}S, ^{13}C^{33}S, ^{13}C^{34}S	10	CH_2NH		9
CN	^{13}CN	16	CH_3CN		24
CP		2	CH_3CCH		7
SiC		8	l-C_3H	$v_4 = 1$, ^{13}CCCH	17
NaCN		38	c-C_3H		12
SiO	^{29}SiO, ^{30}SiO, Si^{18}O	6	C_3N		14
NaCl	Na^{37}Cl	11	PH_3		1
AlCl	Al^{37}Cl	10	H_2CO		3
KCl		9	H_2CS		9
AlF		2	HC_3N	$v_7 = 1$	13
PN		2	c-C_3H_2		16
HNC	$v_2 = 1$, HN^{13}C	3	SiN		4
HCP		2	HCO^+		1
SiC_2	$v_3 = 1$, ^{29}SiC_2, ^{30}SiC_2, Si^{13}CC	132	SiS	$v = 1$, $v = 2$, $v = 3$, $v = 4$, ^{29}SiS, ^{30}SiS, Si^{33}S, Si^{34}S, ^{29}Si^{34}S, ^{30}Si^{34}S, ^{29}SiS $v = 1$, ^{30}SiS $v = 1$, Si^{34}S $v = 1$	47
HCN	(v_1,v_2,v_3) = (1,0,0), (0,1,0), (0,0,1), (0,1,1), (1,1,0), (0,2,0), (0,3,0), (0,4,0), (1,2,0), H^{13}CN, HC^{15}N, H^{13}C^{15}N, H^{13}CN (0,1,0)	17	C_4H	$v_7 = 1^1$, $v_7 = 2^0$, $v_7 = 2^2$, ^{13}CCCCH, C^{13}CCCH, CC^{13}CCH, CCC^{13}CH	124
U		126			
Total number of lines = 717					

Table 4
Molecular Lines Observed in the 1 mm Spectrum of VY CMa

Molecule	Variation	No. of Lines
CO	^{13}CO	2
SiO	$v = 1$, $v = 2$, ^{29}SiO, ^{30}SiO, Si^{18}O, ^{29}SiO $v = 1$, ^{29}SiO $v = 2$, ^{30}SiO $v = 1$	12
SiS	$v = 1$, $v = 2$, ^{29}SiS, ^{30}SiS, Si^{34}S	21
SO	^{34}SO	7
CS		1
CN		3
NS		2
NaCl	$v = 1$, Na^{37}Cl	12
PN		2
PO		6
AlO		2
H_2O	$v_2 = 1$, $v_2 = 2$	3
H_2S		1
HCN	(v_1,v_2,v_3) = (0,1,0), H^{13}CN	3
HNC		1
SO_2	$v_2 = 1$, ^{34}SO_2	35
AlOH		2
HCO^+		1
U		14
Total number of lines		130

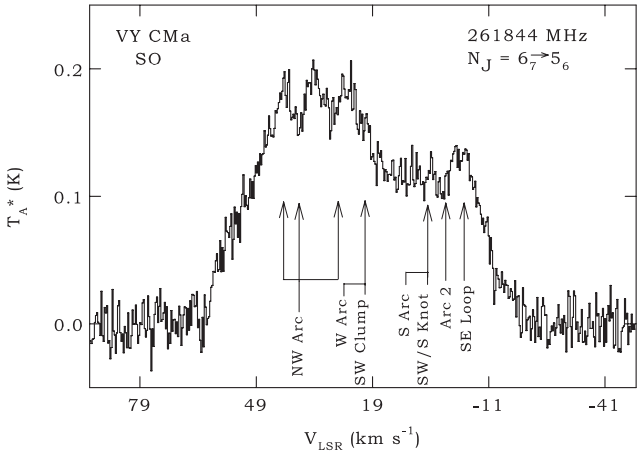

Figure 6. High-resolution (250 kHz per channel) spectrum of the SO, $N_J = 6_7 \rightarrow 5_6$ transition at 262 GHz in VY CMa. V_{LSR} values corresponding to atomic spectra observed at prominent infrared dust features in VY CMa (Humphreys et al. 2007) are denoted with vertical arrows. The three small peaks comprising the broad red-shifted feature, which correspond to the three velocities of the NW arc, highlight the kinematic complexity of the molecular outflows in this source. Molecular emission is also present at the velocities of other IR features (e.g., SE Loop, Arc 2, etc.). The kinematic correspondence between SO emission and the gas associated with infrared dust emission suggests that the molecular outflows and dust structures are associated.

excited SiS, and thermal SiO only arises from the central component.

As discussed in Ziurys et al. (2007, 2009), the unusual molecular line shapes are caused by a highly asymmetric, complex outflow. *Hubble Space Telescope* (*HST*) imaging of dust emission in VY CMa has shown a multitude of jets, arcs, and knots of dust and gaseous material flowing from the star, extending to an angular diameter of ∼12″, or ∼14,000 AU (Smith et al. 2001). More recent slit spectroscopy of CO rovibrational lines at 4.6 μm shows individual knots distributed radially around the star, with no clear large-scale axis of symmetry (Smith et al. 2009). Two of the most prominent outflows traced by dust in the infrared have been designated the Northwest Arc and Arc 2 (Humphreys et al. 2005, 2007). As proposed by Ziurys et al. (2007), molecular emission is likely associated with these dusty outflows and their clumpy structures. This close association is illustrated in Figure 6. Here, one of the survey lines, the $N_J = 6_7 \rightarrow 5_6$ transition of SO, is shown, observed with 250 kHz resolution. What is

Table 5
Narrow Emission Lines in IRC +10216

ν_{rest} (MHz)	Molecule	Transition	ΔV_{HWZP}[a] (km s^{-1})
228439.1	CO, $v = 1$	$J = 2 \rightarrow 1$	3.0 ± 1.0
248232.6	^{29}SiS, $v = 1$	$J = 14 \rightarrow 13$	3.0 ± 1.2
266941.8[b]	SiS, $v = 4$	$J = 15 \rightarrow 14$	3.9 ± 1.1
219257.9	U		4.2 ± 0.7
264862.5	U		4.5 ± 2.3
239284.3	U		4.6 ± 1.3
263518.8	Si^{34}S, $v = 1$	$J = 15 \rightarrow 14$	4.6 ± 1.1
267423.6	U		4.6 ± 1.1
247918.0	U		4.8 ± 1.2
251629.6[b]	SiS, $v = 2$	$J = 14 \rightarrow 13$	4.8 ± 1.2
271552.2	U		4.9 ± 1.1
267264.4	U		4.9 ± 1.1
250976.3	U		5.0 ± 1.2
224229.4	U		5.4 ± 2.6
251910.3	U		6.0 ± 2.4
253231.3	U		6.0 ± 2.4
261567.5	U		6.0 ± 2.0
270449.4	U		6.0 ± 2.2
281075.5	Si^{34}S, $v = 1$	$J = 16 \rightarrow 15$	6.4 ± 1.1
250392.6	SiS, $v = 3$	$J = 14 \rightarrow 13$	6.4 ± 1.2
265384.2	HCN, $(v_1,v_2,v_3) = (1,2^0,0)$	$J = 3 \rightarrow 2$	6.6 ± 1.5
275383.0	U		6.7 ± 4.4
269592.7	SiS, $v = 2$	$J = 15 \rightarrow 14$	7.0 ± 1.1
268663.3	HCN, $(v_1,v_2,v_3) = (0,4^0,0)$	$J = 3 \rightarrow 2$	7.0 ± 1.1
251660.5	U		7.1 ± 1.2
266540.0	HCN, $(v_1,v_2,v_3) = (0,3^{1c},0)$	$J = 3 \rightarrow 2$	7.2 ± 1.1
251081.2	U		7.2 ± 1.2
215697.5	SiS, $v = 2$	$J = 12 \rightarrow 11$	7.6 ± 1.4
283835.7	KCl	$J = 37 \rightarrow 36$	7.6 ± 1.1
251793.9	U		8.3 ± 1.2
243160.8[b]	CS, $v = 1$	$J = 5 \rightarrow 4$	9.0 ± 4.8
222665.5	KCl	$J = 29 \rightarrow 28$	9.1 ± 1.0
256542.5	SiC_2, $v_3 = 1$	$J_{Ka,\,Kc} = 11_{3,\,9} \rightarrow 10_{3,\,8}$	9.7 ± 1.2
269498.7	U		10.0 ± 4.2

Notes.
[a] Half-width at zero power, also referred to as expansion velocity (V_{exp}).
[b] Partially blended with another molecular transition.

striking about this spectrum is the more complex kinematic structure apparent in the three small peaks that make up the red-shifted component. Furthermore, the LSR velocities of all three peaks roughly correspond to velocities of atomic transitions from Humphreys et al. (2007) observed across the Northwest Arc, as indicated in the figure. A similar situation exists for Arc 2 and the blue-shifted wind (see Figure 6). Other velocity components observed by Humphreys et al. (2007) also align with the molecular emission. As shown in Figure 6, the South Arc, Southeast Loop, and South and West knots all fall at V_{LSR} values in the range −5 to 5 km s^{-1}, near the blue-shifted molecular outflow, and the Southwest Clump and West Arc show LSR velocities of ∼21 km s^{-1}, near the central component. Therefore, the presence of three velocity components is probably an oversimplification. In circumstellar envelopes, gas and dust acceleration are intimately linked (e.g., Verhoelst et al. 2009); thus, it is expected that the molecular gas structure would reflect that of the dust. Emission lines from other molecules such as SO_2, HCN, SiS, and CO also show a similar correspondence with the velocities of the dust outflows (see Ziurys et al. 2007, 2009).

SMA observations of SO and CO by Muller et al. (2007) did reveal three outflow components at $V_{LSR} = -5$, 20, and 45 km s^{-1}. Muller et al. interpreted the red- and blue-shifted components as arising from a wide bipolar outflow along the line of sight, but they did note that there was some correspondence to the dust features seen with the *HST*. The spatial resolution of the SMA observations was 2″ (Muller et al. 2007), but the entire angular extent of CO and dust emission is ∼10″–12″ (Ziurys et al. 2009; Smith et al. 2001). The resolution of the SMA observations may have been too coarse to distinguish the small irregular structures found by Humphreys et al. (2007) and Smith et al. (2009).

4.3. A Summary of New Molecular Species and Transitions

In the course of this survey, four new molecules containing refractory elements were discovered in the envelopes of VY CMa and IRC +10216: PO, PH_3, AlO, and AlOH. The details of these observations can be found elsewhere (Tenenbaum et al. 2007; Tenenbaum & Ziurys 2008, 2009, 2010). In the case of AlO and AlOH, transitions at 2 mm were also measured to confirm the identification. PO, AlO, and AlOH were discovered in VY CMa, making this source a new molecular "hunting ground" favoring a unique oxide chemistry. Millimeter-wave lines from all three of these species had been unsuccessfully searched for in the past in a variety of astronomical objects, including molecular clouds and C-rich and O-rich circumstellar envelopes (Turner 1991,

Table 6
Observed Versus Catalog Frequencies for NaCN

Transition	ν_{obs} (MHz)	ν_{rest} [a] (MHz)	$\nu_{obs} - \nu_{rest}$ (MHz)
$J_{Ka,Kc} = 17_{4,14} \rightarrow 16_{4,13}$	266163.7 ± 4	266178.5	−14.8
$J_{Ka,Kc} = 16_{6,11} \rightarrow 15_{6,10}$; $16_{6,10} \rightarrow 15_{6,9}$	249499.3 ± 4	249512.8[b]	−13.5
$J_{Ka,Kc} = 16_{3,13} \rightarrow 15_{3,12}$	252138.2 ± 2	252149.8	−11.6
$J_{Ka,Kc} = 17_{6,12} \rightarrow 16_{6,11}$; $17_{6,11} \rightarrow 16_{6,10}$	265116.7 ± 4	265126.3[b]	−9.6
$J_{Ka,Kc} = 18_{5,14} \rightarrow 17_{5,13}$; $18_{5,13} \rightarrow 17_{5,12}$	281279.0 ± 2	281288.3[b]	−9.3
$J_{Ka,Kc} = 17_{5,13} \rightarrow 16_{5,12}$; $17_{5,12} \rightarrow 16_{5,11}$	265609.1 ± 4	265616.9[b]	−7.8
$J_{Ka,Kc} = 17_{3,14} \rightarrow 16_{3,13}$	268288.7 ± 4	268295.4	−6.7
$J_{Ka,Kc} = 15_{4,11} \rightarrow 14_{4,10}$	234785.0 ± 2	234791.7	−6.7
$J_{Ka,Kc} = 16_{1,15} \rightarrow 15_{1,14}$	254942.2 ± 6	254948.8	−6.6
$J_{Ka,Kc} = 18_{2,17} \rightarrow 17_{2,16}$	278370.4 ± 2	278377.0	−6.6
$J_{Ka,Kc} = 14_{5,10} \rightarrow 13_{5,9}$; $14_{5,9} \rightarrow 13_{5,8}$	218641.7 ± 1	218647.6[b]	−5.9
$J_{Ka,Kc} = 17_{2,15} \rightarrow 16_{2,14}$	273268.6 ± 4	273274.4	−5.8
$J_{Ka,Kc} = 15_{7,9} \rightarrow 14_{7,8}$; $15_{7,8} \rightarrow 14_{7,7}$	233511.0 ± 4	233516.7[b]	−5.7
$J_{Ka,Kc} = 17_{3,15} \rightarrow 16_{3,14}$	266348.9 ± 4	266354.5	−5.6
$J_{Ka,Kc} = 15_{6,10} \rightarrow 14_{6,9}$; $15_{6,9} \rightarrow 14_{6,8}$	233897.0 ± 4	233902.6[b]	−5.6
$J_{Ka,Kc} = 15_{5,11} \rightarrow 14_{5,10}$; $15_{5,10} \rightarrow 14_{5,9}$	234291.5 ± 2	234297.1[b]	−5.6
$J_{Ka,Kc} = 16_{3,14} \rightarrow 15_{3,13}$	250685.6 ± 4	250691.0	−5.4
$J_{Ka,Kc} = 18_{1,17} \rightarrow 17_{1,16}$	285358.2 ± 2	285361.9	−3.7
$J_{Ka,Kc} = 15_{2,13} \rightarrow 14_{2,12}$	240507.1 ± 2	240510.5	−3.4
$J_{Ka,Kc} = 14_{4,11} \rightarrow 13_{4,10}$	219037.6 ± 1	219040.9	−3.3
$J_{Ka,Kc} = 16_{1,16} \rightarrow 15_{1,15}$	238937.4 ± 4	238940.3	−2.9
$J_{Ka,Kc} = 14_{3,12} \rightarrow 13_{3,11}$	219322.0 ± 1	219324.3	−2.3
$J_{Ka,Kc} = 15_{3,12} \rightarrow 14_{3,11}$	236081.3 ± 4	236083.5	−2.2
$J_{Ka,Kc} = 14_{4,10} \rightarrow 13_{4,9}$	219068.0 ± 1	219070.1	−2.1
$J_{Ka,Kc} = 15_{4,12} \rightarrow 14_{4,11}$	234742.1 ± 2	234744.0	−1.9
$J_{Ka,Kc} = 14_{3,11} \rightarrow 13_{3,10}$	220089.0 ± 4	220089.9	−0.9
$J_{Ka,Kc} = 15_{3,13} \rightarrow 14_{3,12}$	235012.7 ± 2	235012.8	−0.1
$J_{Ka,Kc} = 15_{2,14} \rightarrow 14_{2,13}$	232751.4 ± 4	232751.4	0.0
$J_{Ka,Kc} = 17_{1,17} \rightarrow 16_{1,16}$	253616.1 ± 3	253615.9	0.2
$J_{Ka,Kc} = 15_{1,14} \rightarrow 14_{1,13}$	239549.3 ± 2	239549.0	0.3
$J_{Ka,Kc} = 15_{0,15} \rightarrow 14_{0,14}$	226584.8 ± 4	226583.4	1.4
$J_{Ka,Kc} = 14_{1,13} \rightarrow 13_{1,12}$	224035.9 ± 2	224032.5	3.4

Notes.
[a] ν_{rest} is taken from the CDMS database, 2007 April entry.
[b] ν_{rest} is an average of the both listed transition frequencies.

1995; Matthews et al. 1987). PH_3 was found in IRC+10216, but not VY CMa. The higher sensitivity achieved in this survey has been a key factor in finding these long-sought species. Additionally, NaCl, PN, NS, and HCO^+ were observed in VY CMa (Ziurys et al. 2007, 2009), representing the first detections of these molecules in an O-rich CSE. Overall, six phosphorus-containing molecules have currently been observed in circumstellar envelopes (also CP, HCP, and CCP: Milam et al. 2008; Agúndez et al. 2007; Halfen et al. 2008), striking evidence for an active gas-phase chemistry of this element.

The organic molecule methyleneamine (CH_2NH) was also detected in IRC +10216 via nine rotational transitions in the 1 mm band. This molecule has previously been observed in giant molecular clouds (Dickens et al. 1997) and in an ultra luminous infrared galaxy (Salter et al. 2008), but never before in a circumstellar envelope. Line parameters of the observed CH_2NH features are included in Table 1. Details of this detection, including the derived abundance and distribution, and possible formation mechanisms for CH_2NH can be found in Paper I.

Other interesting identifications in the survey arise from highly excited species. The most intense emission line observed in VY CMa arises from the $v_2 = 2$, $J_{Ka,Kc} = 6_{5,2} \rightarrow 7_{4,3}$ transition of H_2O at 268149 MHz—the first detection of a water line in the $v_2 = 2$ state. Previous work showed the presence of radio and infrared lines of water in the $v_2 = 1$ and $v_2 = 0$ states (e.g., Menten et al. 2006; Polehampton et al. 2010). Additional new discoveries include the observation of vibrationally excited NaCl, found in VY CMa, and some new vibrational states of HCN in its bending mode in IRC+10216, as mentioned. The CCH radical was also observed in the first quantum of its bending mode; three clean features were identified, arising from the structure in the *l*-type doublets (see Table 1). The astrophysical implications of these highly excited states are discussed elsewhere (Paper I).

4.4. Directions for Laboratory Spectroscopy and Unidentified Features

A number of emission lines from the T-shaped molecule NaCN showed significant deviations in their observed frequencies from their catalog values, as much as 15 MHz, indicating that the accepted spectroscopic parameters for this molecule should be revised. Table 6 lists the unblended observed transitions of NaCN, along with observed versus catalog frequency differences. Catalog frequencies were taken from the 2007 April entry in the CDMS database, described by He et al. (2008). The laboratory data used in the catalog predictions only consists of 20 transitions, all in the 9–40 GHz range (van Vaals et al. 1984).

Even after an improved spectral fit with additional centrifugal distortion terms (He et al. 2008), the predicted frequencies in the 1 mm region are still inaccurate, as illustrated in Table 6. Because the most unreliable catalog frequencies belong to transitions that are relatively weak in IRC +10216, further laboratory measurements in the 1, 2, and 3 mm ranges should made in order to provide accurate rest frequencies (±0.5 MHz) and refine the spectroscopic constants. Such measurements are currently underway at Arizona (D. T. Halfen et al. 2011, in preparation).

The large number of unidentified lines detected in this survey highlights the need for additional laboratory studies of the rotational spectra of possible circumstellar molecules. Toward IRC +10216 and VY CMa, 126 and 14 U-lines were observed in the 1 mm band, respectively, as mentioned. The majority of these lines are weak, with intensities of $T_A^* \leqslant 10$ mK. An analysis of the set of U-lines in each object did not reveal any harmonically spaced series. This is not surprising, because every line of a given harmonic series would not necessarily be detected, either due to a low signal-to-noise ratio or obscuration by another molecular transition. In IRC +10216, however, a number of the U-lines do appear as closely spaced doublets. For example, a doublet of narrow lines ($T_A^* \sim 4$ mK) is apparent in the IRC +10216 data, centered at 266657 MHz and split by 36 MHz. One can speculate that such "doublets" arise from the same free radical, but relevant laboratory data are clearly needed.

None of observed U-lines appear to be common to both sources. The fact that VY CMa and IRC +10216 show entirely different sets of U-lines is an indication of the contrasting chemical environments in these two objects (see Paper I). It is probable that the U lines in IRC +10216 arise from carbon-bearing molecules, while the unidentified features in VY CMa are due to compounds containing oxygen or sulfur.

Many of the U-lines in VY CMa and IRC +10216 exhibit narrow line widths, and are most likely caused by emission arising from within the dust acceleration zone. In VY CMa, for example, two unidentified lines with $T_A^* \sim 5$ mK and $\Delta V_{1/2} \sim 10$ km s^{-1} are present at 228418 MHz and 279486 MHz. Another example is in IRC +10216, where an 18 mK, narrow ($V_{\rm exp} = 5$ km s^{-1}) feature is observed at 271552 MHz. These and the other narrow U-lines may be coming from vibrationally excited states of known circumstellar molecules, or from new circumstellar species that are formed in the inner envelope region. Additional laboratory efforts should be made to measure rotational spectra of excited species such as CCH ($A^2\Pi$) and of probable inner shell species such as KO. These laboratory efforts will assist line identification not only in this data set, but also in CSE spectra observed with the SMA, Herschel, and in the future, ALMA.

5. CONCLUSIONS

The first continuous millimeter-wave spectral survey of an oxygen-rich circumstellar envelope has proven that these objects have greater chemical complexity than previously thought. VY CMa has now been recognized as a source of new chemical species. This work has also demonstrated that an increase in sensitivity by factors of 5–10 can lead to new discoveries, even for sources that have been well studied such as IRC +10216, in atmospheric windows that have long been accessible (1 mm). The total number of U-lines found in the survey demonstrates the need for additional laboratory spectroscopic measurements, for both new species and known ones such as NaCN. The total number of molecules identified in circumstellar envelopes is now 80, comprising over half of the known molecules in the interstellar medium.

We thank the operators, engineers, and support staff of the ARO for their assistance, and Dr. Aldo Apponi for his input when initiating the survey. We also thank A. Kerr and the National Radio Astronomy Observatory and A. Lichtenberger of the University of Virginia Microfabrication Laboratory for the Band 6 mixer development. Finally, we appreciate Karl Menten for sharing his insights on water emission in VY CMa. This research is supported by NSF grant AST-06-07803 and AST-09-06534 and the NASA Astrobiology Institute under cooperative agreement CAN-02-0SS02 issued through the Office of Space Science. E.D.T. acknowledges support from an NSF graduate research fellowship.

REFERENCES

Agúndez, M., & Cernicharo, J. 2006, ApJ, 650, 374
Agúndez, M., Cernicharo, J., & Guélin, M. 2007, ApJ, 662, L91
Avery, L. W., et al. 1992, ApJS, 83, 363
Bowers, P. E., Johnston, K. J., & Spencer, J. H. 1983, ApJ, 274, 733
Bujarrabal, V., Fuente, A., & Omont, A. 1994, A&A, 285, 247
Cernicharo, J., Guélin, M., & Kahane, C. 2000, A&AS, 142, 181
Cernicharo, J., et al. 1996, A&A, 315, L201
Cherchneff, I. 2006, A&A, 456, 1001
Choi, Y. K., et al. 2008, PASJ, 60, 1007
Decin, L., De Beck, E., Brünken, S., Müller, H. S. P., & Menten, K. M., et al. 2010, A&A, 516, A69
Dickens, J. E., Irvine, W. M., De Vries, C. H., & Ohishi, M. 1997, ApJ, 479, 307
Dorschner, J., & Henning, T. 1995, A&AR, 6, 271
Groesbeck, T. D., Phillips, T. G., & Blake, G. A. 1994, ApJS, 94, 147
Guelin, M., Cernicharo, J., Paubert, G., & Turner, B. E. 1990, A&A, 230, L9
Halfen, D. T., Clouthier, D. J., & Ziurys, L. M. 2008, ApJ, 677, L101
He, J. H., Dinh-V-Trung, Kwok, S., Müller, H. S. P., Zhang, Y., Hasegawa, T., Peng, T. C., & Huang, Y. C. 2008, ApJS, 177, 275
Humphreys, R. M., Davidson, K., Ruch, G., & Wallerstein, G. 2005, AJ, 129, 492
Humphreys, R. M., Helton, L. A., & Jones, T. J. 2007, AJ, 133, 2716
Johansson, L. E. B., Andersson, C., Elder, J., Friberg, P., Hjalmarson, A., Hoglund, B., Oloffson, H., Rydbeck, G., & Irvine, W. M. 1985, A&AS, 60, 135
Kawaguchi, K., Kasai, Y., Ishikawa, S., & Kaifu, N. 1995, PASJ, 47, 853
Matthews, H. E., Feldman, P. A., & Bernath, P. F. 1987, ApJ, 312, 358
Menten, K. M., & Alcolea, J. 1995, ApJ, 448, 416
Menten, K. M., Lundgren, A., Belloche, A., Thorwirth, S., & Reid, M. J. 2008, A&A, 477, 185
Menten, K. M., Philipp, S. D., Güsten, R., Alcolea, J., Polehampton, E. T., & Brünken, S. 2006, A&A, 454, L107
Milam, S. N., Apponi, A. J., Woolf, N. J., & Ziurys, L. M. 2007, ApJ, 668, L131
Milam, S. N., Halfen, D. T., Tenenbaum, E. D., Apponi, A. J., Woolf, N. J., & Ziurys, L. M. 2008, ApJ, 684, 618
Millar, T. J., & Herbst, E. 1994, A&A, 288, 561
Millar, T. J., Herbst, E., & Bettens, R. P. A. 2000, MNRAS, 316, 195
Monnier, J. D., Danchi, W. C., Hale, D. S., Lipman, E. A., Tuthill, P. G., & Townes, C. H. 2000, ApJ, 543, 861
Müller, H. S. P., Schlöder, F., Stutzki, J., & Winnewisser, G. 2005, J. Mol. Struct., 742, 215
Muller, S., Dinh-V-Trung, , Lim, J., Hirano, N., Muthu, C., & Kwok, S. 2007, ApJ, 656, 1109
Omont, A., Lucas, R., Morris, M., & Guilloteau, S. 1993, A&A, 267, 490
Olofsson, H. 2005, in Proc. Dusty Molecular Universe, A Prelude to Herschel and ALMA, ed. A. Wilson (Noordwijk: ESA), 223
Olofsson, H., Johansson, L. E. B., Hjalmarson, A., & Nguyen-Quang-Rieu, 1982, A&A, 107, 128
Olofsson, H., Lindqvist, M., Nyman, L.-Å., & Winnberg, A. 1997, A&A, 329, 1059
Patel, N. A., Young, K. H., Brünken, S., Menten, K. M., Thaddeus, P., & Wilson, R. W. 2009a, ApJ, 691, L55
Patel, N. A., et al. 2009b, ApJ, 692, 1205
Pickett, H. M., Poynter, R. L., Cohen, E. A., Delitsky, M. L., Pearson, J. C., & Müller, H. S. P. 1998, J. Quant. Spectrosc. Radiat. Trans., 60, 883

Polehampton, E. D., Menten, K. M., Van Der Tak, F. F. S., & White, G. J. 2010, A&A, 510, 80
Salter, C. J., Ghosh, T., Catinella, B., Lebron, M., Lerner, M. S., Minchin, R., & Momjian, E. 2008, AJ, 136, 389
Schöier, F. L., & Olofsson, H. 2001, A&A, 368, 969
Shinnaga, H., Moran, J. M., Young, K. H., & Ho, P. T. P. 2004, ApJ, 616, L47
Shinnaga, H., et al. 2009, ApJ, 698, 1924
Smith, N., Hinkle, K. H., & Ryde, N. 2009, AJ, 137, 3558
Smith, N., Humphreys, R. M., Davidson, K., Gehrz, R. D., Schuster, M. T., & Krautter, J. 2001, AJ, 121, 1111
Tenenbaum, E. D., Dodd, J. L., Milam, S. N., Woolf, N. J., & Ziurys, L. M. 2010, ApJ, 720, L102 (Paper I)
Tenenbaum, E. D., Woolf, N. J., & Ziurys, L. M. 2007, ApJ, 666, L29
Tenenbaum, E. D., & Ziurys, L. M. 2008, ApJ, 680, L121
Tenenbaum, E. D., & Ziurys, L. M. 2009, ApJ, 694, L59
Tenenbaum, E. D., & Ziurys, L. M. 2010, ApJ, 712, L93
Tielens, A. G. G. M., & Charnley, S. B. 1997, Orig. Life. Evol. Biosph., 27, 23
Turner, B. E. 1991, ApJ, 376, 573
Turner, B. E. 1995, Ap&SS, 224, 297
Turner, B. E., Steimle, T. C., & Meerts, L. 1994, ApJ, 426, L97
van Vaals, J. J., Meeerts, W. L., & Dymanus, A. 1984, Chem. Phys., 86, 147
Verhoelst, T., Van Der Zypen, N., Hony, S., Decin, L., Cami, J., & Eriksson, K. 2009, A&A, 498, 127
Willacy, K., & Cherchneff, I. 1997, Ap&SS, 251, 49
Ziurys, L. M. 2006, Proc. Natal. Acad. Sci., 103, 12274
Ziurys, L. M., Milam, S. N., Apponi, A. J., & Woolf, N. J. 2007, Nature, 447, 1094
Ziurys, L. M., Savage, C., Highberger, J. L., Apponi, A. J., Guélin, M., & Cernicharo, J. 2002, ApJ, 564, L45
Ziurys, L. M., Tenenbaum, E. D., Pulliam, R. L., Woolf, N. J., & Milam, S. N. 2009, ApJ, 695, 1604